

PATHWAYS FOR C—H ACTIVATION AND FUNCTIONALIZATION BY GROUP 9 METALS

Dale R. Pahls

Dissertation Prepared for the Degree of

DOCTOR OF PHILOSOPHY

UNIVERSITY OF NORTH TEXAS

May 2015

APPROVED:

Thomas Cundari, Major Professor
Weston Borden, Committee Member
Mohammad Omary, Committee Member
LeGrande Slaughter, Committee Member
Martin Schwartz, Committee Member
Karen Goldberg, Committee Member
William Acree, Chair of the Department of
Chemistry
Costas Tsatsoulis, Interim Dean of the
Toulouse Graduate School

Pahls, Dale R. *Pathways for C—H Activation and Functionalization by Group 9 Metals*.

Doctor of Philosophy (Chemistry - Inorganic Chemistry), May 2015, 98 pp., 2 tables, 22 figures, 18 schemes, references, 202 titles.

As fossil fuel resources become more and more scarce, attention has been turned to alternative sources of fuels and energy. One promising prospect is the conversion of methane (natural gas) to methanol, which requires an initial activation of a C-H bond and subsequent formation of a C-O bond. The most well studied methodologies for both C-H activation and C-O bond formation involve oxidation of the metal center. Metal complexes with facile access to oxidation states separated by four charge units, required for two subsequent oxidations, are rare. Non-oxidative methods to perform C-H bond activation or C-O bond formation must be pursued in order for methane to methanol to become a viable strategy. In this dissertation studies on redox and non-redox methods for both C-H activation and C-O bond formation are discussed.

In the early chapters C-O bond formation in the form of reductive functionalization is modeled. Polypyridine ligated rhodium complexes were studied computationally to determine the properties that would promote reductive functionalization. These principles were then tested by designing an experimental complex that could form C-O bonds. This complex was then shown to also work in acidic media, a critical aspect for product stabilization.

In the later chapters, non-oxidative C-H activation is discussed with Ir complexes. Both sigma bond metathesis and concerted metalation deprotonation were investigated. For the former, the mechanism for an experimentally known complex was elucidated and for the latter the controlling factors for a proposed catalyst were explored.

Copyright 2015

by

Dale R. Pahls

ACKNOWLEDGEMENTS

They say that 'no man is an island' and I feel this holds particularly true of a graduate student in the sciences. On our own few graduate student 'islands' would be exposed to the breadth of chemistry necessary to truly grow professionally and without the support of friends and family we would not be able to grow at all.

On the professional side, I would to thank my collaborators for the interesting and challenging projects they have provided over the years. Few experiences have been as satisfying as solving a truly challenging problem with the help of collaborators that both help test and challenge your proposals. Both of the centers with which, I have had the privilege of working have helped by exposing me to new ideas and ways of thinking. In particular the open round table discussions at the yearly meetings were valuable in seeing how some of the most successful individuals in the field identify and approach problems.

I could not thank enough my lab and all its members, both past and present, for making graduate school fun. It is not uncommon for people not to remember this period of life fondly, but the lab environment made this untrue for our lab. The lab jokes, discussions, and interactions both in and out of lab is something I will always remember. The discussions with my advisor, Tom Cundari, both on my work or any random topic was always appreciated. The generally relaxed, yet very productive nature of the lab made it an excellent place to learn.

For my friends and family it has been a particularly long road to my defense. Of my friends in particular I want to thank John Paul Giordano, Marcus Wallace, Terra and Beverly Necessary, and Josh Anderson. Their support and understanding during the stressful times has been invaluable. Their patience especially during this period will not be forgotten.

TABLE OF CONTENTS

	Page
ACKNOWLEDGEMENTS.....	iii
LIST OF TABLES.....	vi
LIST OF FIGURES.....	vii
LIST OF SCHEMES.....	ix
CHAPTER 1 INTRODUCTION.....	1
CHAPTER 2 THEORETICAL STUDY OF REDUCTIVE FUNCTIONALIZATION OF METHYL LIGANDS OF GROUP 9 COMPLEXES SUPPORTED BY TWO BIPYRIDYL LIGANDS: A KEY STEP IN CATALYTIC HYDROCARBON FUNCTIONALIZATION.....	6
2.1 Introduction.....	6
2.2 Results and Discussion.....	11
2.2.1 Structure of the (<i>bis</i> -bipyridine)Rh-alkyl Complexes.....	11
2.2.2 Impact of Ancillary Ligand Modification.....	15
2.2.3 Impact of Supporting Ligand Modification.....	18
2.2.4 Impact of Nucleophile.....	20
2.2.5 Impact of Metal.....	21
2.2.6 Correlation of LUMO Energies and Reaction Barriers.....	22
2.3 Summary and Conclusions.....	26
2.4 Computational Details.....	29
2.5 Acknowledgements.....	29
CHAPTER 3 REDUCTIVE FUNCTIONALIZATION OF A RHODIUM(III)-METHYL BOND BY ELECTRONIC MODIFICATION OF THE SUPPORTING LIGAND.....	31
3.1 Introduction.....	31
3.2 Results and Discussion.....	34
3.3 Conclusions.....	41
CHAPTER 4 REDUCTIVE FUNCTIONALIZATION OF A RHODIUM(III)-METHYL BOND IN ACIDIC MEDIA.....	42

4.1	Introduction	42
4.2	Results and Discussion	45
4.3	Conclusions	51
4.4	Computational Methods.....	53
CHAPTER 5 MECHANISM OF HYDROGENOLYSIS OF AN IRIIDIUM-METHYL BOND: EVIDENCE FOR A METHANE COMPLEX INTERMEDIATE		55
5.1	Introduction	55
5.2	Summary of Experimental Results.....	56
5.3	Computational Results and Discussions	58
CHAPTER 6 DFT STUDIES ON LIGAND OPTIMIZATION OF C-H ACTIVATION BY PheboxIr(OAc) ₂ (H ₂ O).....		62
6.1	Introduction	62
6.2	Computational Methods.....	66
6.3	Reaction Pathway	67
6.3.1	Loss of Water from PheboxIr(OAc) ₂ (H ₂ O).....	67
6.3.2	Hydrocarbon Binding to PheboxIr(OAc) ₂	68
6.3.3	Carbon—Hydrogen Bond Activation.....	69
6.4	Impact of Ligand Modification.....	72
6.4.1	Effect of <i>para</i> -substitution on Aryl Linker	73
6.4.2	Modifications of the Aryl Backbone	74
6.4.3	Effect of Pincer Arm Substitution	76
6.4.4	Effect of Modifying Acetate Base	78
6.5	Summary and Conclusions.....	80
CHAPTER 7 CLOSING REMARKS AND CHAPTER SUMMARY.....		82
REFERENCES.....		88

LIST OF TABLES

	Page
Table 4.1	Calculated free energies (kcal/mol) for the reductive functionalization pathways A and B presented in Scheme 4.2. 46
Table 4.2	Calculated free energies (kcal/mol) for the protonation transition states A-C presented in Figure 4.2. 50

LIST OF FIGURES

		Page
Figure 2.1	The tilt angle of the bipyridine ligands in <i>trans</i> -[(bpy) ₂ RhMe ₂] ⁺	13
Figure 2.2	Optimized ground state of <i>trans</i> -[(bpy) ₂ Rh(Me)(Cl)] ⁺ with the Rh–Cl bond length (Å) shown.	17
Figure 2.3	Plot of scaled calculated difference in free energy barrier ($\Delta\Delta G^\ddagger$) to nucleophilic attack by hydroxide on the Rh–CH ₃ bond of <i>cis</i> -[(bpy) ₂ Rh(Me)X] ⁺ complexes versus Hammett σ_p and σ_m parameters with associated R ² values.	19
Figure 2.4	Plots of the LUMO orbitals.....	23
Figure 2.5	Plot of calculated LUMO energies of Rh(III) complexes (eV) versus ΔG^\ddagger_{NA} (kcal/mol) for attack of hydroxide on the Rh–Me bond of <i>cis</i> -[(Y-bpy) ₂ Rh(Me) ₂] ⁺ complexes.....	24
Figure 2.6	Plot of calculated LUMO energies of Rh(III) complexes versus ΔG^\ddagger_{NA} for hydroxide attack on [(bpy) ₂ Rh(Me)X] ⁿ⁺ (X = HO ⁻ , H ⁻ , H ₃ C ⁻ , Cl ⁻ , CO or Py,) complexes	24
Figure 3.1	DFT-optimized structures of 1'-6' in THF	35
Figure 3.2	Experimental and computed thermodynamics of oxidative addition of MeI to tBu ₃ terpyRhI.....	36
Figure 3.3	Three pathways for reductive functionalization from 9'.....	39
Figure 4.1	Transition state structures and their corresponding energies (kcal/mol) for reductive functionalization of 2' with hydrogen bonding interactions.....	47
Figure 4.2	DFT calculated transition states (A and B) for methane formation from 2' and 3'.....	50
Figure 5.1	DFT-calculated structures of (PONOP)Ir(H)(Me)(H ₂) ⁺ and (PONOP)Ir(CH ₄)(H) ₂ ⁺ ..	59
Figure 5.2	(a) Transition state for hydrogen transfer with an Ir–H bond length of 1.6 Å. (b) Transition state for hydrogen transfer with a restricted Ir–H distance of 2.0 Å.	61
Figure 6.1	Example of CMD reaction of hydrocarbons with (dmPhebox)Ir(OAc) ₂ (H ₂ O).....	63
Figure 6.2	DFT optimized structure of (dmPhebox)Ir(OAc) ₂ (H ₂ O) with selected bond distances shown.....	65

Figure 6.3	Comparison of the free energies of <i>cis</i> and <i>trans</i> - ^{dm} PheboxIr(OAc) ₂ complexes upon methane binding and activation.....	69
Figure 6.4	The structures of <i>cis</i> - ^{dm} PheboxIr(OAc) ₂ (σ-CH ₄), the CMD TS of <i>cis</i> - ^{dm} Phebox(OAc) ₂ (σ-CH ₄), <i>trans</i> - ^{dm} PheboxIr(OAc) ₂ (σ-CH ₄), and the CMD TS of <i>trans</i> -(^{dm} Phebox)Ir(OAc) ₂ (σ-CH ₄)	72
Figure 6.5	Free energy barriers (kcal/mol) for systems with para-substituents on the phenyl backbone.....	73
Figure 6.6	Free energy barriers (kcal/mol) for systems with nitrogen heterocycles as central ligand.	74
Figure 6.7	Free energy barriers (kcal/mol) for systems with protonated or methylated systems.	76
Figure 6.8	Free energy barriers (kcal/mol) for systems with modified side chains.	77
Figure 6.9	Free energy barriers (kcal/mol) for the activation of methane by various carboxylates and acetamide.	79

LIST OF SCHEMES

		Page
Scheme 1.1	Scheme showing a generalization of the current methodology and proposed methodology for the functionalization of alkenes.	2
Scheme 1.2	Current and proposed methodology for transforming methane into methanol. Thermodynamics are reported in the gas phase.	4
Scheme 2.1	General scheme for electrophilic activation and reductive functionalization of alkanes using late transition metal catalysts.	7
Scheme 2.2	Graphical representation of the reaction modeled in Yoh's work.	10
Scheme 2.3	The relative stabilities (ΔG , kcal/mol) of <i>cis</i> and <i>trans</i> isomers of selected $[(bpy)_2Rh(Me)X]^{n+}$ complexes as well as the barrier to nucleophilic attack by hydroxide nucleophile (<i>cis</i> _NA and <i>trans</i> _NA).	12
Scheme 2.4	Calculated relative free energies (kcal/mol) of the ground and transition states for <i>cis</i> - and <i>trans</i> - $[(bpy)_2RhMe_2]^+$ complexes undergoing nucleophilic attack by hydroxide.	15
Scheme 2.5	Effect of the <i>trans</i> ligand on the calculated free energy barrier (kcal/mol) to nucleophilic attack on a Rh(III)-methyl bond by hydroxide starting from <i>trans</i> - $[(bpy)_2Rh(Me)X]^{n+}$ and hydroxide.	16
Scheme 2.6	Calculated free energy barriers (kcal/mol) to nucleophilic attack of complexes with varied bipyridine ligands.	18
Scheme 2.7	Effect of nucleophile on the free energy barrier (kcal/mol) to nucleophilic attack on the Rh-CH ₃ bond of <i>cis</i> - $[(bpy)_2Rh(Me)_2]^+$	20
Scheme 2.8	Effect of the transition metal on the free energy barrier to nucleophilic attack by hydroxide on <i>cis</i> - $[(bpy)_2M(Me)_2]^+$ complexes.	21
Scheme 3.1	The electrophilic catalytic cycle for the partial oxidation/ functionalization of methane using late transition metals.	32
Scheme 3.2	DFT calculated thermodynamics for the reaction of 1' and 2' with MeX. All free energies (kcal/mol) are listed as $L_nRh^I + MeX \rightarrow L_nRh^{III}$	37
Scheme 4.1	The proposed "Shilov" catalytic cycle for the partial oxidation/functionalization of methane using Pt ^{II} salts (X = OH ⁻ , Cl ⁻ ; L = H ₂ O).	43

Scheme 4.2	Two proposed pathways for reductive functionalization from $[(\text{NO}_2)_3\text{terpy}]\text{Rh}(\text{Me})(\text{Cl})\text{I}$ ($X = \text{I}^-$).	45
Scheme 4.3	A potential mechanism for electrophilic catalytic cycle using Rh-based catalysts.	53
Scheme 5.1	Two Possible Pathways for Hydrogenolysis of a $\text{M}-\text{CH}_3$ Bond	56
Scheme 5.2	Hydrogenolysis of Complex 1 at Low Temperature.....	57
Scheme 5.3	Two Potential Mechanisms for Interconversion of 2 and 5.	60

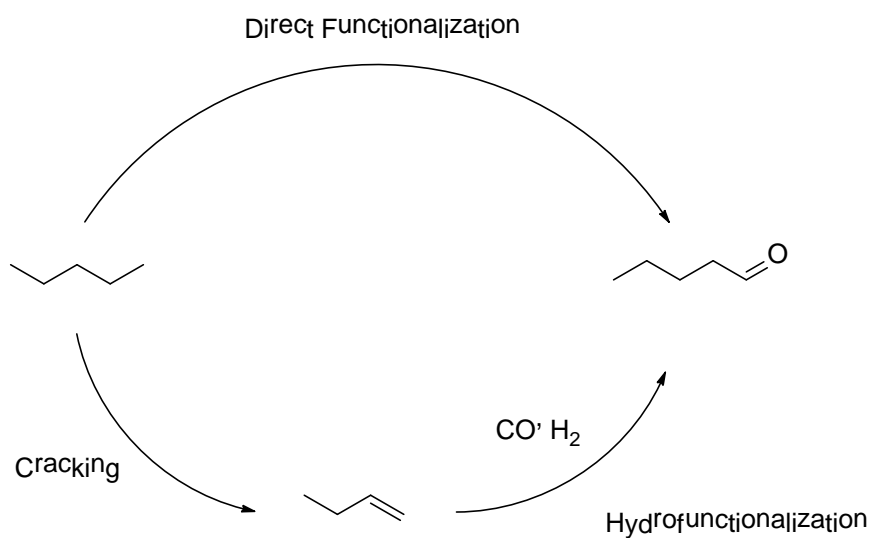
CHAPTER 1

INTRODUCTION

Petroleum is one of the primary carbon feedstocks.¹ After separation, it provides access to a variety of alkanes and arenes.² Alkanes are historically difficult to functionalize selectively.³ To overcome this difficulty, industry “cracks” the alkanes in petroleum by breaking a carbon-carbon bond in long chain alkanes to form a shorter length alkene and alkane.² Industry has developed a wide array of processes that can very effectively utilize alkenes including hydroformylation, a transformation utilized quite often by industry.⁴ Cracking has several drawbacks. The first is that cracking is a very energy intensive process, as might be expected when C-C and C-H σ -bonds are being cleaved. Often temperature upwards of 500 K are necessary.⁵ Also, small hydrocarbons such as methane and ethane are formed in the process. These hydrocarbons are difficult to capture and transport and so have little commercial value. As methane is a worse greenhouse gas than carbon dioxide these gases are instead burned, a waste of potential resources. As the consequences of chemical waste on the environment become more pressing, regulations are calling for newer processes that are more atom and energy efficient, i.e., “greener.” As outlined above, cracking is neither energy nor atom efficient, but is still necessary to produce the alkene feedstocks that the chemical industry needs. Clearly an alternative to this process would be valuable to develop.

One potential alternative would be metal mediated direct activation and functionalization of alkanes, (Scheme 1.1) which has the potential to be both more atom and energy efficient than the current methodology. Such a process would involve activation of the alkane by a metal center and the transformation of the resulting metal-alkyl bond to yield a functionalized product.

Development of these processes are difficult not only because of the low reactivity of the alkanes, but also due to the requirements of industry. To be a useful reaction, the process must not only activate and functionalize alkanes, but must do so both selectively (only one product) and efficiently (extremely high turnover numbers). Developing a catalyst that can meet all these requirements is naturally very challenging and so theory is often relied upon to facilitate catalyst development. Calculations can facilitate catalyst development by understanding the mechanism of a reaction and applying that knowledge to suggest directions for experiment that would improve catalyst performance. These improvements could be a more active, selective, or robust catalyst depending on what properties are most desirable.

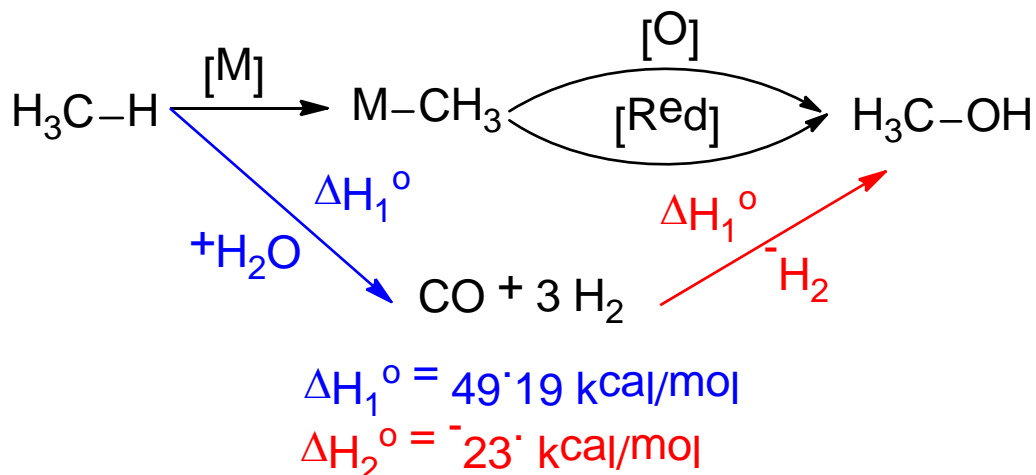


Scheme 1.1 Scheme showing a generalization of the current methodology and proposed methodology for the functionalization of alkenes.

The work described in this dissertation will focus on the activation and functionalization of methane. One particular challenge of using methane in catalysis is that being the smallest alkane, it has one of the strongest C-H bonds. Catalysts capable of methane C-H activation should also be capable of C-H activation at other primary carbon centers barring a strong steric

preference. Investigation of methane C-H activation also provides an added benefit of being of value to the natural gas market. Methane is the primary component of natural gas, which is currently used primarily as an energy source not as a chemical feedstock.¹ The United States has access to large quantities of natural gas and these reserves grow as new drilling techniques such as horizontal drilling are developed.¹ However, it is costly to condense and transport natural gas, limiting the range for which it may be used as energy. Excess methane is typically flared in the same manner that smaller chain alkanes are when alkanes are cracked. A process that could selectively functionalize methane into a more value added, easier to transport compound is thus a tantalizing target.

One potential target is the mono-oxidation of methane to methanol.¹ Methanol is a very useful product that sees use as a fuel, in the formation of biodiesel, and as a precursor to various plastics, gasoline, and alkenes.¹ As a liquid it both avoids the issue of concentration that faces methane and can also use the infrastructure in place to transport gasoline. The current process to form methanol from methane requires steam reforming of the methane to form carbon monoxide and hydrogen gas, which can then be combined to form methanol.⁶ Although the second step is exothermic, this first step, steam reforming, is very energy intensive. If a direct pathway were to be developed then this energy intensive step could be removed. Metal mediated C-H activation is one potential alternative method to the selective formation of methanol (Scheme 1.2). The main challenge for methane to methanol catalysis is selectivity. Methane oxidation is extremely easy, but stopping that oxidation before methane is fully oxidized to carbon dioxide is a difficult task.



Scheme 1.2 Current and proposed methodology for transforming methane into methanol. Thermodynamics are reported in the gas phase.⁷

The first step in this reaction, C-H activation, has been studied by multiple groups with various metals, ligands, and hydrocarbons including methane.⁸ A large number of these studies have focused on oxidative addition and the parameters that control this reaction are fairly well understood.⁹ Ligands and complexes have been developed to assist this reaction which formally oxidizes the metal center. The second step, C-O bond formation, is far less well understood. One such method that our group has investigated to form C-O bonds is oxy-insertion.¹⁰ Oxy-insertion is the formal insertion of the oxygen atom of a metal-oxygen multiple bond into a metal-carbon bond. In oxy-insertion an oxygen atom transfer reagent delivers the oxygen atom and formally oxidizes the metal center. Oxidative addition and oxy-insertion are unlikely to be compatible reactions within a catalytic cycle as both steps oxidize the metal and would require stable oxidation states separated by both two and four charge units, a trait few metals possess. As such an alternate method to either oxidative addition or oxy-insertion is likely necessary to develop a complete catalytic cycle. The work discussed within will focus on reductive methods for C-O bond

formation, non-oxidative methods for C-H activation, and the potential to bypass the metal-oxygen double bond (oxo complexes), and thus oxidation of the metal center.

CHAPTER 2

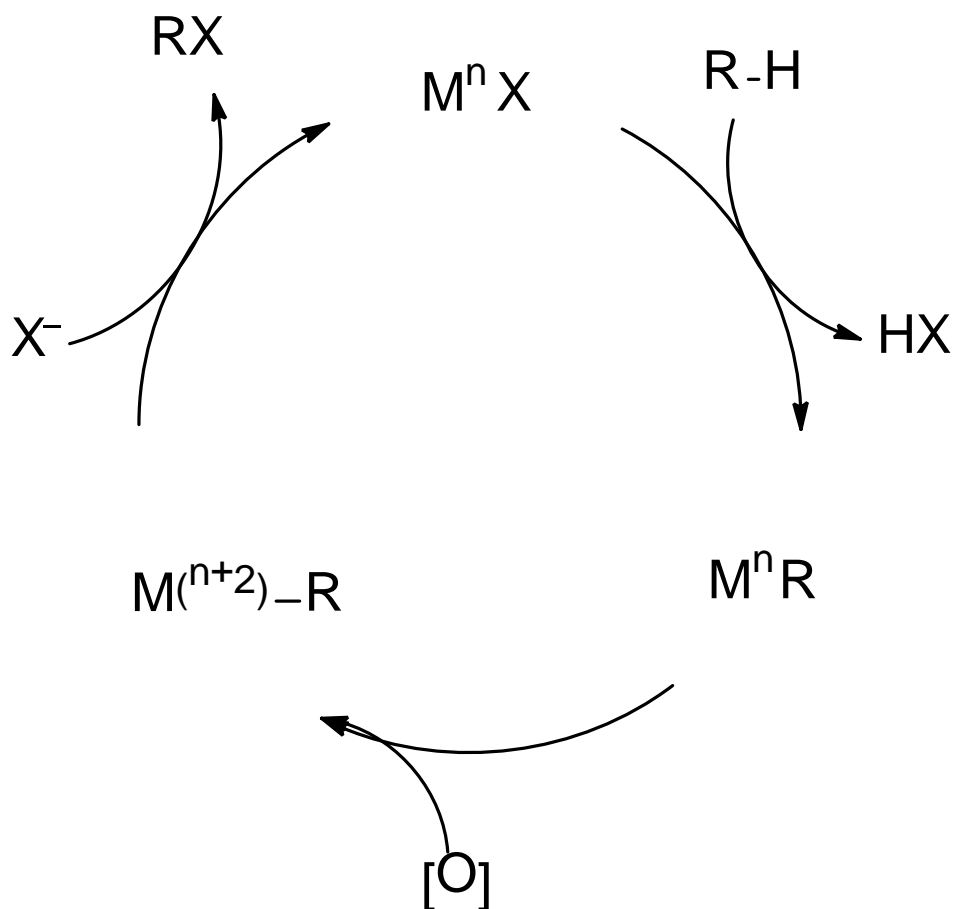
THEORETICAL STUDY OF REDUCTIVE FUNCTIONALIZATION OF METHYL LIGANDS OF GROUP 9 COMPLEXES SUPPORTED BY TWO BIPYRIDYL LIGANDS: A KEY STEP IN CATALYTIC HYDROCARBON FUNCTIONALIZATIONⁱ

2.1 Introduction

A method for the direct selective partial oxidation of alkanes is a highly sought transformation, especially for the conversion of methane to methanol.^{11,12,13,14,15,16,17} A commercially viable low temperature and low pressure (≤ 250 °C and ≤ 500 psi) process for the direct formation of alcohol from light alkanes could expand the use of natural gas as a transportation fuel and chemical feedstock.¹⁸ One strategy for alkane functionalization is the use of electrophilic late transition metals that mediate C–H activation and a reductive functionalization of the resulting metal-hydrocarbyl bond (Scheme 2.1), and catalysts based on Pt, Pd, Au, Hg, Rh and Tl have been reported.^{12,15,19,20,21,22,23} One advantage of late transition metal catalysts is their tolerance of acidic media (HX). This provides a strategy for protection of the functionalized methyl group through formation of MeX (X = electron withdrawing group), which can decrease the rate of electrophilic C–H activation.^{12,20,24} Among the most heavily studied complexes is the Shilov catalyst system,²⁵ which incorporates a simple Pt(II) salt as catalyst and stoichiometric Pt(IV) as the oxidant. Later work has incorporated N-based ligands on Pt(II) to enable detailed studies, especially of the C–H activation step,^{13,26,27,28,29,30,31} as well as

ⁱ Reprinted with permission from **Theoretical Study of Reductive Functionalization of Methyl Ligands of Group 9 Complexes Supported by Two Bipyridyl Ligands: A Key Step in Catalytic Hydrocarbon Functionalization**, D. R. Pahls, J. T. Groves, T. B. Gunnoe, T. R. Cundari, *Organometallics*, **2014**, 33, 1936-1944. DOI: [10.1021/om4010093](https://doi.org/10.1021/om4010093). Copyright 2014 American Chemical Society.

improvements in catalyst efficacy.¹³ Application of the Shilov and more recent Pt(II) catalysts has been hampered by product or water inhibition, difficulty incorporating scalable oxidants, and slow rates of catalytic turnover.^{15,22}



Scheme 2.1 General scheme for electrophilic activation and reductive functionalization of alkanes using late transition metal catalysts.

For the Shilov and related catalysts, it has been suggested that the C–H activation occurs at Pt(II) while the functionalization of an electrophilic alkyl ligand occurs at Pt(IV).^{24,26,27,32} Thus, the catalyst requires access to formal oxidation states that provide d^8 and d^6 electronic states. Similarly, it has been proposed that bisulfate serves as a nucleophile for reductive functionalization of methyl-Hg(II) bonds using a Hg(II) catalyst that operates in sulfuric acid,²⁴ and presumably related processes occur for related Au and Tl catalysts.²² Despite the success of

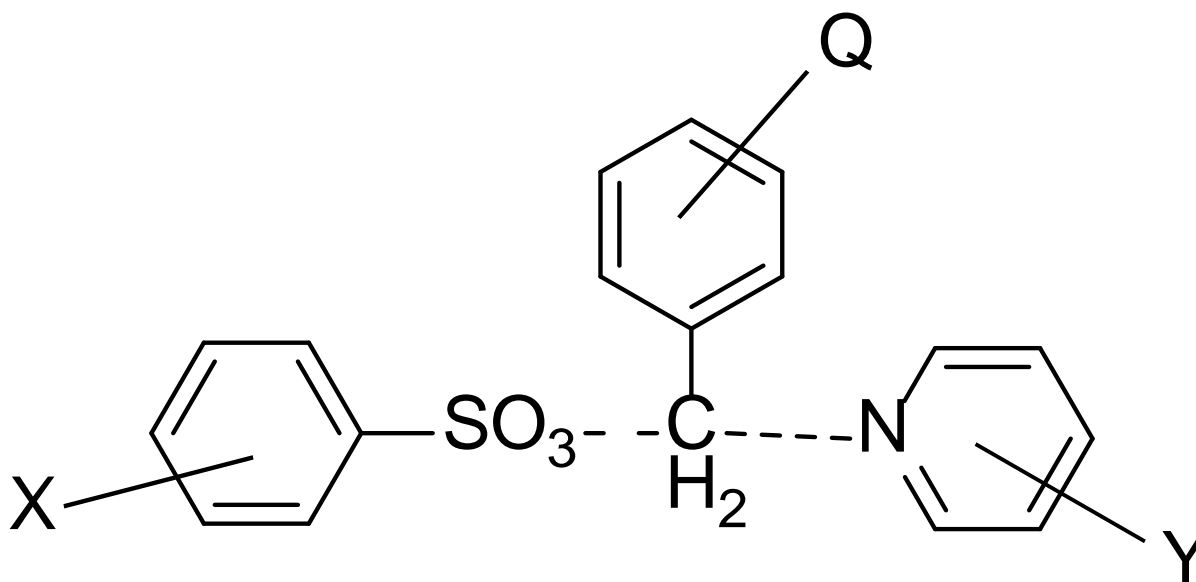
several different metals for electrophilic catalytic functionalization of methane, relatively little computational work has been directed toward alkane functionalization using electrophilic complexes similar to the Shilov system that take advantage of umpolung reactivity where an alkyl ligand is electrophilic and functionalized by a nucleophile.^{33,34,35,36,37}

Moving earlier in the transition series (compared to the Group 10 triad) may reduce metal electrophilicity and thus decrease the predilection toward product or water inhibition. Rhodium provides a viable target since it can readily access d^8 [Rh(I)] and d^6 [Rh(III)] states. Also, C–H activation by Rh(I) and Rh(III) complexes has precedent.^{38,39,40,41,42,43,44,45,,46,47,48,49,50} Despite the potential of Rh catalysts,³³ few systematic studies of reductive functionalization of Rh(III)-alkyl moieties have been reported. DiMugno and coworkers used perfluorinated tetraphenylporphyrin-rhodium complexes and demonstrated that after activation of methane, the resulting rhodium-methyl bond can be functionalized by phosphine nucleophilic attack to yield a phosphonium salt.⁵¹ It was proposed that the electron-poor perfluoroporphyrin ligand stabilizes the resulting anionic Rh(I) complex and hence facilitates the functionalization of the Rh(III)-methyl bond.⁵¹ Groves and coworkers have shown that pendent oxygen and nitrogen nucleophiles are capable of intramolecular nucleophilic addition to Rh-alkyl groups supported by tetraphenylporphyrin.^{52,53,54} Fu and coworkers have reported similar intermolecular ring closure from β -hydroxyalkyl groups to form D₁-propylene oxide from (TPP)Rh(CDH)CH(CH₃)(OH).⁵⁵ The observed inversion of stereochemistry at the carbon bound to the metal is consistent with a nucleophilic attack mechanism.^{54,55} Varshavsky and coworkers have demonstrated that addition of triphenylphosphine to a room temperature solution of *cis*-[Rh(β -diketonate)(PPh₃)₂(CH₃)(CH₃CN)][BPh₄] gives the Rh(I) complex Rh(β -diketonate)(PPh₃),

[MePPh₃][BPh₄] and free acetonitrile.⁵⁶ Although a reductive elimination pathway was proposed, intermolecular nucleophilic attack of free phosphine on the Rh–Me ligand appears plausible. Most recently Milstein and coworkers have published on sterically hindered ^tBuPNP (^tBuPNP= 2,6-bis-(di-*tert*-butylphosphinomethyl)pyridine) pincer ligated rhodium complexes of the form [(^tBuPNP)Rh(CH₃)X][BF₄] where X = (Cl⁻, Br⁻, and I⁻). They proposed, based on solvent effects, that the sterically hindered ^tBuPNP complexes underwent reductive elimination of CH₃X by nucleophilic attack for X= I⁻, and Br⁻, but by a concerted fashion for X = Cl⁻ upon presence of coordinating or noncoordinating ligands.⁵⁷

As part of an interest in modeling routes for metal-mediated C–X bond formation (where X is a halide or heterofunctional group), we seek to compare and contrast metal-mediated variants of classic organic routes.⁵⁸ In one especially comprehensive study that incorporated theory and experiment, Yoh and coworkers investigated the nucleophilic attack of substituted (Q)-benzyl-(X)-benzenesulfonates with (Y)-pyridines to determine the relative effects of changing the electronic properties of the leaving group (benzenesulfonate), electrophile (benzyl group) and nucleophile (pyridine) on the rate (Scheme 2.2).⁵⁹ They found that changing the electronic properties of the pyridine nucleophile (Y) had the largest effect on the rate of reaction, while modifying the electronic properties of the benzenesulfonate leaving group (X) had a similar but slightly diminished effect on the rate of S_N2 substitution. Modification of the benzyl group (Q) had the smallest effect on the rate of the nucleophilic substitution reaction. To wit, even the largest Hammett ρ determined for changing the benzyl group was smaller than the smallest ρ calculated for either the benzenesulfonate leaving group or the pyridine nucleophile. The study

by Yoh *et al.* thus suggests an order of importance for what parameters most affect this organic S_N2 reaction in polar, aprotic media, viz nucleophile > leaving group >> electrophile.⁵⁹



Scheme 2.2 Graphical representation of the reaction modeled in Yoh's work. We have replaced the Z nomenclature with Q to avoid any potential confusion with olefin isomers. Adapted from reference 59.

The observation of Hammett "indifference" to electrophile in the study by Yoh *et al.* is interesting in comparison to our recent computational study of the migration of an aryl ligand coordinated to Pt(II) to the O atom of a pyridine-*N*-oxide ligand (*i.e.*, an organometallic Baeyer-Villiger (OMBV) reaction).^{58f} The study of the Pt(II)-mediated OMBV reaction predicted that the activation barrier for aryl migration would be highly sensitive to substituents on the aryl ligand. However, in Baeyer-Villiger type reactions, methyl is a reluctant migrating group,⁶⁰ which is a potential impediment to exploitation of the OMBV mechanism in a methane-to-methanol catalytic cycle. It is thus interesting to assess and expand the scope of the functionalization of electrophilic rhodium alkyl groups by nucleophiles for C-X bond formation. As outlined above, Rh complexes supported by porphyrin ligands have been studied.^{49,51,54} Based on differences in

charge, exchanging the dianionic porphyrin ring with two neutral bipyridine (bpy) ligands, $[(bpy)_2Rh(Me)L]^{n+}$ ($n = 1$ or 2 depending on charge of L) and an additional ancillary ligand might be anticipated to improve the reactivity toward reductive functionalization of Rh(III) methyl ligands. The resulting complexes would be either mono or dicationic, depending on the choice of the ancillary ligand, and therefore are reasonably expected to be more electrophilic than the corresponding charge neutral porphyrin complexes.

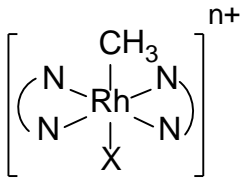
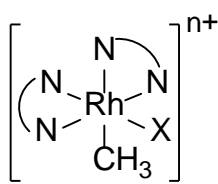
This account will compare reductive functionalization of methyl ligands of *bis*-bipyridyl complexes with previously reported rhodium porphyrin complexes as well as probe the impact on C–X bond formation of (a) the electronic properties of the ancillary ligands including the bipyridine ligands and the ligand occupying the sixth coordination site, (b) the identity of the nucleophile, and (c) the identity of the metal. Salient electronic characteristics of the metal complex are sought that would render nucleophilic routes to C–X bond formation by Group 9 metal complexes with hydrocarbyl ligands viable.

2.2 Results and Discussion

2.2.1 Structure of the (*bis*-bipyridine)Rh-alkyl Complexes

Two geometric isomers exist for the $[(bpy)_2Rh(Me)X]^+$ ($X = Me, HO^-, PMe_3,$ or pyridine (Py)) complexes. The methyl and ancillary ligands X can either occupy a trans or a cis configuration. Since either of these isomers could be the reactive entity and examples of both are known,^{61,62,63,64,65} the relative stabilities and barriers to reaction for the two isomers were compared. For this comparison the relative stabilities of complexes corresponding to $X = H_3C^-, HO^-, PMe_3,$ and pyridine were studied (Scheme 2.3) to afford the analysis of an array of ligand donor properties. The *cis*- $[(bpy)_2Rh(Me)_2][BAr'_4]$ ($Ar' = 3,5-(CF_3)_2C_6H_3$) complex has been

reported. Treatment of *cis*-[(bpy)₂Rh(Me)₂][BAR'₄] with triflic acid forms *cis*-[(bpy)₂Rh(Me)(OTf)][BAR'₄], and the triflate anion can undergo exchange with other ligands.^{63,64} The hydroxide and phosphine complexes were deemed of interest, as they would be expected to displace the triflate and open up other reactive pathways leading to functionalized products.^{50,51,52} Pyridine was chosen to determine the relative importance of two stereoelectronic effects, which will be discussed below.

	X, n^+	<i>cis</i> -NA	<i>cis</i>	<i>trans</i>	<i>trans</i> -NA
	$CH_3, 1^+$	31.5	0.0	23.4	44.2
	$OH, 1^+$	25.2	0.0	17.4	44.2
	$PMe_3, 2^+$	16.5	0.0	10.7	25.2
	$C_5H_5N, 2^+$	14.0	0.0	9.4	18.4
<i>trans</i>					
					
<i>cis</i>					

Scheme 2.3 The relative stabilities (ΔG , kcal/mol) of *cis* and *trans* isomers of selected [(bpy)₂Rh(Me)X]ⁿ⁺ complexes as well as the barrier to nucleophilic attack by hydroxide nucleophile (*cis*_NA and *trans*_NA). All values are relative to the lower energy *cis*-[(bpy)₂Rh(Me)X]ⁿ⁺ complex. The overall charge of the Rh complexes is n⁺.

For all of the systems studied, the *cis* complex was found to be more stable than the *trans* isomer by at least 9 kcal/mol (Scheme 2.3). The [(bpy)₂RhMe₂]⁺ complex showed the greatest difference (23.4 kcal/mol) in the stability of the two isomers, and [(bpy)₂RhMe(Py)]²⁺ showed the least difference in *cis*-*trans* stability (9.4 kcal/mol). We propose that the relative stabilities of the *cis* and *trans* isomers are due to a combination of two factors: (1) steric interactions between the two bipyridine ligands (particularly the 6 and 6' hydrogens) in the *trans* isomer, and (2) the greater *trans* influence of the methyl ligand versus a pyridyl ring of the bipyridine ligand. When both bipyridine ligands occupy the same plane of an octahedron, forcing the X and Me to be *trans* to each other, the interaction of the 6 and 6' C-H bonds of the two bipyridine ligands forces these

ligands to distort from planarity.⁶¹ This interaction would, therefore, destabilize the trans complex relative to its cis isomer in which the bipyridine ligands do not distort. The calculated tilt angles (Figure 2.1), *i.e.*, the extent that the C_{bridging}-C_{bridging}-N-C_{ortho} dihedral angle deviates from 180°, for [(bpy)₂Rh(Me)(PMe₃)]²⁺ range from 12.2° to 13.4°, which is slightly smaller than the average tilt angle of 15.5° in the known rhodium complex *trans*-[(bpy)₂Rh(H₂O)(Cl)][OH][ClO₄].⁶¹

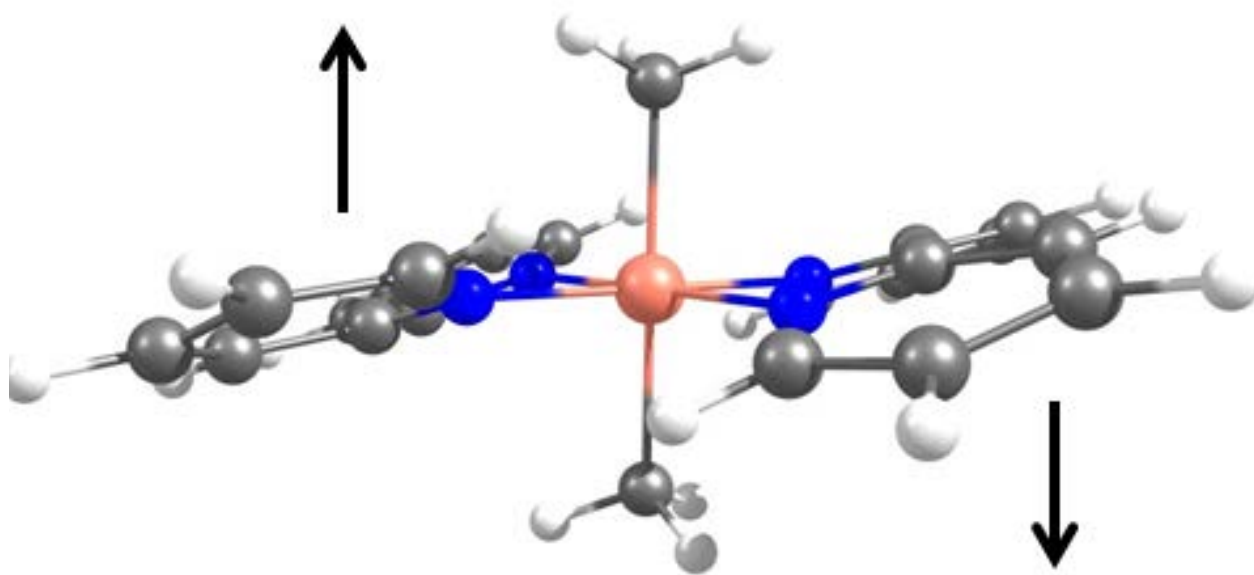
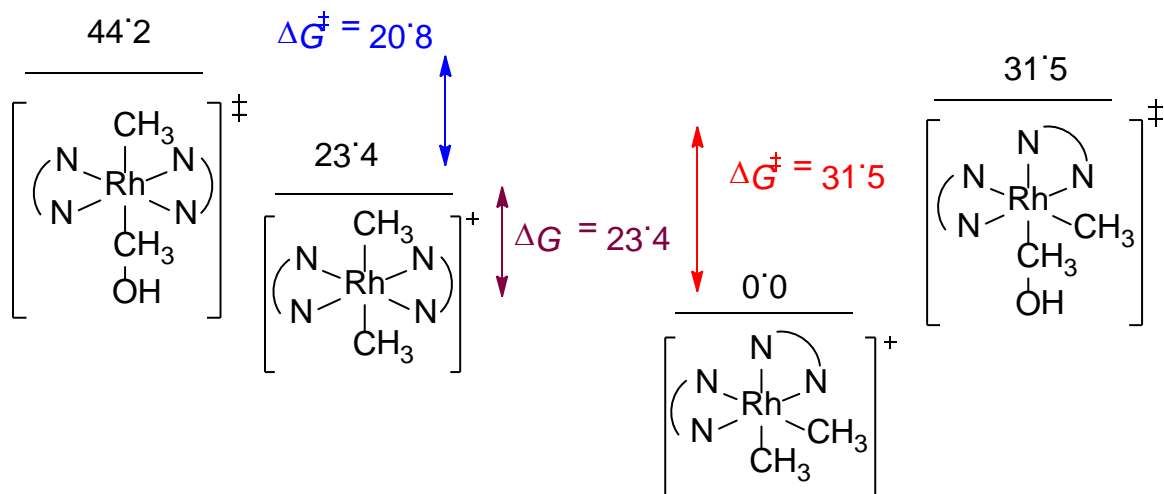


Figure 2.1 The tilt angle of the bipyridine ligands in *trans*-[(bpy)₂RhMe₂]⁺.

The second factor affecting the relative stability of the two [(bpy)₂Rh(Me)X]⁺ isomers is the strength of the trans influence of the ligand trans to the methyl group in the two complexes. For *trans*-[(bpy)₂RhMe₂]⁺, the influence of the strong trans influencing methyl ligand likely destabilizes the complex. As the X group trans to the methyl becomes a weaker trans influencing ligand, the complex should be less destabilized and the difference in ground state energies should lessen, as is observed computationally (Scheme 2.3). To help delineate the effects of the trans influence from the destabilization of the bipyridine ligands arising from tilting, the complexes

with a pyridine ancillary ligand were modeled since the difference in the trans influences of pyridine and bipyridine should be minimal. The *trans*- $[(bpy)_2Rh(Me)(Py)]^{2+}$ isomer is 9.4 kcal/mol less stable than the *cis*- $[(bpy)_2Rh(Me)(Py)]^{2+}$ isomer. This destabilization accounts for most of the energy difference between the cis and trans isomers of $[(bpy)_2Rh(Me)(PMe_3)]^{2+}$ (10.7 kcal/mol), but only about half of the energy difference for the cis and trans isomers of $[(bpy)_2Rh(Me)(OH)]^+$ and $[(bpy)_2Rh(Me)_2]^+$ (Scheme 2.3).

Although the cis complexes are computed to be more stable, if the trans orientation is kinetically accessible the reductive functionalization could occur from *trans*- $[(bpy)_2Rh(Me)X]^{n+}$. Thus, the barriers to nucleophilic attack on methyl ligands of the cis and trans complexes were compared (Scheme 2.3). The calculated barriers for the trans complexes are lower than the analogous barriers for the cis complexes for all ancillary ligands studied except hydroxide. However, the differences in barriers are less than the relative stabilities of the ground states. Hence, the cis nucleophilic attack transition states are lower in free energy than their corresponding isomeric trans nucleophilic attack transition states (see Scheme 2.4 for the example of $[(bpy)_2Rh(Me)_2]^+$). For this reason, we focused most of the remaining calculations on *cis*- $[(bpy)_2Rh(Me)X]^+$ complexes. Additionally, the calculations provide a possible clue as to a potential advantage of the Rh-porphyrin complexes. The conjugated porphyrin necessitates a trans arrangement of the alkyl and ancillary ligand X. By extension, simulations imply that modifications to $[(bpy)_2M(Me)X]^+$ that lower the cis-trans free energy difference would be desirable vis-à-vis nucleophilic reductive functionalization of M-methyl bonds.



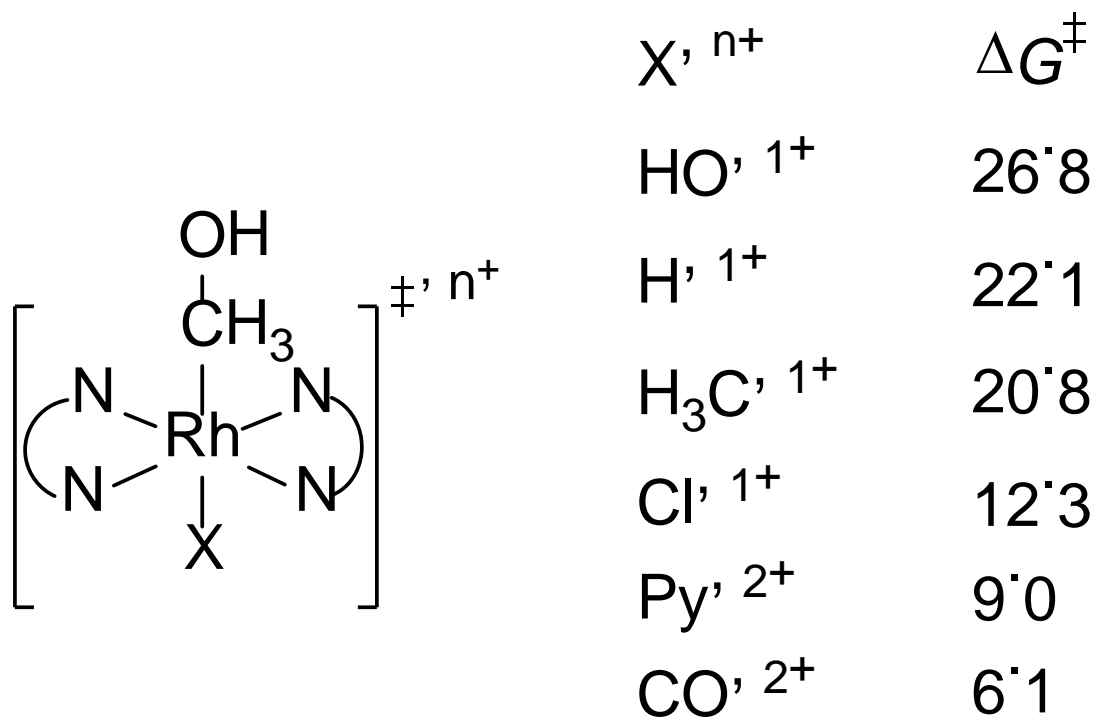
Scheme 2.4 Calculated relative free energies (kcal/mol) of the ground and transition states for *cis*- and *trans*-[(bpy)₂RhMe₂]⁺ complexes undergoing nucleophilic attack by hydroxide.

2.2.2 Impact of Ancillary Ligand Modification

To examine the effect of the ancillary ligand that is trans to the methyl ligand on the C–X bond formation reaction, a series of complexes of the form *trans*-[(bpy)₂Rh(Me)X]ⁿ⁺ was investigated where X = HO[−], H[−], H₃C[−], Cl[−], CO, and Py (Scheme 2.5). These ligands were chosen to give a mix of neutral and anionic σ-donating ligands (H[−], H₃C[−], Py), π-donating ligands (HO[−], Cl[−]), and π-accepting ligand (CO). Although the *cis* complex is more stable, in octahedral complexes the ligand trans to the reacting ligand tends to have the largest impact on the reaction, so *trans* complexes were emphasized for this portion of the study. Hydroxide was utilized as the nucleophile in all of these model reactions, and the implicitly modeled solvent, DMSO, is a polar, aprotic solvent (ε = 47).

Complexes with anionic *trans* ligands are computed to have higher free energy barriers to nucleophilic attack than the corresponding neutral ligands (Scheme 2.5). Barriers to nucleophilic attack were calculated to increase in the order of π-accepting ligand < σ-donating ligands < π-donating ligands. The exception to this trend is the *trans*-[(bpy)₂Rh(Me)(Cl)]⁺ complex,

which has the lowest barrier to nucleophilic attack of the complexes with anionic ancillary ligands, but we propose that this is a special case (see below).



Scheme 2.5 Effect of the trans ligand on the calculated free energy barrier (kcal/mol) to nucleophilic attack on a Rh(III)-methyl bond by hydroxide starting from *trans*- $[(bpy)_2Rh(Me)X]^{n+}$ and hydroxide. For anionic X ligands $n^+ = +1$, and for neutral X ligands $n^+ = +2$.

The data in Scheme 2.5 can be explained by three factors. The first factor is the overall charge of the complex. A dicationic complex should be more electrophilic and hence more reactive towards nucleophilic attack than an analogous monocationic complex. The second factor is the trans influence of X. A stronger trans influence ligand in this case weakens the Rh-CH₃ bond. A weaker bond should be easier to activate; therefore, strong trans influencing ligands will lower the barrier to C-O bond formation. This proposal is supported by the computed free energy barriers for the complexes with H₃C⁻ and H⁻ ligands, which were calculated to have a lower barrier

to reaction (20.8 kcal/mol and 22.1 kcal/mol, respectively) than the complex with the HO⁻ ligand (26.8 kcal/mol).

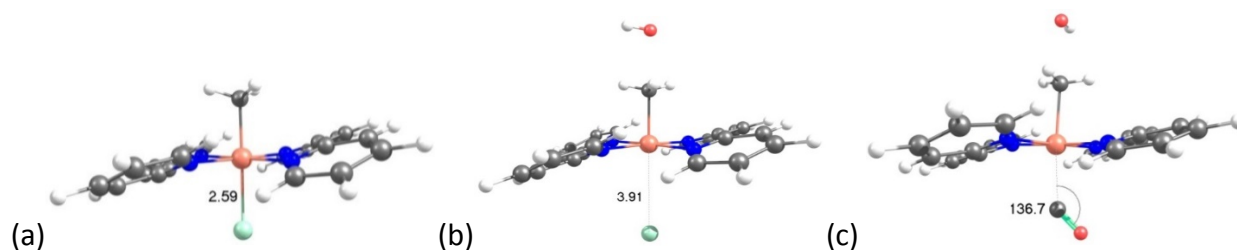
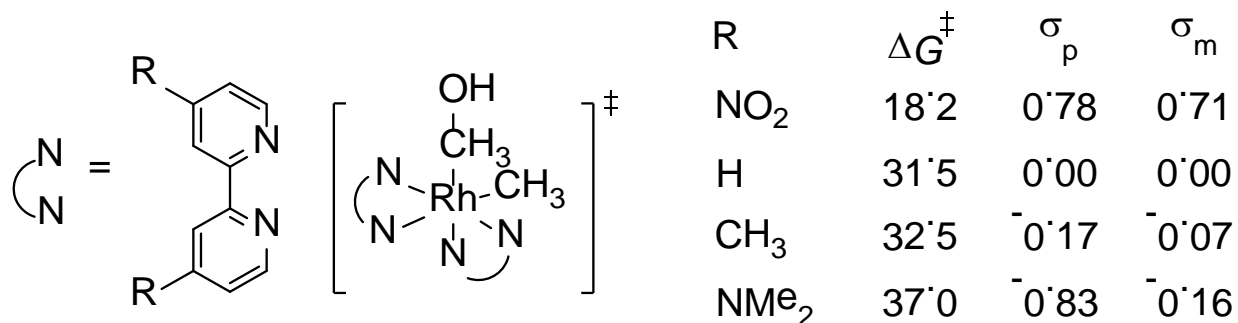


Figure 2.2 (a) Optimized ground state of *trans*-[(bpy)₂Rh(Me)(Cl)]⁺ with the Rh–Cl bond length (Å) shown. (b) Optimized transition state for nucleophilic attack of *trans*-[(bpy)₂Rh(Me)(Cl)]⁺ by HO⁻ with the elongated Rh–Cl bond length shown. (c) Optimized transition state for nucleophilic attack of *trans*-[(bpy)₂Rh(Me)(CO)]²⁺ by HO⁻ with the Rh–C–O bond angle shown. Rhodium = peach, nitrogen = blue, carbon = gray, oxygen = red.

The third factor that contributes to the activation barriers for hydroxide nucleophilic attack is the ability of the *trans* ligand to accept electron density. The effect can be seen most clearly when chloride is the ancillary ligand (Figure 2.2a) as the chloride ligand is nearly dissociated (calculated Mulliken charge on dissociated Cl = -0.9 *e*⁻) from the rhodium complex (Rh–Cl = 3.91 Å) in the transition state (Figure 2.2b). The carbonyl complex also shows this effect as the transition state reveals that the Rh–C–O bond angle is bent at an angle of 137° rather than linear (Figure 2.2c) (note that the computed Rh–C–O angle in the ground state of *trans*-[(bpy)₂Rh(Me)(CO)]²⁺ is linear). The bent Rh–C–O angle indicates transfer of electron density from the methyl ligand to the carbonyl ligand in the transition state and implies that the carbonyl ligand should be thought of more akin to a carbonyl radical anion than a carbonyl ligand. These calculations suggest that strong π-accepting ancillary ligands may be of interest in nucleophilic routes to C–O bond formation as they have both a strong *trans* influence and can accept electron density.



Scheme 2.6 Calculated free energy barriers (kcal/mol) to nucleophilic attack of complexes with varied bipyridine ligands.

2.2.3 Impact of Supporting Ligand Modification

To investigate the effects of modifying the electronic properties of the bipyridine ligand for the C–O bond formation reaction, *cis*-Rh(Me)X complexes containing bipyridine ligands substituted at the 4 and 4' positions with NO₂, NMe₂ and CH₃ were compared (Scheme 2.6). Figure 2.3 shows the Hammett correlations. The barrier to reaction was found to increase in the order Y = NO₂ < H < CH₃ < NMe₂. The complex containing the electron-withdrawing nitro-substituted bipyridine ligands has a significantly lower barrier than the parent (Y = H) system ($\Delta\Delta G^\ddagger = 13.3$ kcal/mol), while the complex containing the electron-donating dimethylamino-substituted bipyridine ligands has a 5.5 kcal/mol higher barrier than the parent system. Adding methyl substituents raises the barrier, but only slightly (by *ca.* 1 kcal/mol).

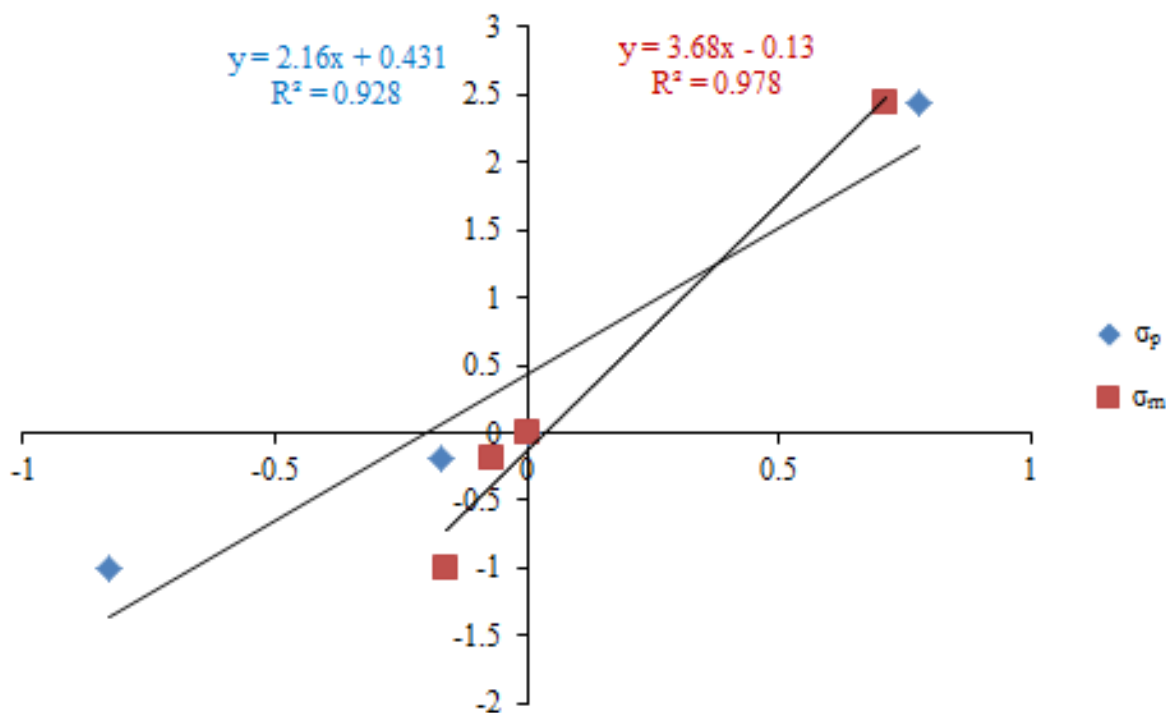
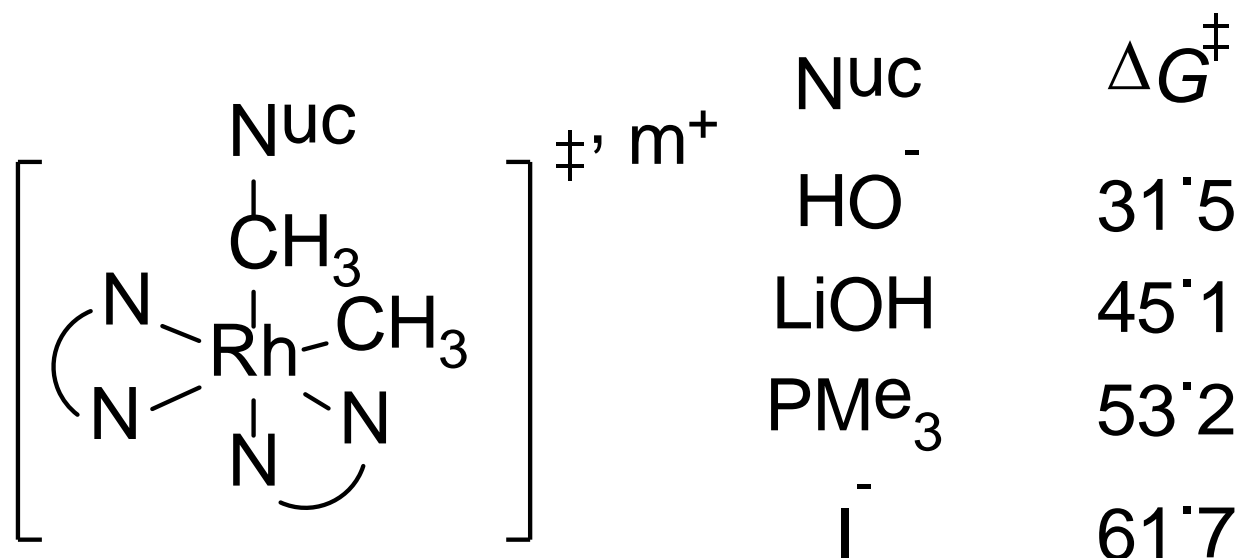


Figure 2.3 Plot of scaled calculated difference in free energy barrier ($\Delta\Delta G^\ddagger$) to nucleophilic attack by hydroxide on the Rh-CH₃ bond of *cis*-[(bpy)₂Rh(Me)X]⁺ complexes versus Hammett σ_p (blue diamonds) and σ_m (red squares) parameters with associated R² values. Values reported are scaled by ¼ to represent the effect of 1 substituent.

The σ_p Hammett values of NO₂ and NMe₂ substituents are of similar magnitude, but opposite in direction ($\sigma_p = 0.78$ and -0.83 ,⁶⁶ respectively). The difference in magnitude between the effect of the NO₂ substituent and the NMe₂ substituent implies that mainly considering the π -system will not explain the calculated trend. If only the inductive effects of the NO₂ and NMe₂ substituents are considered and the σ_m Hammett values ($\sigma_m = 0.71$ and -0.16 ,⁶⁶ , respectively) compared, then the Hammett values match the calculated data more closely (Figure 2.3), implying that inductive effects are more important than resonance effects for understanding the impact of modifying the electronic properties of the bipyridine ligand. The ρ value of 3.7 is approximately twice the ρ values ($\rho = 1.6$ to 1.9) obtained in the work of Yoh and coworkers for the effect of the leaving group.⁵⁹ Electron-withdrawing groups facilitating the reductive

nucleophilic reduction of the Rh–Me moiety is consistent with the reported reactions of electron-poor porphyrin complexes.^{49,50,51} Moreover, a less electron donating bipyridine ligand would lead to a more electrophilic metal center, which should be more reactive towards nucleophilic attack. This represents a promising experimental lead in the search for Rh(III) hydrocarbon functionalization catalysts based on C–X bond formation via a Shilov-type mechanism.

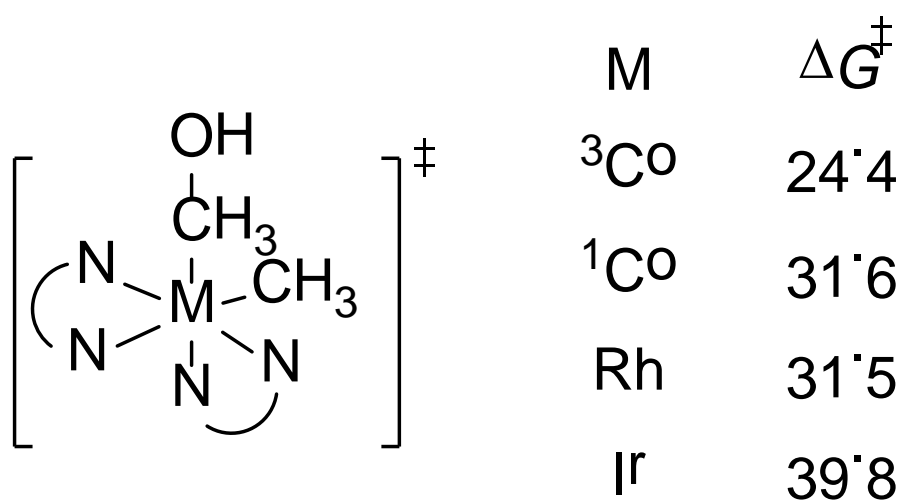


Scheme 2.7 Effect of nucleophile on the free energy barrier (kcal/mol) to nucleophilic attack on the Rh–CH₃ bond of *cis*-[(bpy)₂Rh(Me)₂]⁺.

2.2.4 Impact of Nucleophile

To determine the effect of the nucleophile on the reaction of interest, HO⁻, LiOH, PMe₃, and I⁻ were investigated as potential nucleophiles (Scheme 2.7).⁵¹ The barriers to nucleophilic attack on the Rh–CH₃ bond of *trans*-[(bpy)₂Rh(Me)₂]⁺ increased in the order HO⁻ < LiOH < PMe₃ < I⁻. The calculated activation barriers (see above) for modifications to the Rh complex range approximately 20 kcal/mol ($\Delta\Delta G^\ddagger = 18.8$ kcal/mol for bipyridine effects, and $\Delta\Delta G^\ddagger = 20.7$ kcal/mol

for trans ligand effects), while the calculated barrier range for changing the nucleophile is 30.2 kcal/mol ($\Delta\Delta G^\ddagger$). The effect of adding the Lewis acid Li^+ to the reaction with hydroxide increases the calculated activation barrier by 13.6 kcal/mol, which is approximately equivalent in impact to adding two very strongly electron withdrawing nitro groups to each bipyridine supporting ligand. Germane here is the use of a crown ether to facilitate nucleophilic addition to (porphyrin)Rh(III) alkyl ligands.⁵²



Scheme 2.8 Effect of the transition metal on the free energy barrier to nucleophilic attack by hydroxide on $\text{cis}-[(\text{bpy})_2\text{M}(\text{Me})_2]^+$ complexes. Values for cobalt are given relative the most stable (singlet) ground state.

2.2.5 Impact of Metal

To determine whether or not rhodium is the most effective metal for this transformation, complexes of the Group 9 congeners were investigated (Scheme 2.8). The barrier to nucleophilic attack of hydroxide onto the $\text{cis}-[(\text{bpy})_2\text{Co}(\text{Me})_2]^+$ complex on the singlet surface ($\Delta G^\ddagger_{\text{NA}} = 31.6$ kcal/mol) is identical (within anticipated error of the calculations) to the analogous rhodium complex ($\Delta G^\ddagger_{\text{NA}} = 31.5$ kcal/mol). The iridium complex, however, has a significantly higher barrier to reaction ($\Delta G^\ddagger_{\text{NA}} = 39.8$ kcal/mol). The reaction of $\text{cis}-[(\text{bpy})_2\text{Co}(\text{Me})_2]^+$ along the triplet surface

was also considered. Triplet *cis*-[(bpy)₂Co(Me)₂]⁺ is 7.5 kcal/mol less stable than the singlet *cis*-[(bpy)₂Co(Me)₂]⁺ complex; however, the barrier to nucleophilic attack from the triplet *cis*-[(bpy)₂Co(Me)₂]⁺ complex is only 16.8 kcal/mol, 14.8 kcal/mol less than the calculated barrier for the singlet surface. The combined barrier of changing the spin state followed by hydroxide nucleophilic attack is thus only 24.4 kcal/mol, the lowest barrier observed for the Group 9 complexes. Cobalt complexes are thus of interest for future study, particularly as it is a considerably less expensive and more Earth-abundant element than rhodium. Iridium complexes are expected to be much less reactive than Rh(III) and Co(III) methyl complexes. Of course, for development of catalytic cycles for alkane functionalization, barriers for C–H activation and possible M–Me bond homolysis must also be considered. Here, Co is likely to be disadvantaged because of the possibility of weak Co–R bonds, which could lead to facile bond homolysis and higher activation barriers for the C–H bond cleavage step. However, Chirik *et al.* have demonstrated that a series of cobalt pincer complexes of the form (LNL)CoR (L = P,N and R = Me, CH₂SiMe₃) are capable of accomplishing C–H activation of arenes and alkynes, plus activation of H₂.^{67,68} The arenes could then be further functionalized. Neither of these classes of substrates is amenable to the chemistry described here, but these reactions show that cobalt-methyl complexes may be competent catalysts.

2.2.6 Correlation of LUMO Energies and Reaction Barriers

Our calculations have indicated that modifications to [(bpy)₂Rh(Me)X]⁺ complexes that allow for better acceptance of the electron density lower the activation barrier for reductive nucleophilic addition to the methyl ligand. Hence, the computed LUMOs were analyzed to

investigate correlations with calculated activation barriers for the reductive functionalization of the Rh(III) methyl bonds.

The LUMOs of both the *cis*- and *trans*-Rh(III)-complexes are generally localized on the bipyridine rings (Figure 2.4) with a small component corresponding to a metal d orbital. In some cases there are contributions from the other ligands, such as the contribution from the methyl ligand in *trans*- $[(\text{bpy})_2\text{Rh}(\text{Me})_2]^+$, but this contribution is small and inconsistent for all the complexes modeled. Although the energies of unoccupied orbitals may be circumspect, comparison of similar complexes should minimize the uncertainties of the method and allow for a meaningful analysis.⁶⁹

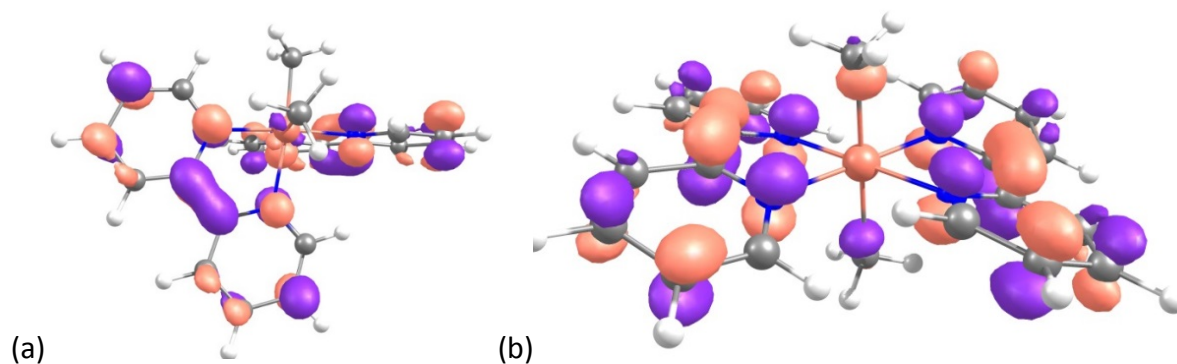


Figure 2.4 Plots of the LUMO orbitals for (a) *cis*- $[(\text{bpy})_2\text{Rh}(\text{Me})_2]^+$ (b) *trans*- $[(\text{bpy})_2\text{Rh}(\text{Me})_2]^+$. Orbitals shown at an Isovalue of 0.045.

Although a comparison of the free energy barriers and the LUMOs for all complexes studied did not show a linear correlation, analysis of subsets of similar complexes did show good correlations between the LUMO energy and the calculated free energy barrier to nucleophilic attack. The first subset of complexes studied are 4,4'-substituted bipyridine ligands (Figure 2.5). These complexes show a very strong linear correlation between the LUMO of the reactant complex and the calculated free energy barriers to nucleophilic attack ($R^2 = 1.00$) with complexes

with more stabilized LUMOs having lower activation barriers.

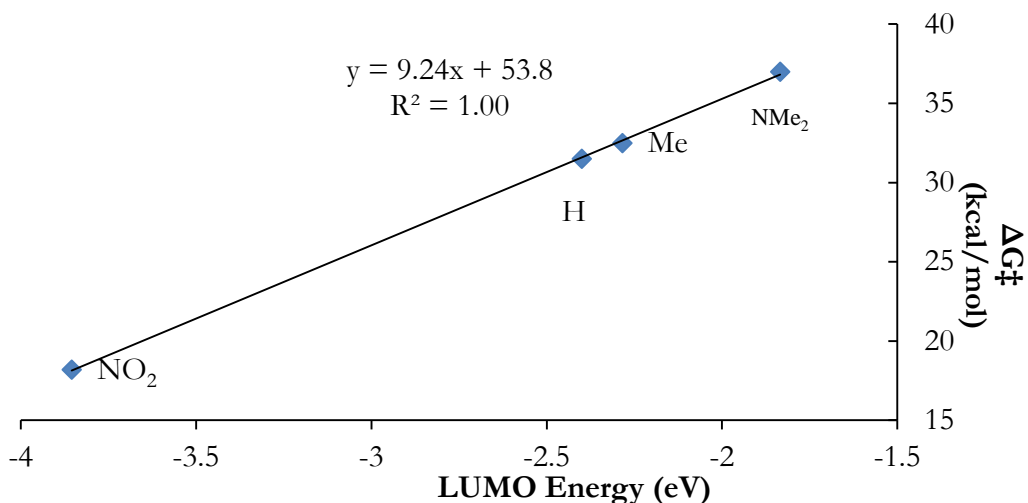


Figure 2.5 Plot of calculated LUMO energies of Rh(III) complexes (eV) versus ΔG_{NA}^\ddagger (kcal/mol) for attack of hydroxide on the Rh–Me bond of *cis*-[(Y-bpy)₂Rh(Me)₂]⁺ complexes. Scheme 2.6 contains the 4,4'-bpy substituents (Y) that were modeled.

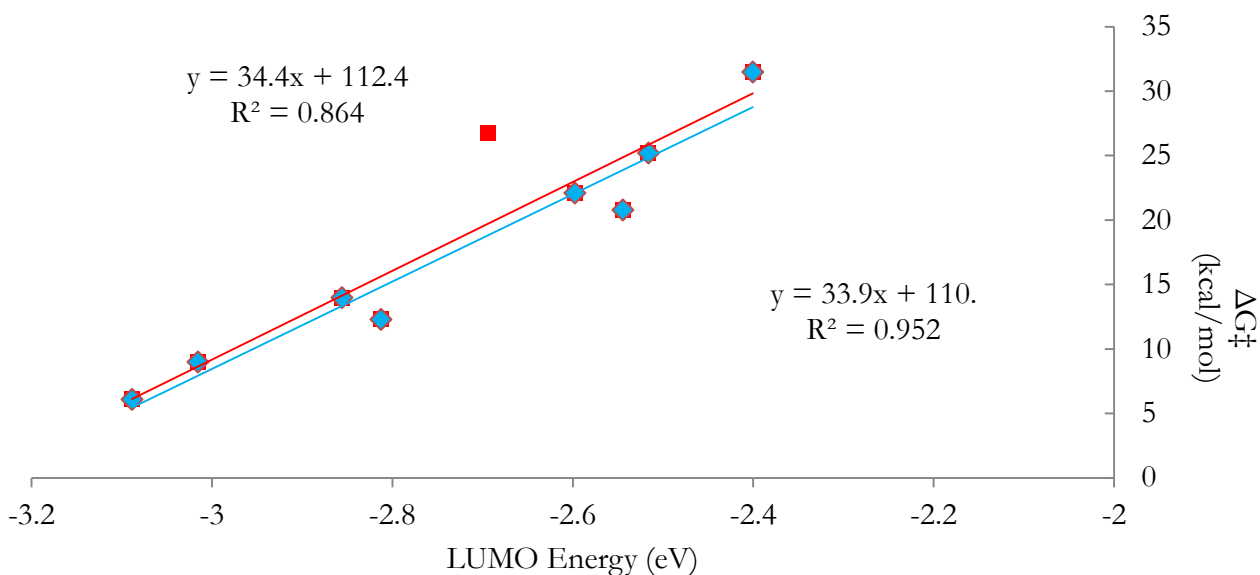


Figure 2.6 Plot of calculated LUMO energies of Rh(III) complexes versus ΔG_{NA}^\ddagger for hydroxide attack on [(bpy)₂Rh(Me)X]ⁿ⁺ (X = HO⁻, H⁻, H₃C⁻, Cl⁻, CO or Py₂) complexes. The red best fit line includes the *trans*-[(bpy)₂Rh(Me)(OH)]⁺ complex (red square) and the blue best fit line excludes this point.

The second set of complexes that shows a linear correlation between the LUMO orbital energy of the reactant complex and the free energy barrier for hydroxide attack on the Rh–CH₃ bond is *cis*- and *trans*-[(bpy)₂Rh(Me)X]ⁿ⁺ (X = HO⁻, H⁻, H₃C⁻, Cl⁻, CO, and Py₂) complexes (Figure 2.6). For this set of complexes we have highlighted the point corresponding to *trans*-[(bpy)₂Rh(Me)(OH)]⁺ (red square). Inclusion of this complex (red line, R² = 0.86) reduces the correlation (blue line, R² = 0.95). It is currently unclear why this complex behaves differently than the rest of the closely related complexes. For example, the LUMO of *trans*-[(bpy)₂Rh(Me)(OH)]⁺ is similar to the *cis* complexes, in that it is a bipyridine-based π* orbital. Nonetheless, the correlations in Figures 2.5 and 2.6 show that within closely related systems comparisons of the LUMOs can give an indication of which complexes are predicted to react faster.

While it is tempting to directly compare the slopes of the two graphs (Figures 2.5 and 2.6) for the two classes of complexes, such a comparison may give false conclusions. The LUMOs of all bpy-ligated Rh(III) complexes studied here are bipyridine based π* orbitals. Adding substituents, especially π-donating or withdrawing substituents, directly to the bipyridine ring would thus be expected to affect the energy of the LUMO orbital more than changing the substituents on the metal center to which the bipyridine is bound. This effect can be observed by comparing the range of LUMO energies for the substituted bipyridine set of complexes (-3.85 to -1.83 eV) and the narrower range of LUMO energies for the second set (-3.09 to -2.40 eV) (see Figures 2.5 and 2.6). The range of LUMO energies for the first subset of Rh(III) complexes is nearly three times larger than that of the second subset. When the calculated free energies of activation are compared (18.2 to 37.0 kcal/mol and 6.1 to 31.5 kcal/mol for the first and second sets, respectively), the range of free energies of activation is more similar. Therefore, the difference

in slopes for the linear correlations is due more to the change in the energy level of the bipyridine π^* orbitals (LUMO) than the ease of nucleophilic attack ($\Delta G^\ddagger_{\text{NA}}$). Since the LUMOs in these complexes are ligand-based orbitals and hence indirectly impacted by the metal's electrophilicity, analysis of ground state LUMO energies of Group 9 alkyl complexes within related subsets of complexes can give a useful measure of expected reactivity. However, trying to use the LUMO energies to compare more chemically disparate complex sets than these (see SI) gives no useful information, as the LUMOs are no longer directly comparable in their orbital composition.

2.3 Summary and Conclusions

The present DFT studies detailing the factors that control nucleophilic attack on the methyl ligand of bipyridine-ligated Rh(III) complexes have allowed an understanding of why these complexes are resistant to nucleophilic attack and have illuminated strategies to overcome high barriers to reaction. As a result, promising routes forward for C–X functionalization may be suggested. These are summarized below.

1) The Rh(III) complexes show a strong dependence of the calculated barrier to C–X formation on the strength of the nucleophile. For example, the addition of a Lewis acid such as Li^+ to hydroxide increases the activation barrier to nucleophilic addition by over 13 kcal/mol. Use of crown ethers or cations that do not form tight ion pairs with hydroxide thus seems a viable strategy to ensure the lowest barriers to C–X bond formation,⁵² but such a tactic is likely to be viable for only stoichiometric reactions and not for catalytic processes. For catalytic reactions performed in acidic media, the nucleophile will in most cases be limited to the conjugate base.

2) Modifications to the coordination sphere that reduce electron density, whether through more electron poor ligands (*e.g.*, $\text{bpy} \rightarrow 4,4'\text{-NO}_2\text{-bpy}$) or ligands that easily dissociate

as a stable anion (*e.g.*, Cl⁻), reduce the activation barriers to nucleophilic functionalization. All of the modifications that result in a lower activation barrier stabilize the metallo-leaving groups, which in the present case are d⁸ complexes.

3) Within closely related sets of compounds, the relative reactivity can be determined by analyzing the LUMO energies of the reacting Group 9 complex. Although porphyrin and bis-bipyridine complexes are too disparate to allow a direct comparison of the reactivity of the complexes by a LUMO comparison, the insight gained from the other studies may allow an understanding of why the porphyrin complexes appear to be more reactive. Groves has shown that reactions of porphyrins occur at room temperature.^{52,55} Most of the reactions described herein would not be expected to react at room temperature given the calculated free energies of activation. Since in both of these cases the metal center (Rh) and nucleophile (OH⁻) are the same, the difference must lie in the stability of the resulting metal complexes. In all rhodium systems studied here, the metallo-leaving group is a d⁸ Rh(I) complex and would be expected to prefer a square planar or square pyramidal geometry depending on the supporting ligands. For example, the *cis*-[(bpy)₂Rh(Me)X]⁺ complexes need to rearrange after nucleophilic attack on the methyl group to a configuration with the bpy ligands in a single square plane in order to minimize trans influence interactions. However, the *trans*-[(bpy)₂Rh(Me)X]⁺ complexes exhibit unfavorable 6,6'-C-H interactions, and their kinetic superiority to *cis* isomers cannot overcome their ground state inferiority (*i.e.*, $\Delta\Delta G > \Delta\Delta G^\ddagger$). Porphyrin ligands enforce a square planar geometry, a perpendicular d_z^2 orbital for Rh(I) species, without any steric hindrance, and therefore, are “preorganized” to be good d⁸-metallo-leaving groups.

4) As for the capability of the metallo-leaving group to accept electron density, the pKa's of the hydrogen ligand in Rh(III) hydride complexes supported by tetraphenylporphyrin and perfluorinated-tetraphenylporphyrin ligands are both known (11.0 and 2.1 in DMSO, respectively).⁵¹ Hence, anionic Rh(I) porphyrin complexes are reasonably accessible. Structures of the four-coordinate Rh(I) complexes *trans-bis*-bipyridine Rh(I) perchlorate (*trans*-[(bpy)₂Rh(H₂O)(Cl)][OH][ClO₄]) and *cis*-bis(1,10-phenanthroline-5,6-dione)Rh(I) are known, but the majority of square planar Rh(I) complexes containing bidentate pyridine-type ligands contain π -withdrawing ligands such as isonitriles,⁷⁰ olefins,⁷¹ or carbonyl⁷² ligands to stabilize the Rh(I) product. Thus, porphyrin ligands seem to stabilize square planar Rh(I) complexes better than the *bis*-bipyridine framework. The present calculations indicate that the Rh-porphyrin systems are both preorganized and better able to accept electron density than *bis*-bipyridine rhodium complexes, and thus the former likely have a greater predilection toward reaction with nucleophiles despite the fact that the porphyrin ligand is a dianion. In order to find a non-porphyrin system that can take advantage of the higher electrophilicity of cationic systems, then at least one, if not both, of the challenges that hinder the reaction of bis-bipyridine Rh(III) complexes, preorganization and poor ability to accept electron density, needs to be solved.

5) Cobalt complexes may be of interest for future studies on reductive functionalization of metal-alkyl ligands. Replacing rhodium, a very expensive metal, with a less expensive metal such as cobalt would be beneficial for a commercial process. The calculations predict that analogous complexes of both metals will react through similar barriers on the singlet surface. However, cobalt complexes also exhibit a propensity to access high spin states and react on the triplet surface, in which case the barrier to reductive functionalization was found to be much

lower at only 16.8 kcal/mol. For the bis-bipyridine Co complex, the singlet spin state is 7.5 kcal/mol more stable than the triplet spin state. Designing complexes that stabilize a triplet ground state and are capable of accepting the electron pair may open up new reductive functionalization pathways. Challenges with C–H activation and possible Co–alkyl bond homolysis could present problems. In contrast, the use of Ir complexes, which may have an advantage for C–H activation, is predicted to result in higher activation barriers for reductive functionalization of Ir-hydrocarbyl units. Thus, incorporation of Ir catalysts might require another mechanism for hydrocarbyl functionalization *or* access to oxidation states higher than Ir(III).

2.4 Computational Details

Density functional theory (DFT) was used to calculate the barriers to nucleophilic attack by a variety of group 9 metal-methyl complexes. The Gaussian 09⁷³ software package was used to optimize the geometries of the complexes and calculate frequencies. Ground and transition states were confirmed by calculating the energy Hessian and identifying either 0 or 1 imaginary frequency respectively. Optimization and frequency calculations were performed with the implicit solvation of DMSO ($\epsilon = 46.826$) by CPCM^{74,75} as implemented by Gaussian 09. The complexes were modeled by the B3LYP^{76,77} exchange-correlation functional with the CEP-31G(d)^{78,79} basis set. Free energies are reported at STP in kcal/mol and LUMO energies are reported in eV. Spin states other than singlets were considered only for the cobalt complexes.

2.5 Acknowledgements

This work was solely supported as part of the Center for Catalytic Hydrocarbon Functionalization, an Energy Frontier Research Center funded by the U.S. Department of Energy,

Office of Science, Office of Basic Energy Sciences, under Award No. DE-SC0001298. The authors would like to acknowledge Drs. Erika Milzcek and Joanna Webb for helpful discussions.

CHAPTER 3

REDUCTIVE FUNCTIONALIZATION OF A RHODIUM(III)-METHYL BOND BY ELECTRONIC MODIFICATION OF THE SUPPORTING LIGANDⁱⁱ

3.1 Introduction

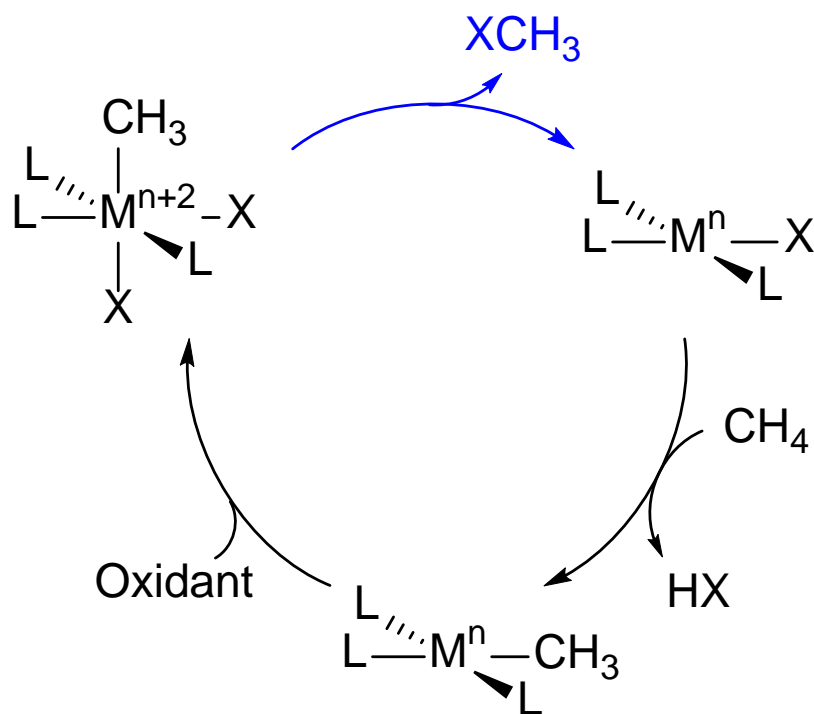
The partial oxidation of hydrocarbons into alcohols is of considerable economical interest for the production of transportation fuels and commercial chemicals.^{80,81,82,83} The development of catalytic systems that can mediate an overall insertion of an oxygen-atom into a C–H bond without over-oxidation remains a substantial challenge.^{14,83,84,85,86,87,88,89} Among the catalytic systems that mediate hydrocarbon functionalization,²² Shilov's Pt-based system (Scheme 3.1) exerts good selectivity against over-oxidation but uses costly Pt^{IV} as the oxidant.⁹⁰ Substantial advances were made by Periana and coworkers by replacing the Pt^{IV} oxidant with H₂SO₄, but a slow turnover frequency (10⁻³ s⁻¹) and low turnover numbers caused by product inhibition and dilution with water impedes commercial application.¹³ Thus, considerable research has been directed at new catalytic systems to functionalize hydrocarbons with improved efficiency.²² One possible approach to improve Shilov-type chemistry is to use Rh complexes, which in general should be less electrophilic than analogous Pt complexes.

The Rh^I/Rh^{III} redox couple offers three attractive properties compared to Pt-based systems. The less electrophilic metal should form weaker coordination bonds to water and functionalized product, potentially delaying the onset of product inhibition. The easily accessible

ⁱⁱ This chapter is adapted from **Reductive Functionalization of a Rhodium(III)-methyl Bond by Electronic Modification of the Supporting Ligand**, Matthew E. O'Reilly, Dale R. Pahls, Joanna, R. Webb, Nichols C. Boaz, Subhojit Maumdar, Carl D. Hoff, John T Groves, Thomas R. Cundari, T. Brent Gunnoe., *Dalton Trans.*, 2014, **43**, 8273-8281. DOI: 10.1039/C4DT00234B - Reproduced by permission of The Royal Society of Chemistry.

RhI/RhIII redox cycle^{91,92} could allow for milder and possibly air-recyclable oxidants to be used. The formation of Rh(s) is less thermodynamically favorable than for Pt(s).^{92,93} However, developing a Rh-based catalyst presents some challenges.^{94,95}

Reductive Functionalization



Scheme 3.1 The electrophilic catalytic cycle for the partial oxidation/ functionalization of methane using late transition metals.

A key step in the functionalization of hydrocarbons by Shilov-based Pt catalysts is the reductive elimination (RE) of MeX ($X = \text{halide or pseudo-halide: } Cl^-, CF_3CO_2^-, HSO_4^-, HO^-, \text{ etc.}$) from a $X\text{-Pt(IV)-}CH_3$ intermediate (Scheme 3.1).^{96,97} In fact, RE of alkyl, acyl, and aryl halides is a relatively rare transformation compared to the reverse process, oxidative addition.^{98,99,100,101} The majority of examples feature high-valent late transition metal complexes: Pt^{IV} ,^{102,103,104,105,106,107,108} Pd^{IV} ,^{109,110,111,112,113,114} Pd^{III} ,^{115,116} Au^{III} ,^{117,118} and Ni^{III} .¹¹⁹ RE from earlier and/or low oxidation state metals is more thermodynamically challenging.

Nevertheless, Hartwig^{120,121,122} and others^{123,124,125} showed that RE of R-X from Pd^{II} can be achieved by employing sterically bulky phosphine ligands, and the Rh-based Monsanto acetic acid process has been shown to reversibly add C(sp³)-I¹²⁶ while ultimately eliminating C(sp²)-I from a Rh^{III} center prior to acetic acid formation.¹²⁷

While the reductive functionalization from Rh^{III}-R bonds with strong phosphorus,^{51,56} oxygen,^{52,53,55} and nitrogen nucleophiles⁵² has been reported, the RE of alkyl halides can be challenging. Milstein and coworkers recently reported the RE of an alkyl halide from a Rh^{III} complex using a combination of sterically bulky PCP and PNP pincer ligands to destabilize the Rh^{III}-CH₃ moiety. For these reactions, the addition of π -acidic ligands (CO, CNR, MeCN) was used to trap the RhI complex.^{57,128} Steimann and coworkers reported an in-situ Rh^{III}-CH₃ complex formed by decarbonylation, which also provides a π -acidic CO ligand to drive RE.¹²⁹

In designing a Rh^I/Rh^{III} system capable of hydrocarbon functionalization, the question remains whether RE of an alkyl halide or pseudo-halide is thermodynamically feasible without significant steric destabilization. The use of large steric groups may raise the barrier for C-H activation. Hence, the thermodynamic potential for reductive functionalization should ideally be controlled by electronic modifications to the supporting ligand(s).

The terpyridine ligand provides a reasonable ligand platform to investigate the reductive functionalization from a Rh^{III}-CH₃ since the electronic properties of the terpyridine are easily modulated without appreciably impacting steric factors by appending electron-donating and withdrawing groups to the 4, 4' and 4'' positions. The merit of using a tridentate ligand is an increased coordination stability while minimizing the electronic donation to the Rh^{III} metal center. Herein, we show that incorporating electron-withdrawing nitro groups on a terpyridine

ligand sufficiently reduces the electronic stabilization of a $\text{Rh}^{\text{III}}\text{-CH}_3$ complex to permit reductive functionalization of MeX $\{\text{X} = \text{Cl}^- \text{ or } \text{CF}_3\text{CO}_2^- \text{ (TFA}^-)\}$, which, to our knowledge, marks the first RE of an alkyl halide from a $\text{Rh}^{\text{III}}\text{-CH}_3$ without steric destabilization or the use of a trapping agent.

3.2 Results and Discussion

To investigate the electronic requirements for reductive functionalization, experimental collaborators at the University of Virginia and Princeton (Matthew O'Reilly, Nicholas Boaz, Jay Groves, T. Brent Gunnoe), sought to synthesize $\text{Rh}^{\text{III}}\text{-CH}_3$ complexes featuring 4,4',4''-tri-tert-butylterpyridine [tBu_3terpy] and 4,4',4''-trinitroterpyridine [$(\text{NO}_2)_3\text{terpy}$] ligands. Incorporating tert-butyl groups on the terpyridine ligand enhances the solubility, while the three appended nitro groups are, on the basis of the simulations presented in the previous chapter,¹³⁰ the best suited terpyridine ligand for reductive functionalization. They were able to synthesize both complexes and showed that the tBu_3terpy and $(\text{NO}_2)_3\text{terpy}$ complexes could undergo oxidative addition (OA) of MeI . The $(\text{NO}_2)_3\text{terpy}$ complex could also undergo reductive elimination (RE) with OA or RE being favored depending on the conditions. Heating a solution of $(\text{NO}_2)_3\text{terpy}$ RhCl with excess MeI at 70 °C in THF results in $[(\text{NO}_2)_3\text{terpy}]\text{Rh}(\text{Me})(\text{Cl})\text{I}$ while heating $[(\text{NO}_2)_3\text{terpy}]\text{Rh}(\text{Me})(\text{Cl})\text{I}$ in nitromethane to 90 °C releases halomethanes and Rh^{I} complexes. These results suggested the $\text{Rh}^{\text{I}}/\text{Rh}^{\text{III}}$ equilibrium was near thermoneutral, however, the poor solubility of the trinitroterpyridine complexes prevented a full kinetic and thermodynamic investigation.

Therefore, DFT calculations were employed to investigate the thermodynamics and mechanism of RE from $[(\text{NO}_2)_3\text{terpy}]\text{Rh}(\text{Me})(\text{Cl})\text{I}$. To best model experimental systems, structures were optimized and free energies computed in the appropriate experimental solvent using the

CPCM model: THF for thermodynamics and nitromethane for mechanistic studies of reductive elimination (vide infra). Figure 3.1 depicts the lowest energy DFT-optimized structures for complexes 1'-6'. For simplicity, the appended ^tBu groups were removed from ^tBu₃terpy since test simulations indicate that this modification impacts absolute reaction free energies by ~0.2 kcal/mol, and relative ΔG's are expected to vary by even less.

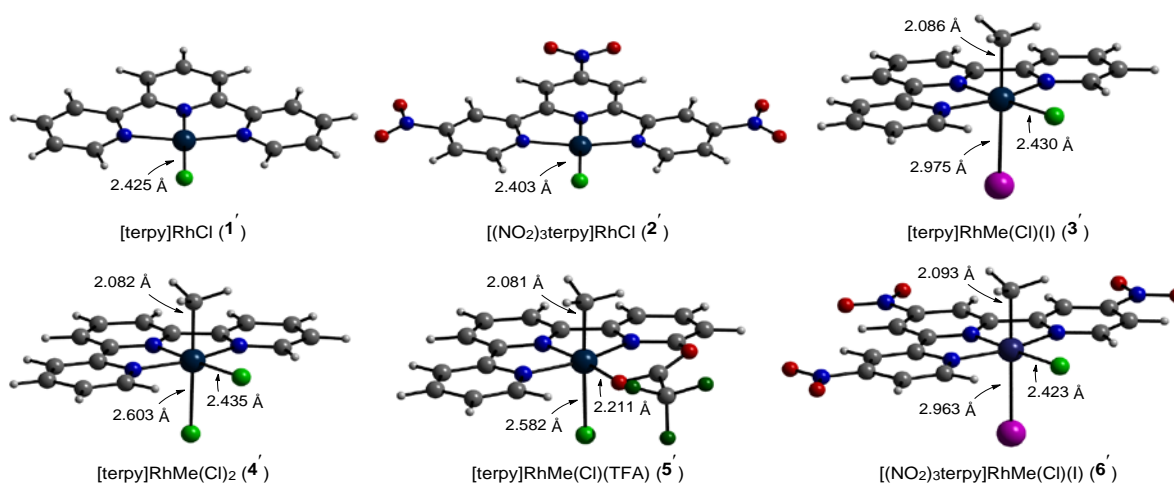


Figure 3.1 DFT-optimized structures of 1'-6' in THF. Rhodium = navy blue, carbon = gray; hydrogen = white; chlorine = lime green; iodine = purple; nitrogen = blue; oxygen = red; fluorine = forest green.

The optimized structures were calculated with the Rh-CH₃ bond in the axial position relative to the meridional terpyridine ligand, which is consistent with the crystallographic structures of analogous diiminepyridine Rh^{III}-CH₃ complexes.¹³¹ In the mixed halide or pseudo-halide complexes 3', 5', and 6', there are two possible coordination isomers (assuming the methyl ligand remains in the axial position). Placing the more weakly coordinating iodide trans to the Rh-CH₃ bond lowers the energy by ~2.5 kcal/mol for 3' and 6'; however the two coordination isomers of 5' are nearly thermoneutral (ΔG = 0.3 kcal/mol). The geometry of optimized structures

show moderate changes in the trinitroterpyridine ligand, while the Rh–CH₃ bonds are relatively unchanged.

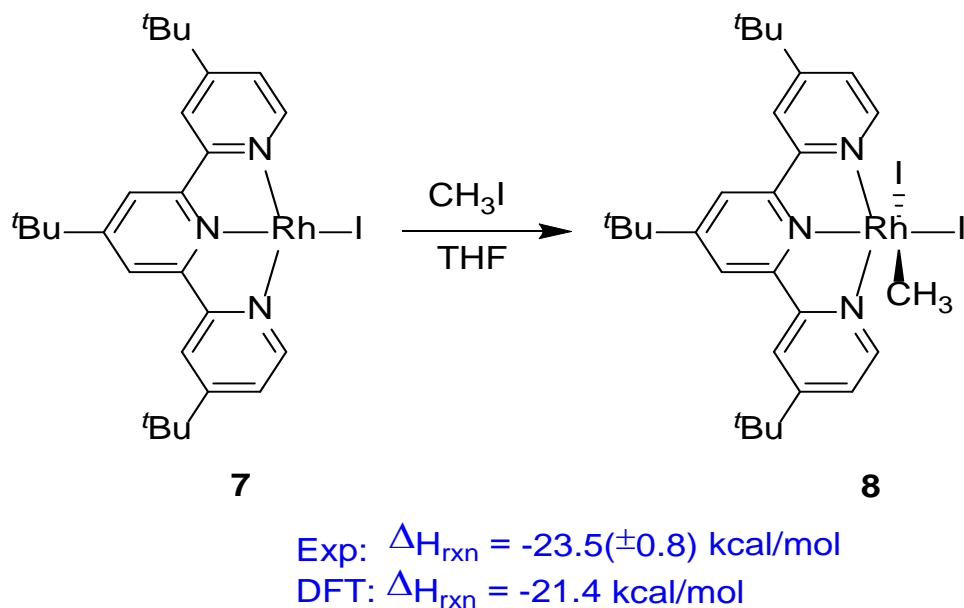
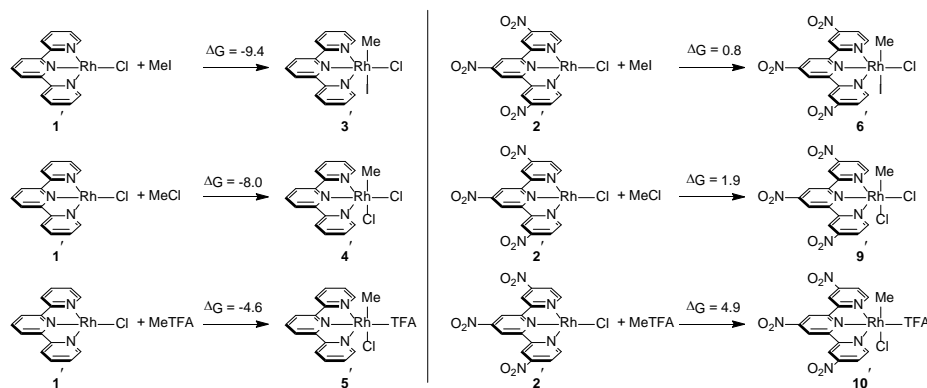


Figure 3.2 Experimental and computed thermodynamics of oxidative addition of MeI to tBu₃terpyRhI

Solution calorimetric experiments performed by collaborators at the University of Miami (Carl Hoff, Subhojit Majumdar) were used to calibrate the computational methods. However, oxidative addition of MeX (X = Cl⁻, and TFA⁻) to complex 1 yields considerable amounts of halide-exchange products or uses MeCl(g), which complicates solution calorimetry experiments. To eliminate these problems, collaborators synthesized [tBu₃terpy]RhI by stirring a THF solution of [tBu₃terpy]RhCl with excess NaI for 12 h. Treating complex [tBu₃terpy]RhI with MeI cleanly affords [tBu₃terpy]RhMeI₂. Solution calorimetry experiments for the oxidative addition reaction were performed in triplicate and yielded an averaged ΔH_{rxn} of -23.5 (±0.8) kcal/mol. The corresponding reaction was modeled by DFT using [tBu₃terpy]RhI (7') and [tBu₃terpy]RhMe(I)₂ (8'). The full ligand was modeled for the calibration to minimize approximations. These parameters yielded a

computed $\Delta H_{\text{rxn}} = -21.4$ kcal/mol, which is within 2 kcal/mol of the experimental value (Figure 3.2). The agreement between the experimental and theoretical thermochemistry supports the reliability of the employed computational methods.



Scheme 3.2 DFT calculated thermodynamics for the reaction of 1' and 2' with MeX. All free energies (kcal/mol) are listed as $\text{L}_n\text{Rh}^{\text{I}} + \text{MeX} \rightarrow \text{L}_n\text{Rh}^{\text{III}}$. Numerical values are calculated thermodynamics in continuum THF solvent.

Next, the thermodynamics of oxidative addition of MeX ($X = \text{I}^-$, Cl^- , TFA^-) to 1' and 2' were investigated computationally, and the results are presented in Scheme 3.2. The formation of 3', 4', and 5' from 1' was found to be exothermic by -9.4, -8.0, and -4.6 kcal/mol, respectively, while oxidative additions of MeCl and MeTFA by 2' are uphill (1.9 and 4.9 kcal/mol). The calculations agree with the observed reactivity of complexes 1 and 2. Perhaps more importantly, DFT calculations show a consistent ~ 10 kcal/mol difference for the oxidative addition reactions between complexes 1' and 2', illustrating the substantial influence of the NO₂ groups on the free energy potentials. A surprising result is that the calculated free energy for the oxidative addition of MeI by 2' to give 6' is 0.8 kcal/mol uphill. The mild free energy difference corresponding to a $K_{\text{eq}} = 0.16$ $\{K_{\text{eq}} = [6']/([2'][\text{MeI}])\}$ suggests a near thermoneutral reaction. Experimental evidence seems to support this assertion, though the reaction conditions are complicated due to solubility, side-reactions, and temperature. Nevertheless, the 10-fold excess of MeI in THF at 70 °C may

drive the reaction towards the formation of $[(\text{NO}_2)_3\text{terpy}]\text{Rh}(\text{Me})(\text{Cl})\text{I}$, while in the absence of MeI, $[(\text{NO}_2)_3\text{terpy}]\text{Rh}(\text{Me})(\text{Cl})\text{I}$ was shown to reductively eliminate a small percentage of MeI along with MeCl in CD_3NO_2 at 90 °C.

The mechanism of RE, the microscopic reverse of oxidative addition, has been proposed to occur by either concerted RE, $\text{S}_{\text{N}}2$, or radical pathways.¹²⁷ Often more than one mechanism may be operable depending on the nature of X^- .^{57,83} More electron donating X^- favor concerted RE mechanism over an $\text{S}_{\text{N}}2$ pathway. For instance, Milstein and coworkers propose a concerted RE of MeCl(g) while an $\text{S}_{\text{N}}2$ RE pathway was operative for MeBr and MeI.

In our case, we sought to investigate the mechanism of reductive functionalization of MeCl from complex 6' with free Cl^- present in solution for two reasons. First, the RE of MeCl from $[(\text{NO}_2)_3\text{terpy}]\text{Rh}(\text{Me})(\text{Cl})\text{I}$ with three equivalents of $[\text{Bu}_4\text{N}]\text{Cl}$ exclusively yields MeCl, and secondly, NMR data indicate that the coordinated iodide is substituted with chloride upon adding $[\text{Bu}_4\text{N}]\text{Cl}$, providing $[(\text{NO}_2)_3\text{terpy}]\text{RhMe}(\text{Cl})_2$ (9') as a reasonable starting position. We calculated three pathways (Figure 3.3), and for each pathway we modeled six-coordinate and five-coordinate Rh (formed by dissociation of Cl^- from 9') transition states. Here, we present results supporting an $\text{S}_{\text{N}}2$ RE mechanism through a five-coordinate $[(\text{NO}_2)_3\text{terpy}]\text{RhMe}(\text{Cl})^+$ (11') intermediate.

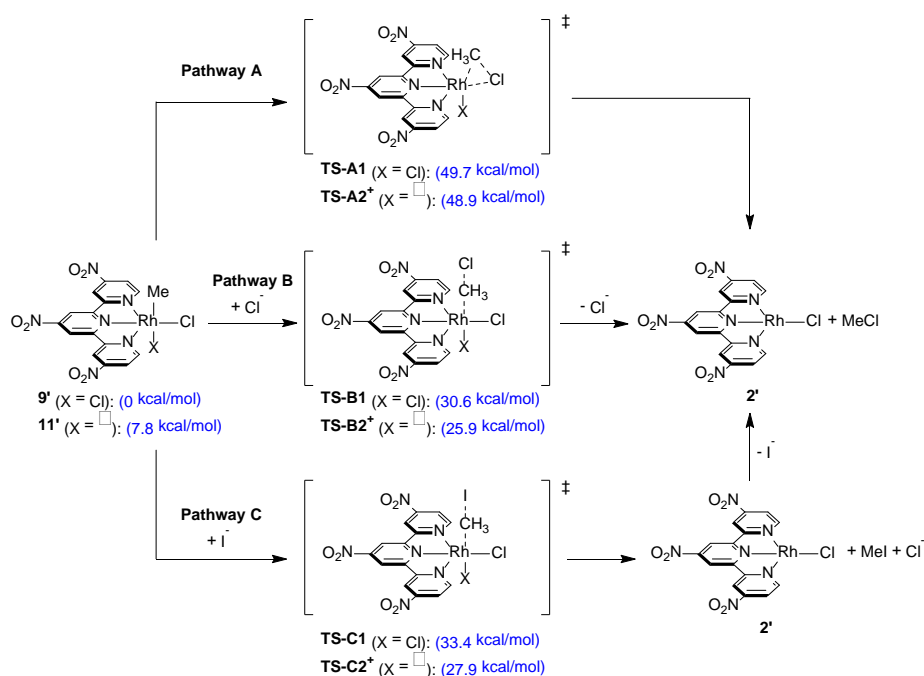


Figure 3.3 Three pathways for reductive functionalization from 9'. Pathway A: Concerted RE, Pathway B: Cl⁻ initiated S_N2 RE, and Pathway C: I⁻ initiated S_N2 RE. Numerical values are calculated free energies (kcal/mol) in continuum CH₃NO₂ solvent relative to 9'. TS-1 involves six-coordinate Rh transition states, TS-2 involves five-coordinate Rh transition states (square denotes a vacant coordination site).

To keep the calculations consistent with the experimental work, we employed the same level of theory used in our previous calibration study, but changed the continuum solvent to CH₃NO₂. In this solvent, the RE of MeCl from 9' is calculated to be modestly favorable (-0.3 kcal/mol). Figure 3.3 depicts three different plausible mechanisms for RE labeled as Pathways A, B, and C. We excluded a radical mechanism since CH₃NO₂ is a known radical trap.^{132,133,134} To simplify matters, complete separation of ions was assumed, so no tetrabutyl ammonium cations were modeled as spectator cations. All isolated anions were modeled in continuum CH₃NO₂ solvent to balance equations.

Pathway A features a concerted RE of MeCl. The calculated free energy barrier from 9' (TS-A1) is 49.7 kcal/mol. One approach to mitigate the high transition state barrier is to remove

trans-Cl⁻ (forming 11') prior to the reductive functionalization step. Previous RE studies reveal that odd-coordinate complexes yield overall lower energy pathways for RE.^{96,97,103,104,107,128,135} The initial loss of chloride ion from 9' yielding 11' is mildly endergonic (7.8 kcal/mol), but lowers the overall TS barrier by 0.8 kcal/mol (TS-A2+, 48.9 kcal/mol). Regardless, both transition states are exceptionally high for a reaction that proceeds at 90 °C.

Pathways B and C (Figure 3.3) involve a nucleophilic attack upon the Rh—Me bond by free Cl⁻ or I⁻, respectively. This mechanism – an S_N2 mechanism – parallels organic substitution reactions. A nucleophilic attack by the chloride (Pathway B) directly on 9' (TS-B1) gives a barrier of 30.6 kcal/mol. By removing the trans-chloride ligand prior to reductive functionalization, the transition state barrier (TS-B2+) is lowered by 4.7 kcal/mol, yielding the lowest computed free energy barrier of 25.9 kcal/mol (relative to 9'). This energetic barrier appears reasonable in relation to the required reaction conditions. The other possible pathway for reductive functionalization (Pathway C) is a nucleophilic attack by I⁻, which is also present in solution. Iodide serves an intermediary role by forming MeI, which would then react with free Cl⁻ to generate MeCl. The calculated transition state barrier for iodide attack on complexes 9' and 11' yielded slightly higher free energies, 33.4 and 27.9 kcal/mol, respectively, than for Pathway B (Figure 3.3).

The DFT calculations provide three insights into the mechanism of reductive functionalization from 9'. (1) An S_N2 pathway is heavily favored over a concerted RE mechanism. (2) Dissociating the trans-halide to form cationic complex 11' prior to reductive functionalization lowers the transition state barrier to nucleophilic attack by ~5 kcal/mol. (3) While Pathway B yields the lowest transition state barrier, it is possible that Pathway C is also operable since the

calculations reveal only a slight 2 kcal/mol difference for chloride (TS-B2+) versus iodide (TS-C2+) attack on 11'.

3.3 Conclusions

Oxidative addition of MeI by $[(\text{NO}_2)_3\text{terpy}]\text{RhCl}$ provides access to a trinitroterpyridine ligated $\text{Rh}^{\text{III}}\text{-CH}_3$ complex $[(\text{NO}_2)_3\text{terpy}]\text{Rh}(\text{Me})(\text{Cl})\text{I}$ in order to investigate reductive functionalization. Heating complex $[(\text{NO}_2)_3\text{terpy}]\text{Rh}(\text{Me})(\text{Cl})\text{I}$ in CD_3NO_2 reductively eliminates MeCl along with MeI. Upon addition of free Cl^- and TFA^- complex $[(\text{NO}_2)_3\text{terpy}]\text{Rh}(\text{Me})(\text{Cl})\text{I}$ undergoes reductive functionalization to produce MeCl and MeTFA, respectively. DFT calculations support an $\text{S}_{\text{N}}2$ reductive functionalization pathway through a five-coordinate intermediate $[(\text{NO}_2)_3\text{terpy}]\text{RhMe}(\text{Cl})^+$ (11'). The slight energetic difference between transition state for Cl^- and I^- attack on 11' suggests that both routes are competitive.

Net reductive elimination of RX is a key step in overall catalytic cycles for hydrocarbon functionalization. Thus, a primary limitation to use of Rh complexes as catalysts for hydrocarbon functionalization through the "Shilov" route (Scheme 3.1) is the energetic inhibition (both kinetic and thermodynamic) of RX elimination. For the first time, we are able to establish that the RE of an alkyl halide (MeCl) and pseudo-halide (MeTFA) from a Rh^{III} complex can be achieved without using sterically bulky ligands or a trapping agent to stabilize the $\text{Rh}(\text{I})$ product. These results are promising for Rh-based electrophilic catalysts for hydrocarbon functionalization. Ongoing work focuses on developing new systems capable of both RE and C-H bond activation, and progressing towards the conditions needed for catalytic hydrocarbon functionalization.

CHAPTER 4

REDUCTIVE FUNCTIONALIZATION OF A RHODIUM(III)-METHYL BOND IN ACIDIC MEDIAⁱⁱⁱ

4.1 Introduction

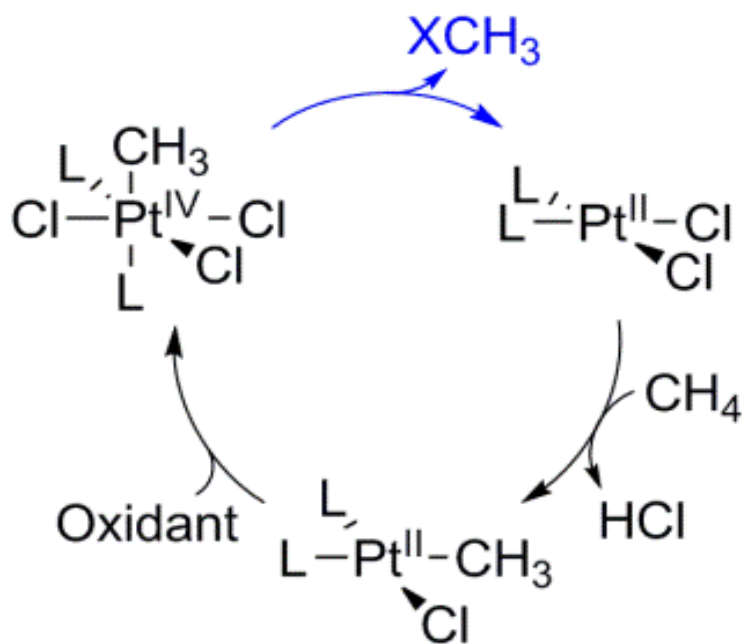
The selective and economical mono-functionalization of hydrocarbons to alcohols is of interest for the production of transportation fuels and commercial chemicals.^{14,80,81,82,83,84,85,86,87,88,89} Since Shilov's initial discovery of Pt-mediated alkane functionalization (Scheme 4.1),¹³⁶ a growing number of late transition and main group elements have been found to catalyze (Co,^{33,137} Rh,^{11,13} Pd,^{138,139,140,141} Pt,^{142,143} Au²³ and Hg^{12,144,145} or stoichiometrically convert (IO₃⁻,¹⁴⁶ Tl^{147,22} and Pb¹⁴⁷) methane to mono-functionalized product in acidic media. The acidic (HX) medium is an important ingredient to this reaction as it does not compete with methane coordination, and the electron-withdrawing conjugate base (X⁻) deactivates the functionalized MeX product towards further oxidation.¹⁴⁸ However, the acidic solvent can result in competitive protonation of methyl ligands and inhibit the reductive functionalization step by attenuating the nucleophilicity of X⁻ towards an S_N2-type attack¹⁴⁹ of a M–R species. Hence, the selection of the transition metal offers distinct tradeoffs. Late metal ions (Pt, Tl, Pb, Au and Hg) in high oxidation states can provide a large thermodynamic impetus for reductive functionalization, but re-oxidation becomes more thermodynamically difficult.

An advantage for using an earlier subset of transition metals (e.g., Group 9 and 10) is that milder and potentially O₂-recyclable oxidants can be used to re-oxidize the metal. Work by

ⁱⁱⁱ Reprinted with permission from **Reductive Functionalization of a Rh(III)-methyl Bond in Acidic Media: A Key Step in the Electrophilic Functionalization of Methane**, M. E. O'Reilly, D. R. Pahls, T. R. Cundari, T. B. Gunnoe. *Organometallics*, 2014, 33, 6504-6510. DOI:[10.1021/om5008456](https://doi.org/10.1021/om5008456) Copyright 2014 American Chemical Society.

Straßner and co-workers has demonstrated aerobic mono-functionalization of propane using Pd complexes in HTFA (TFA = CF₃CO₂).¹⁵⁰ Also, the oxidation of Pt^{II}-Me complexes using O₂ as a direct oxidant has been reported.^{151,152,153,154} Additionally, Co^{III} salts have been shown to catalyze methane functionalization via a radical mechanism using O₂.^{33,137}

Reductive Functionalization



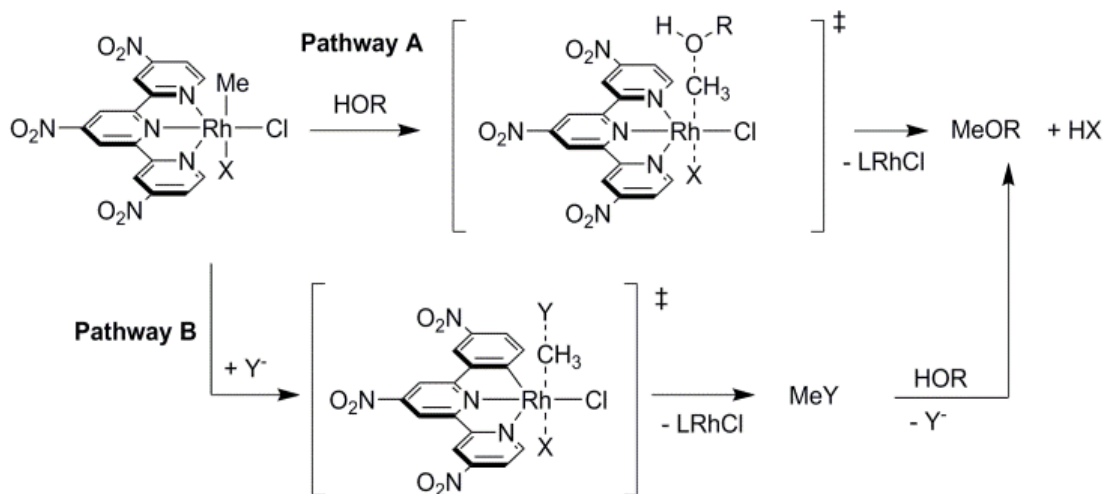
Scheme 4.1 The proposed "Shilov" catalytic cycle for the partial oxidation/functionalization of methane using Pt^{II} salts (X = OH⁻, Cl⁻; L = H₂O). Highlighted in blue is the product forming step, which is a reductive functionalization of the Pt^{IV}-Me bond.

Using an earlier (than Group 10) transition metal such as Rh offers attractive properties for electrophilic hydrocarbon functionalization. The move towards less electronegative metals could potentially allow less acidic media to be used while keeping similar product selectivity. Sen and co-workers reported acetic acid production from CH₄, CO and O₂ using RhCl₃ with Cl⁻ and I⁻ salts.¹⁵⁵ Later, the authors reported that changing the solvent from H₂O to perfluorobutyric acid altered product selectivity from acetic acid to methanol.¹³ The difference in selectivity was

attributed to competitive pathways of CO insertion and reductive functionalization from a Rh–Me species. Wayland and co-workers demonstrated (porphyrin)Rh^{II} complexes can reversibly activate C–H bonds of methane and ethane in benzene via a bimetallic radical pathway,^{21,49} and subsequent work by DiMugno and co-workers demonstrated functionalization of a Rh^{III}–CH₃ bond with strong nucleophiles such as PR₃.⁵¹

Despite examples of Rh-mediated C–H activation,^{156,157,158} very little is known about reductive functionalization of the Rh^{III}–Me bond in acids. To date, only a few instances of alkyl halide reductive elimination from Rh^{III} complexes have been reported; however, to our knowledge, none of these occur in acidic media.^{57,126,128,129} Similar to Sen's catalyst, these examples often require π -acidic ligands (e.g., CO) to drive reductive elimination. An evitable drawback to such a strategy is that CO can be consumed to form CO₂. Our groups investigated computationally the role of nucleophiles, leaving groups, and coordination geometry to aid the understanding of Rh-mediated reductive functionalization processes.¹³⁰ We also recently reported an experimental example of reductive elimination of MeX from Rh–Me without π -acid supporting ligands.¹⁵⁹ Mechanistic experimental and computational studies were utilized to understand the impact of supporting ligand modification upon the thermodynamics and kinetics of reductive functionalization. Herein, details surrounding successful reductive functionalization of a Rh^{III}–CH₃ bond in acidic media are reported.

4.2 Results and Discussion



Scheme 4.2 Two proposed pathways for reductive functionalization from $[(\text{NO}_2)_3\text{terpy}]\text{Rh}(\text{Me})(\text{Cl})\text{I}$ ($X = \text{I}$). Pathway A: direct attack by charge neutral acid ($R = -\text{C}(\text{O})\text{Me}$, $-\text{C}(\text{O})\text{CF}_3$, $-\text{H}$) on the $\text{Rh}-\text{Me}$ bond of $[(\text{NO}_2)_3\text{terpy}]\text{Rh}(\text{Me})(\text{Cl})\text{I}$ to form MeOR . Pathway B: nucleophilic attack by anionic Y^- ($\text{Y} = \text{I}$, Cl , OAc or TFA) on the $\text{Rh}-\text{Me}$ bond to form MeY , followed by metathesis with HTFA . DFT calculations employed $[(\text{NO}_2)_3\text{terpy}]\text{Rh}(\text{Me})(\text{Cl})_2$ and $\{[(\text{NO}_2)_3\text{terpy}]\text{Rh}(\text{Me})(\text{Cl})\}^+$ ($3'$; no ligand in X position) as models for the two pathways.

Our collaborators at the University of Virginia (Matthew O'Reilly, T. Brent Gunnoe) extended the work with the $[\text{NO}_2\text{terpy}]\text{Rh}(\text{Me})(\text{Cl})\text{I}$ complex to protic media. They observed that reductive functionalization was observed, but only at higher temperatures and with attenuated yields. Addition of halide additives ($[\text{NBu}_4]\text{Cl}$, $[\text{NBu}_4]\text{I}$) were found to improve MeX yields with iodide giving higher yields. The lower yields were attributed to the concurrent formation of methane gas.

DFT calculations were performed to investigate the reductive functionalization of the $\text{Rh}-\text{Me}$ bond with the various potential nucleophiles present in solution. Initial calculations used $[\text{NO}_2\text{terpy}]\text{RhMeCl}_2$ ($2'$) and $\{[\text{NO}_2\text{terpy}]\text{RhMeCl}\}^+$ ($3'$) in acetic acid continuum solvent and the same level of theory that was previously corroborated by bomb calorimetry experiments.¹⁵⁹ For simplicity, the effect of hydrogen bonding was excluded in our preliminary investigation (vide

infra). Table 4.1 lists the calculated ΔG^\ddagger 's, and two striking trends emerge. Pathway A, featuring an attack of a charge neutral acid on 2' or 3' by either HTFA or AcOH, yielded extremely high transition state energies (Table 4.1, Pathway A, $\Delta G^\ddagger > 50$ kcal/mol). Even a nucleophilic attack by water on the Rh–Me bond has a free energy barrier greater than 50 kcal/mol. The barrier to reductive functionalization was computed to be substantially diminished when anionic nucleophiles were employed (Table 4.1, Pathway B). Acetate was calculated to have the lowest free energy barrier of ~ 23 kcal/mol, followed by Cl^- (24 - 26 kcal/mol), and then TFA^- (31 - 32 kcal/mol).

Table 4.1 Calculated free energies (kcal/mol) for the reductive functionalization pathways A and B presented in Scheme 4.2.

R	Pathway A		Y ⁻	Pathway B	
	Complex	ΔG^\ddagger		Complex	ΔG^\ddagger
-C(O)Me	2'	53.4 ^a	AcO ⁻	2'	23.4
	3'	61.2 ^a		3'	24.0
-C(O)CF ₃	2'	66.1 ^a	TFA ⁻	2'	31.6
	3'	72.4		3'	31.4
-H	2'	51.3	Cl ⁻	2'	24.1
	3'	60.0		3'	25.8

^aThe lowest reductive functionalization barrier involves nucleophilic attack from the carbonyl O-atom. The square indicates an open coordination site.

The second interesting feature to emerge from DFT calculations is the slight energetic preference for nucleophilic attack on a 6-coordinate 2' over the 5-coordinate 3'. This result in acetic acid solution contrasts our previous experimental and computational studies on this system in a more polar (nitromethane) solvent, which concluded that nucleophilic attack was most facile through the cationic (5-coordinate) 3' generated after dissociation of a halide ligand from 2'.¹⁵⁹ In continuum nitromethane solvent, dissociation of the chloride ligand (trans to methyl) had a computed energetic cost (ΔG) of only 7.8 kcal/mol, while in acetic acid the free energy cost of chloride dissociation increases to 21.4 kcal/mol. The larger energetic cost for

halide loss is not unexpected as the dielectric constant of acetic acid is 6.2528, while the dielectric constant of nitromethane is 36.562. Given the large decrease in solvent polarity for acetic acid, a nucleophilic attack on a charge-neutral 6-coordinate $\text{Rh}^{\text{III}}\text{-Me}$ species becomes competitive. These calculations reveal that the nucleophilic attack on either 5- or 6-coordinate $\text{Rh}^{\text{III}}\text{-Me}$ complex is likely to be solvent dependent.

Next, we probed the effect of added 3 equivalents of $[\text{Bu}_4\text{N}]\text{TFA}$ in HTFA for the reductive functionalization from $\{[\text{NO}_2\text{terpy}]\text{RhMeCl}\}^+$. Our initial DFT calculations predicted a low barrier calculated for TFA^- attack (Table 4.2). However, no functionalized product was observed when 3 was heated with TFA^- . Additionally, heating complex $[\text{NO}_2\text{terpy}]\text{RhMeCl}$ with 3 equivalents of $[\text{Bu}_4\text{N}]\text{OAc}$ in acetic acid did not enhance yields of functionalized product. While initial DFT calculations predicted low transition state barriers for nucleophilic attack by TFA^- and AcO^- , initial models did not incorporate hydrogen-bonding effects, which might be expected to diminish the nucleophilicity of TFA^- and AcO^- .

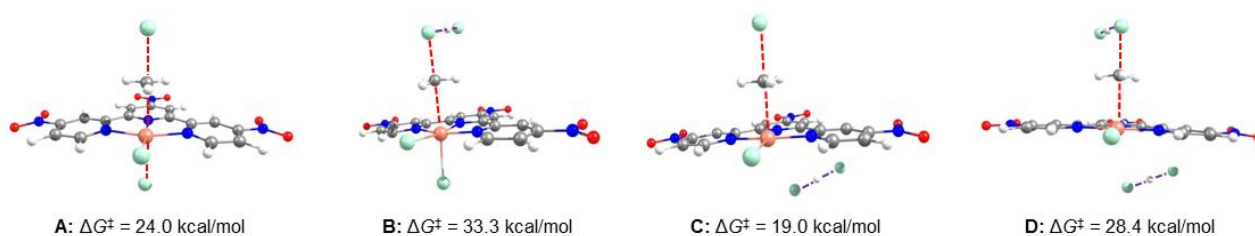


Figure 4.1 Transition state structures and their corresponding energies (kcal/mol) for reductive functionalization of 2' with hydrogen bonding interactions. Barriers for structures B-D are relative to ground state reactants with preformed hydrogen bonds. Red lines depict bond forming/breaking during the transition state. Purple lines depict hydrogen bonding interactions. Atom labels: chloride (light blue), rhodium (pink), oxygen (red), nitrogen (blue), carbon (gray) and hydrogen (white).

Figure 4.1 depicts the changes in transition state energies incorporating H-bonding with a simple HCl model. Modeling H-bonding effects by adding explicit acid molecules during

reductive functionalization presents a substantial added computational and conformational complexity to the system, but the results summarized in Figure 4.1 are instructive vis-à-vis reductive functionalization in protic media. Adding a single hydrogen bond to the attacking chloride (Figure 4.1; B) raises the barrier from 24.0 to 33.3 kcal/mol. The latter is consistent with previous computational studies¹³⁰ of reductive functionalization by related Rh-alkyl complexes in that reduced nucleophilicity shows large increases in the barrier to reductive functionalization at Rh^{III}-CH₃ bonds. Interestingly, hydrogen bonding an equivalent of HCl to the axial-chloride (Figure 4.1; C) decreases the reductive functionalization barrier by 5 kcal/mol to 19.0 kcal/mol. In light of previous studies,¹³⁰ this result can be explained on the basis of hydrogen-bonding interaction making the ligand trans to the Rh^{III}-CH₃ active site a better leaving group (Cl₂H⁻ versus Cl⁻), thereby reducing the reductive functionalization barrier. Combining both of the hydrogen bonding interactions yielded a transition state barrier of 28.4 kcal/mol (Figure 4.1; D). H-bonding HCl to the equatorial Cl had no impact on reductive functionalization barriers ($\Delta\Delta G^\ddagger < 1.0$ kcal/mol). An interesting consequence of hydrogen bonding interaction in structures C and D is that the axial chloride is completely dissociated from the Rh metal center (calculated Rh-Cl_{ax} > 4.97 Å). Hence, the H-bonding effectively moves the transition states towards what could be considered a 5-coordinate intermediate, which the present and past studies of reduction functionalization of Rh^{III}-CH₃ bonds implicate is kinetically advantageous if the 5-coordinate state can be accessed from its 6-coordinate precursor without a substantial free energy penalty.

The reductive functionalization of [NO₂terpy]RhMe(Cl)I in D₂O is unusual compared to acetic acid or trifluoroacetic acid. Additional amounts of Bu₄NI and Bu₄NCl do not increase the yield of functionalized product. In addition, the formation of MeI or MeCl as potential

intermediates was not observed. However, soft halides appear to play a necessary role during reductive functionalization since heating $[[\text{NO}_2\text{terpy}]\text{RhMeCl}]^+$ in D_2O yielded only 10% methanol, while at least 60% of the Rh–Me complex remains intact. Meaningful interpretation is more difficult since water coordination may be a significant factor.

We considered three options for methane formation from the Rh–Me bond. An initial hypothesis was that Rh– CH_3 protonation would proceed through a reverse concerted metallation deprotonation (CMD) mechanism (Figure 4.2, structure A). However, calculated free energy barriers of >55 kcal/mol were obtained, which weigh against this proposal.

The second possibility considered is the simple direct protonation of the $\text{Rh}^{\text{III}}\text{–Me}$ bond as depicted in Figure 4.2, structure B. The protonation barriers seem reasonable for strong acids such as HI (23.2 kcal/mol) and HCl (28.7 kcal/mol). As anticipated, reasonable correlations between pK_a of the acid and protonation barriers were found (see Supporting Information). However, the calculated barriers to protonation with weaker acids are unreasonably high (HTFA = 35.4 kcal/mol; AcOH = 47.3 kcal/mol; H_2O = 70.7 kcal/mol). The simulations thus point away from a direct protonation mechanism since the solvents employed (HOAc and HTFA) have prohibitively large calculated free energy barriers for protonation (Table 4.2).

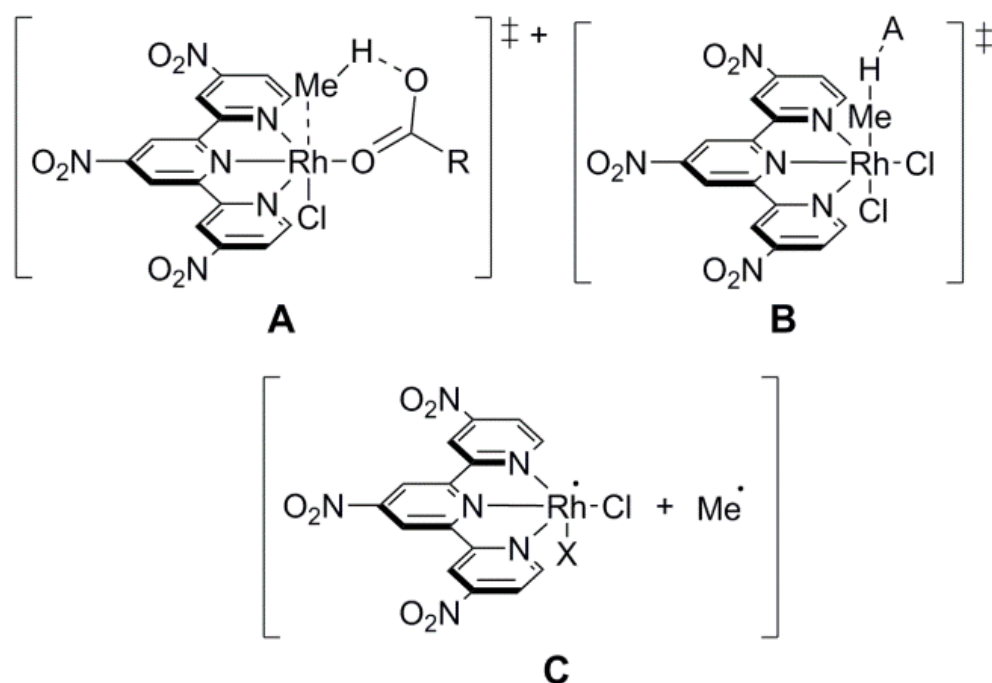


Figure 4.2 DFT calculated transition states (A and B) for methane formation from 2' and 3'. A: reverse concerted metalation deprotonation (revCMD); B: direct protonation; and C: Rh—Me bond homolysis.

Table 4.2 Calculated free energies (kcal/mol) for the protonation transition states A-C presented in Figure 4.2.

Transition State A		Transition State B		Species C	
R	$\Delta G^{\ddagger a}$	HA	ΔG^{\ddagger}	X	ΔG
Me	56.6	HI	23.2	Cl	26.0
CF ₃	58.1	HCl	28.7	-	29.8
		HTFA	35.4		
		AcOH	47.3		
		H ₂ O	70.7		

^aCalculated free energies relative to 2 and HA.

A third proposal for methane formation involves a methyl radical formation via Rh—Me bond homolysis (Figure 4.2, structure C). DFT calculations of 2' and 3' reveal a 26.0 and 29.8 kcal/mol free energy to homolytically cleave the Rh—Me bond. In part, the low Rh—Me bond energy arises from stabilization of the metalloradical by diffusion of the spin density over both the metal, supporting ligand and trans ligand. Taken together, the DFT calculations suggest a

surprising mechanism for CH₄ formation via Rh–Me bond homolysis rather than simple protonation. The high temperature (150 °C) of these experiments seemingly renders Rh–Me bond homolysis a viable option. Several attempts were made by our collaborators to demonstrate the presence of radicals during the reductive functionalization reactions; however, the results could not conclusive support the existence of a methyl radical.

4.3 Conclusions

Selective hydrocarbon functionalization by transition metal catalysts remains a substantial challenge balancing environmental and economic considerations along speed, selectivity, and overall yields. Electrophilic metals later than group 10 have been effective for alkane C–H bond activation and reductive functionalization; however, re-oxidation can be difficult, especially aerobically. In some cases, a super-acidic medium is required.²² Using earlier transition metals (group 9-10) allows for easier re-oxidation, but will inevitably present new challenges. The results presented herein suggested two strategies to promote reductive functionalization of Rh^{III}–R bonds: the use of electron withdrawing ligands and the addition of iodide as a co-catalyst.

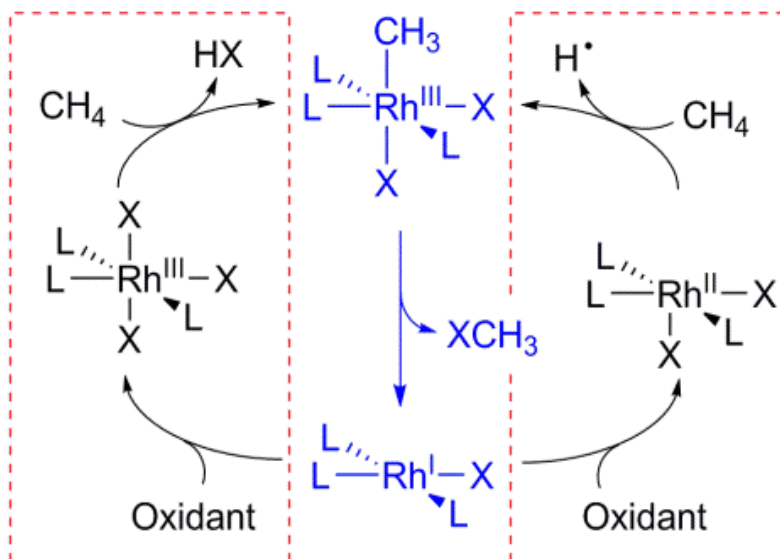
In addressing these new challenges, we report reductive functionalization of Rh^{III}–Me in acids achieving ~60% conversion to MeX under optimized conditions. The reaction is a critical step for electrophilic functionalization of small alkanes. The choice of metal and supporting ligand to modulate the electrophilicity of the methyl moiety is presumably a key factor in diminishing protonation side reactions. In that regard, the reactivity of [NO₂terpy]RhMe(Cl)I in acids is intriguing by yielding both CH₄ and MeX formation, since previous reductive functionalization studies using Pt^{IV}–Me did not observe concomitant protonation.^{96,97,160} The fact that net

protonation is observed from $\text{Rh}^{\text{III}}\text{-Me}$ indicates a different challenge compared to Pt catalysts, which has consequence for the catalytic cycle of alkane functionalization. For Pt-based systems, the oxidation step must occur rapidly to prevent competing protonation of the $\text{Pt}^{\text{II}}\text{-Me}$ species.¹⁶¹ However, for Rh-based catalysts, the reductive functionalization step must be competitive with methane formation. Therefore, soft halides are likely required to mediate reductive functionalization.

Even if concomitant net protonation was not observed for $[\text{NO}_2\text{terpy}]\text{RhMe}(\text{Cl})\text{I}$, DFT calculations reveal that an $\text{S}_{\text{N}}2$ -attack by the acid solvent has a remarkably high activation barrier and would still require soft halides. We suspect that the less electrophilic rhodium ion does not provide a strong thermodynamic impetus for nucleophilic attack by the acid or water at the methyl ligand, highlighting another difference from Pt-based systems.

Overall, the reductive functionalization of the methyl ligand of $[\text{NO}_2\text{terpy}]\text{RhMe}(\text{Cl})\text{I}$ in acids suggests the viability of a new process for hydrocarbon functionalization for Rh-based systems. While we are unable to conclusively determine the mechanism of methane formation, Scheme 4.3 depicts two possible mechanisms to reach $\text{Rh}^{\text{III}}\text{-Me}$ complex, although the present evidence best supports a radical-based bond homolysis. It is possible to envisage a catalyst where a metalloradical mediates C–H bond activation in an acidic medium. An example of radical initiated functionalization of methane in oleum has been reported.¹⁶² Furthermore, Wayland has demonstrated the viable Rh^{II} metalloradical to activate methane.^{51,156} More importantly, designing a Rh-based catalyst for methane functionalization must consider that net protonation is likely to be competitive with functionalization. Lowering the barrier to reductive functionalization of $\text{Rh}^{\text{III}}\text{-Me}$ bonds is a key factor to a successful catalyst. In this regard, the

present research highlights the critical importance of metal-ligand design, and the role of halides to assist the key steps needed for electrophilic hydrocarbon functionalization.



Scheme 4.3 A potential mechanism for electrophilic catalytic cycle using Rh-based catalysts. Left box highlights high-valent route where CH bond activation occurs at a Rh^{III} species. Right box highlights a radical route to achieve a high valent Rh–CH₃ species.

4.4 Computational Methods

The thermodynamics and kinetics of Rh–Me bond functionalization by substituted terpyridine ligated rhodium complexes was studied using DFT. All optimization and frequency calculations were performed by the Gaussian 09 software package.⁷³ The number of imaginary frequencies in the energy Hessian was examined to determine if a structure was a ground (0) or transition state (1). Optimization and frequency calculations were performed with implicit solvation using the CPCM^{74,75} method as employed by Gaussian 09. To most closely model experimental conditions, for the thermodynamics of oxidative addition AcOH ($\epsilon = 6.2528$) was used as solvent. The systems were modeled by the B3LYP^{76,77} exchange-correlation functional with the CEP-31G(d)^{78,79} basis set. Free energies are reported at STP in kcal/mol. All complexes

not involved in bond homolysis were calculated as singlets those involved in bond homolysis were calculated as doublets.

CHAPTER 5

MECHANISM OF HYDROGENOLYSIS OF AN IRIDIUM-METHYL BOND: EVIDENCE FOR A METHANE COMPLEX INTERMEDIATE^{iv}

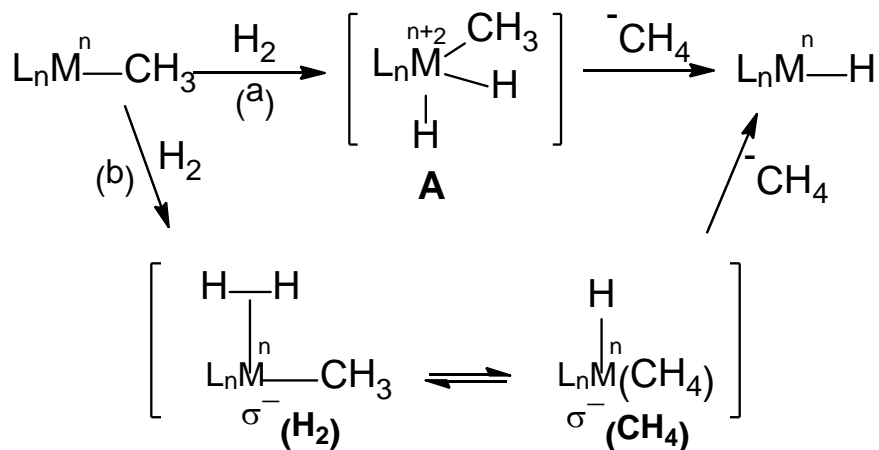
5.1 Introduction

σ -Bond metathesis is a fundamental transformation exhibited by complexes of metals across the periodic table and plays an important role in many catalytic and stoichiometric processes.¹⁶³ Hydrogenolysis of metal–alkyl bonds is a particularly significant reaction for both early and late transition metal alkyls.¹⁶⁴ For example, hydrogenolysis of d^0 metal–alkyl bonds provides an important method for controlling polymer molecular weights in olefin polymerization reactions.¹⁶⁵ In both early- and late-metal systems, hydrogenolysis of metal–alkyl bonds releases the alkane in hydrogenation reactions in which the catalytic cycle involves olefin insertion into a metal monohydride.

In the case of d^0 metal–alkyl complexes, the σ -bond metathesis reaction cannot occur via an oxidative addition/reductive elimination process.^{156,166} Density functional theory (DFT) calculations suggest that σ -complex intermediates intervene along the pathway, but such species are sufficiently high in energy that, to date, they have escaped observation. In the case of late-transition-metal systems, there are multiple possibilities for the exact pathways followed during σ -bond metathesis, as revealed by both DFT studies and experimental observations.¹⁶⁷ A simplified scheme is shown in Scheme 5.1 for the basic hydrogenolysis reaction, cleavage of a M–CH₃ bond by H₂. Pathway (a) involves the formation of oxidative addition intermediate **A** followed

^{iv} Reprinted with permission from **Mechanism of Hydrogenolysis of an Iridium-Methyl Bond: Evidence for a Methane Complex Intermediate**, J. Campos, E. Carmona, M. Brookhart, S. Kundu, D. R. Pahls, T. R. Cundari *J. Am. Chem. Soc.*, 2013, 135 1217-1220. DOI: [10.1021/ja310982v](https://doi.org/10.1021/ja310982v). Copyright 2013 American Chemical Society.

by reductive elimination of CH₄. Pathway (b) involves the formation of a σ-H₂ complex, conversion to a σ-methane (σ-CH₄) complex, and release of methane. While these are two “simplified” schemes, experimentally relevant pathways are certainly more complex. σ-Complex intermediates likely intervene in the formation and decay of **A** in pathway (a). In pathway (b), a higher-energy oxidative addition intermediate such as **A** may connect the σ-H₂ and σ-CH₄ intermediates or the interconversion of these species may be a concerted process. The latter case, in which there is no higher oxidation state intermediate along the pathway, has been termed σ-complex-assisted metathesis (σ-CAM).¹⁶⁸ The extent of the M–H interaction in this transition state may also vary substantially.



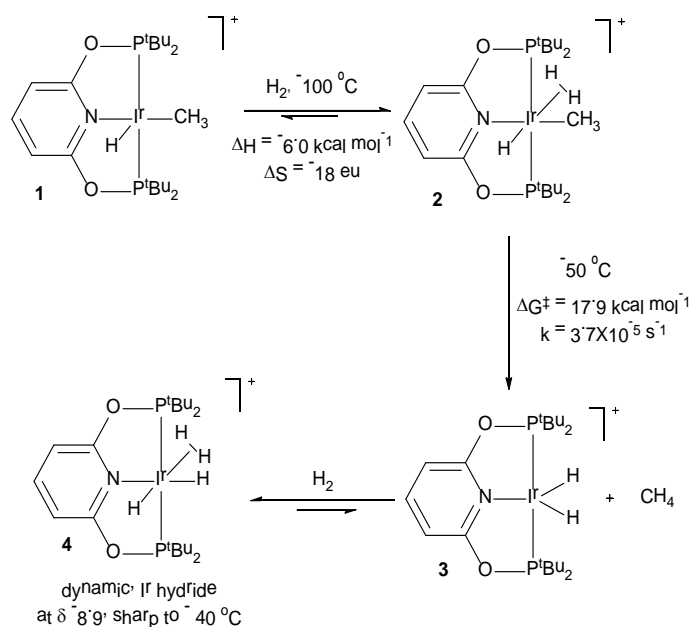
Scheme 5.1 Two Possible Pathways for Hydrogenolysis of a M–CH₃ Bond

5.2 Summary of Experimental Results

Here we report the hydrogenolysis of the Ir–CH₃ bond of a cationic iridium complex wherein the σ-H₂ intermediate can be observed spectroscopically. Deuterium labeling experiments provided evidence for interconversion of the σ-H₂ complex with the σ-CH₄ complex prior to release of methane. DFT calculations revealed the energy difference between the σ-

H₂ and σ-CH₄ complexes and the nature and structure of the transition state connecting these species.

Collaborators in the Brookhart and Carmona labs (Jesús Campos, Sabuj Kundu, Maurice Brookhart, Ernesto Carmona) had previously reported that exposure of the cationic, coordinately unsaturated Ir(III) methyl hydride complex (PONOP)Ir(H)(Me)⁺ (**1**) [PONOP = 2,6-bis(di-*tert*-butylphosphinito)pyridine] to H₂ at -100 °C results in the formation of the η²-H₂ complex **2** in equilibrium with **1**¹⁶⁹ (Scheme 5.2). Warming to -50 °C results in loss of methane and formation of dihydride complex **3**, which under H₂ forms tetrahydride complex **4**.¹⁷⁰ The equilibrium ratio of **1** and **2** at known H₂ concentrations was examined over the temperature range from -110 to -60 °C. A van't Hoff plot revealed ΔH° = -6.0 kcal/mol and ΔS° = -18 eu. With this correction for the equilibrium between **1** and **2**, we were able to determine the first-order rate constant for loss of methane from **2** as 3.7 × 10⁻⁵ s⁻¹ at -50 °C, corresponding to ΔG[‡] ≈ 17.9 kcal/mol.



Scheme 5.2 Hydrogenolysis of Complex 1 at Low Temperature

5.3 Computational Results and Discussions

To ascertain if a σ -CH₄ complex is an intermediate in the loss of methane from **2** our experimental collaborators in the Carmona and Brookhart labs complex **2-d₂** was prepared by addition of D₂ to **1**. Deuterium scrambling to both the methyl and terminal hydride groups at the same rate was observed strongly implying the reversible formation of an intermediate σ -CH₄ complex. Rapid tumbling in the σ -CH₄ complex coupled with the equivalence of the two terminal hydride positions results in equal rates of deuterium scrambling into the two sites. The free energy barrier (ΔG^\ddagger) for this exchange was found to be 13.6 kcal/mol.

To gain further insights into this σ -bond metathesis reaction, this transformation was investigated using DFT. We modeled our system using the PBE0 functional¹⁷¹ with the Stuttgart basis set including an additional f polarization function with an exponent of 0.685 for Ir and the 6-311G** basis set¹⁷² for all other elements. Recent publications on similar systems^{169,173} have found success with this functional using basis sets of double- ζ quality. All of the structures were optimized in the gas phase with a single-point solvent correction using the SMD solvation model¹⁷⁴ (solvent = CH₂Cl₂) as implemented in Gaussian 09.⁷³

The DFT-computed structures of **2** and the methane complex **5** are shown in Figure 5.1. The H–H distance of 0.84 Å in the σ^2 -H₂ ligand is consistent with the observed J_{HD} value of 34 Hz,¹⁷⁵ and the Ir–H distances of 1.57 and 1.80 Å are in the expected ranges for a terminal Ir–H and an η^2 -H₂, respectively. In the σ -CH₄ complex **5**, CH₄ is bound primarily through one C–H bond (M–H distance of 1.78 Å, in contrast to next-nearest geminal C–H \cdots Ir distance of 2.58 Å). The σ^2 -H₂ complex **2** was calculated to be 8.6 kcal/mol more stable than the σ -CH₄ isomer **5** in a

continuum CH_2Cl_2 solution. This value provides an estimate of $17.9 - 8.6 = 9.3$ kcal/mol for ΔG^\ddagger for dissociation of methane from 5.

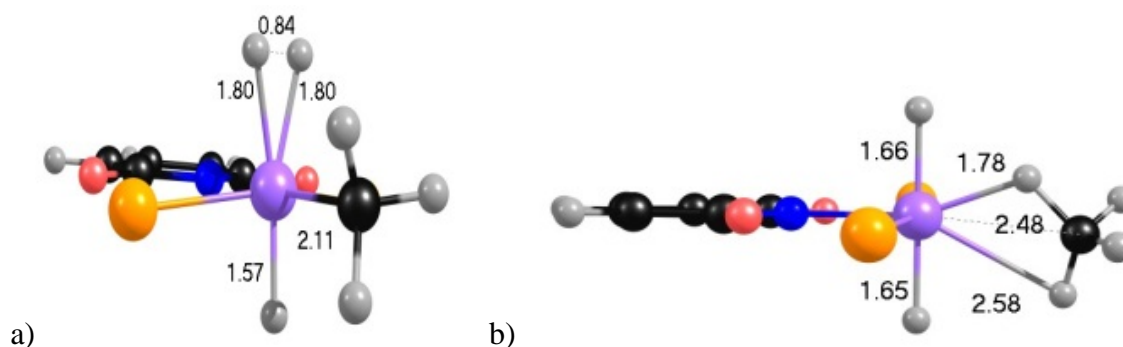
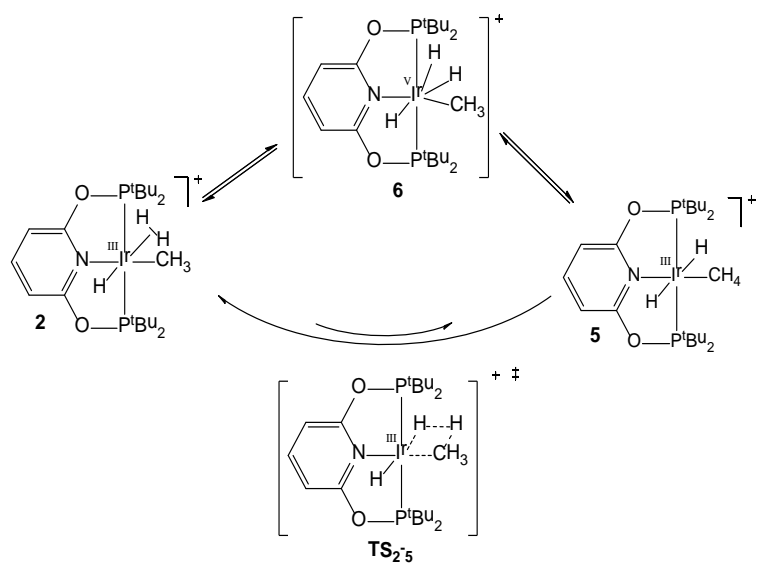


Figure 5.1 DFT-calculated structures of (a) $(\text{PONOP})\text{Ir}(\text{H})(\text{Me})(\text{H}_2)^+$ and (b) $(\text{PONOP})\text{Ir}(\text{CH}_4)(\text{H})_2^+$ (**5**). The *tert*-butyl substituents have been omitted for clarity. Ir, purple; C, black; H, gray; O, red; P, orange; N, blue.

We considered that $\sigma\text{-H}_2$ complex 2 could be converted into $\sigma\text{-CH}_4$ complex 5 by either a two-step or a one-step mechanism (Scheme 5.3). In the two-step mechanism, the H_2 ligand would undergo oxidative addition to give a seven-coordinate trihydride complex, 6, which in turn would undergo reductive elimination to form the CH_4 adduct. The one-step concerted mechanism would involve a direct hydrogen transfer from the H_2 ligand to the CH_3 ligand to form the CH_4 adduct. The single hydrogen-transfer step could proceed via transition state TS_{2-5} with either substantial or little involvement of the metal.



Scheme 5.3 Two Potential Mechanisms for Interconversion of 2 and 5.

We were not able to locate a minimum on the potential energy surface corresponding to 6. All attempts to locate this trihydride complex optimized to the σ -H₂ complex 2. The lack of a stable iridium trihydride complex is strong evidence against an oxidative addition/reductive elimination pathway for the interconversion of the σ -H₂ and σ -CH₄ complexes.

The free energy of the transition state for the one-step conversion of H₂ to CH₄ was calculated to be $\Delta G^\ddagger = 13.3$ kcal/mol in CH₂Cl₂, which is in close agreement with the experimental free energy barrier of 13.6 kcal/mol derived from the H/D scrambling experiments. In the transition state, the Ir–H distance for the hydrogen being transferred is 1.60 Å (Figure 5.2a). This short metal–hydride distance (which can be compared to the distances of 1.80 Å for the η^2 -H₂ ligand in 2) indicates a very significant interaction of the metal with the hydrogen being transferred in the transition state, which therefore seems closer to a trihydride structure. To determine whether this interaction with the metal was necessary for reactivity, I searched for a transition state with a reduced Ir–H interaction. This was accomplished by freezing the distance

between the Ir center and the H being transferred and optimizing the rest of structure. With this procedure, a second transition state with a frozen Ir–H distance of 2.00 Å was located (Figure 5.2b). This structure does not represent a true saddle point on the potential energy surface because one coordinate was not allowed to optimize, and therefore, the energy of this structure is not physically meaningful. When the constraint was removed and the full system was allowed to optimize, a structure with an Ir–H distance of ~2.0 Å was not obtained. Instead, the optimized structure had an Ir–H distance of 1.6 Å, similar to the structure discussed previously. This preference for the shorter Ir–H distance suggests that the Ir–H interaction is important in stabilizing the transition state and is thus consistent with a σ -CAM mechanism. Thus experimental and computational evidence support the intermediacy of a σ -CH₄ complex in the hydrogenolysis of the Ir–Me bond by dihydrogen.

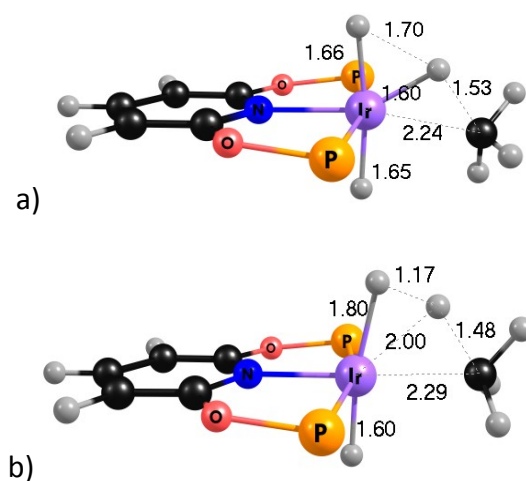


Figure 5.2 (a) Transition state for hydrogen transfer with an Ir–H bond length of 1.6 Å. (b) Transition state for hydrogen transfer with a restricted Ir–H distance of 2.0 Å. The tert-butyl substituents have been omitted for clarity.

CHAPTER 6

DFT STUDIES ON LIGAND OPTIMIZATION OF C-H ACTIVATION BY PheboxIr(OAc)₂(H₂O)^v

6.1 Introduction

Selective activation and subsequent functionalization of hydrocarbons is of great interest. Metal complexes that can activate C—H bonds, and the mechanisms by which such activations occur, have been studied to better understand how to achieve this difficult transformation. Concerted metallation-deprotonation (CMD) is one such mechanism wherein the M-R bond is formed when an internal base, typically a carboxylate, deprotonates a metal σ -bound hydrocarbon (RH) (Figure 6.1).^{176,177} This mechanism has been thoroughly studied for arene activation at Pd(II) centers.^{178,179} However, studies have shown that the CMD mechanism is active for other metal complexes such as those of Au(I),^{23,180} Ru(II),^{181,182,183,184} Co(III),¹⁸⁵ Rh(III),^{182,186,187} and Ir(III).^{188,189,190,191,192,193,194} Moreover, while CMD has been studied most intensively for arene C—H activation, it is also a viable mechanism for the activation of alkenes and alkanes.^{178,187,188,193,194}

^v Reprinted with permission from **Understanding the Effect of Ancillary Ligand on Concerted Metalation Deprotonation by PheboxIr(OAc)₂(H₂O): A DFT Study** *Organometallics*, D. R. Pahls, T. R. Cundari, *Organometallics*, 2014, 33, 6413 - 6419. DOI: [10.1021/om500752m](https://doi.org/10.1021/om500752m) Copyright 2014 American Chemical Society.

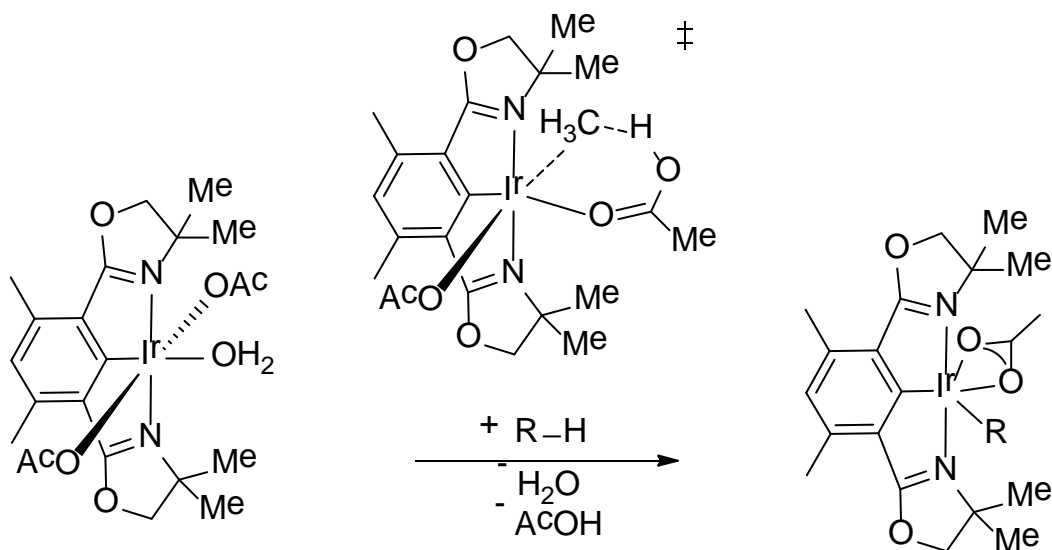


Figure 6.1 Example of CMD reaction of hydrocarbons with $(^{dm}\text{Phebox})\text{Ir}(\text{OAc})_2(\text{H}_2\text{O})$.

The first theoretical studies on the CMD mechanism of which we are aware were performed by Sakaki and coworkers. These researchers examined the activation of benzene and methane by $\text{Pd}(\text{O}_2\text{CH})_2$.¹⁷⁸ Activation of benzene and methane by a 6-membered ring CMD pathway from the formate complex was calculated to have a lower activation barrier than activation of either substrate by $(\text{PH}_3)_2\text{Pd}$, which effected C—H bond activation via an oxidative addition pathway. MacGregor and coworkers investigated the cyclometallation of dimethylbenzylamine (DMBA) by $\text{Pd}(\text{OAc})_2$ using DFT methods.¹⁷⁹ They showed that the lowest energy transition state (TS) was an acetate-assisted 6-membered ring TS after initial agostic binding of an ortho C-H bond of DMBA.¹⁷⁹ Fagnou and Gorelsky later published a combined experimental-computational study utilizing the activation-strain analysis of the TS for a variety of heterocycles and benzene.^{195,196} Their decomposition analysis suggested that the energy to distort the palladium complex from the ground to transition state geometry remained roughly constant for a series of complexes. The activation barriers were largely determined, therefore, by the energy required to distort the arene fragment, and the interaction energy (energy gain from

bringing the reactive fragments together). They further found that these two parameters were largely inversely correlated. Electron rich arenes had large Pd-arene interaction energies, but suffered from large arene distortion energies. Electron poor arenes, had lower arene distortion energies, but gained less interaction energy upon Pd-arene association. Substrates that had small deformation energies, but large interaction energies, such as thiazole-*N*-oxides, were calculated to have the lowest CMD barriers.

MacGregor *et al.* also modeled cyclometallation of DMBA at [CpIrOAc]⁺.¹⁸⁹ They calculated that the 6-membered ring CMD transition state was most favorable, but in this system a σ -adduct was not calculated to precede activation. Goddard *et al.* looked at the activation of benzene and methane from Ir(acac)₂(X) (X = OH, OAc; acac = acetylacetonate).¹⁸⁸ The transition states for a 4- or 6-membered CMD mechanism as well as electrophilic substitution were examined. Goddard and coworkers found that reaction through the 6-membered ring TS was the lowest energy pathway and that the TS had ambiphilic character, whereby both charge transfer from the reacting C-H bond to the Ir, and charge transfer from the acetate to the C-H bond were both important in stabilizing the transition state

As stated above, the majority of applications utilizing CMD mechanisms for hydrocarbon functionalization have employed arene substrates. Recent publications by both the Nishiyama and Goldberg groups have shown that the iridium complex (^{dm}Phebox)Ir(OAc)₂(H₂O) (^{dm}Phebox = 2,6-bis(4,4-dimethyloxazoliny)-3,5-dimethylphenyl) (Figure 6.2) is active for activation of both alkanes and arenes to give Ir-alkyl and -aryl complexes, respectively.^{193,194} Nishiyama showed that arenes were activated at 100 °C without the need for external base, and alkanes were activated at 160 °C with potassium carbonate as external base.

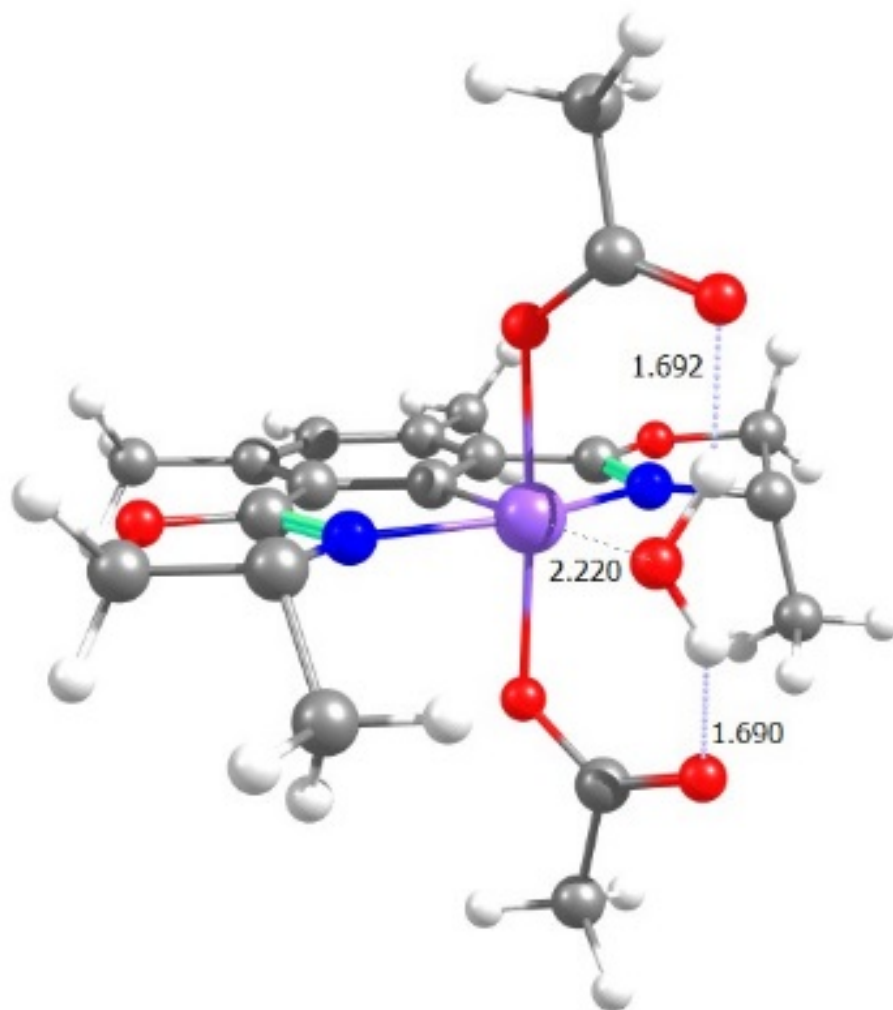


Figure 6.2 DFT optimized structure of $(^{dm}\text{Phebox})\text{Ir}(\text{OAc})_2(\text{H}_2\text{O})$ with selected bond distances shown. Two of the oxazoline methyl groups have been removed for clarity. Purple = iridium, red = oxygen, blue = nitrogen, gray = carbon, white = hydrogen.

Nishiyama *et al.* attempted the activation of benzene with $(^{dm}\text{Phebox})\text{Ir}(\text{Cl})_2(\text{H}_2\text{O})$; however, no reaction was observed, indicating that the acetate anion is crucial to the transformation. A series of mono-substituted arene substrates ($\text{C}_6\text{H}_5\text{X}$, X = OMe, Cl, COMe, NO_2) showed no linear correlation with the Hammett parameter (σ) of the substituent upon activation by $(^{dm}\text{Phebox})\text{Ir}(\text{OAc})_2(\text{H}_2\text{O})$, arguing against an electrophilic activation mechanism. Kinetic isotope effect (KIE) studies on benzene- d_6 and octane- d_{18} each showed a large KIE (2.9 and 4.0,

respectively), leading Nishiyama *et al.* to conclude that C—H activation was the rate determining step and that a CMD type mechanism would be plausible.

Goldberg *et al.* showed that when the reaction of alkanes with $(^{dm}Phebox)Ir(OAc)_2(H_2O)$ was performed at 200 °C without external base, the Ir-alkyl complex formed would release alkene via β -hydride elimination to generate the corresponding Ir-hydride product, $(^{dm}Phebox)Ir(H)(OAc)$. Also $(^{dm}Phebox)Ir(OAc)_2(H_2O)$ showed no loss of activity in the presence of dinitrogen or alkenes, and increased activity in the presence of water; all three of these small molecules are known to deactivate $^{tBu}PCPIr$ dehydrogenation catalysts.^{197,198} It is well established that $^{tBu}PCPIr$ dehydrogenation catalysts activate C-H bonds by C-H oxidative addition.^{199,200,201}

Given the paucity of studies – experimental and computational – on CMD activation of alkanes, computations can play an important role in discerning guiding principles for future catalyst development. Also, Ir^{III}-pincer complexes are of broad interest in catalytic cycles for hydrocarbon functionalization and understanding ligand modifications that promote C—H activation in these systems could allow for milder operating conditions that may allow for expanded reactivity.

In this paper an investigation on the effects of ligand modification on the $(^{dm}Phebox)Ir(OAc)_2(H_2O)$ system is reported including the effect of changing the electronic properties and identity of the aryl linker, modifying the pincer arms, and the identity of the carboxylate base upon the barrier to activation of methane by a CMD mechanism.

6.2 Computational Methods

The PBE0 functional¹⁷¹ was used in conjunction with the 6-311G** basis set on nonmetals and the SDD basis set and ECP on iridium with an additional f polarization function (exponent =

0.685) as implemented by Gaussian 09.^{73,172} Optimizations were performed in the gas phase and the nature of the stationary points as ground states or first order transition states were confirmed by analyzing the energy Hessian. To ensure that the gas phase calculations were sufficient the effect of solvent, temperature, BSSE, and level of theory were investigated. The activation of methane and ethane were used as a basis of comparison. Inclusion of these effects mentioned above changed the $\Delta\Delta G^\ddagger$ of reaction by 2.1 kcal/mol. The calculations that explore the effects of temperature, solvent, level of theory, and BSSE are summarized in Supporting Information.

6.3 Reaction Pathway

6.3.1 Loss of Water from PheboxIr(OAc)₂(H₂O)

In order for the 18-electron ^{dm}PheboxIr(OAc)₂(H₂O) complex to activate a hydrocarbon substrate it must presumably first lose a ligand to open up a coordination site. Loss of water from ^{dm}PheboxIr(OAc)₂(H₂O) is computed to be 13.5 kcal/mol uphill in free energy. Acetate linkage isomers – κ^1 or κ^2 – were considered for ^{dm}PheboxIr(OAc)₂; attention here is focused on the most stable linkage isomer found, the bis- κ^1 species.²⁰²

There are two potential isomers of ^{dm}PheboxIr(OAc)₂ that could be reactive. The isomer where the compound does not rearrange after loss of water and the open coordination site is *trans* to the phenyl ligand of the pincer backbone, hereafter referred to as the *trans* isomer. The other isomer requires a rearrangement of the acetate ligands to place the open coordination site *cis* to the phenyl ligand and is referred to as the *cis* isomer. The *cis* isomer could not be located as a stable point on the reaction coordinate, and always optimized to the *trans* isomer, implying that the *trans*-^{dm}PheboxIr(OAc)₂ isomer is significantly more stable than the *cis*-^{dm}PheboxIr(OAc)₂ isomer. Attempts at constraining the complex in a *cis* orientation resulted in optimization to

structures with imaginary frequencies implying that these constrained geometries are not ground states. The Davies and Macgregor groups have found that the κ^2 - κ^1 transition is important to understanding the reactivity of several iridium systems operating via a CMD mechanism;^{179,189,190} however, in the present system, the second oxygen atom of the acetate is weakly bound; (2.41 Å for shortest Ir-O distance to open coordination site, compared to 2.04 – 2.07 Å for the Ir-O bonds), suggesting that, for this complex, the κ^1 - κ^2 isomerization will be less important.

6.3.2 Hydrocarbon Binding to PheboxIr(OAc)₂

Subsequent association of a methane molecule to form a σ -methane complex precedes C—H bond activation. Both coordination isomers of ^{dm}PheboxIr(OAc)₂(CH₄) were located. Association of methane is calculated to be endergonic for both the *trans* and *cis* isomers of PheboxIr(OAc)₂(CH₄). The *trans*-^{dm}PheboxIr(OAc)₂(CH₄) isomer was calculated to be 10.7 kcal/mol more stable than the *cis*-^{dm}PheboxIr(OAc)₂(CH₄) isomer, and 16.2 kcal/mol uphill in free energy relative to separated ^{dm}PheboxIr(OAc)₂ plus methane (Figure 6.3). Since both isomers of the methane complex can be located, this suggests that a complete coordination sphere is necessary to form a *cis*-bis-acetate arrangement, even if it is a weakly binding ligand such as an alkane. Therefore, it is reasonable to assume that a *cis*- σ -complex requires a rearrangement of the acetates and association of methane.

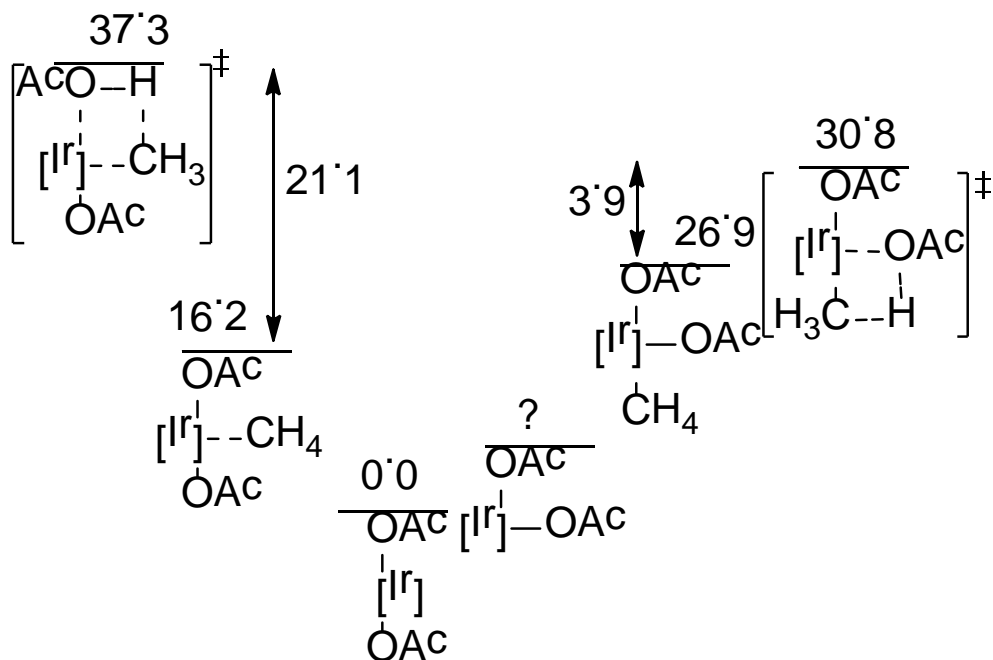


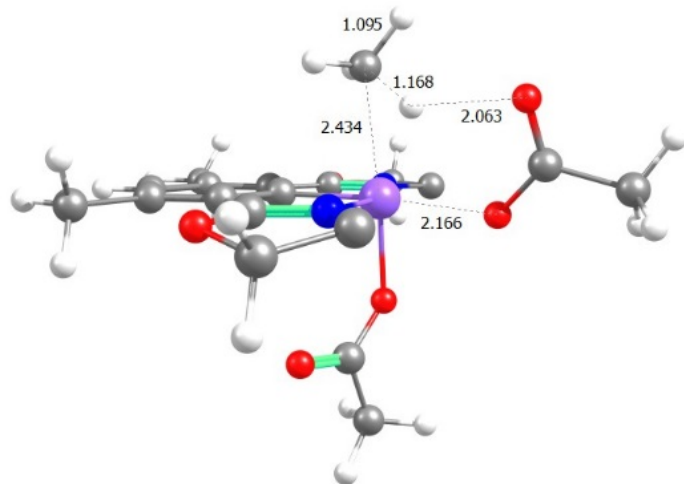
Figure 6.3 Comparison of the free energies of *cis* and *trans*-^{dm}PheboxIr(OAc)₂ complexes upon methane binding and activation. The *cis*-^{dm}PheboxIr(OAc)₂ complex could not be located (denoted by ?) as all input geometries optimized to the *trans*-^{dm}PheboxIr(OAc)₂ complex.

6.3.3 Carbon—Hydrogen Bond Activation

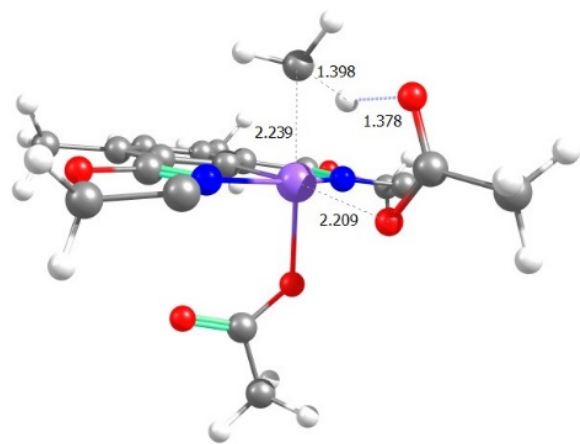
Activation of methane from the σ -methane complex could occur either by a two-step oxidative addition/reductive elimination (OA/RE) pathway, or by a concerted metallation-deprotonation (CMD) pathway. All CMD pathways were calculated as a 6-centered ring transition state, as previous computational studies have shown that a 4-centered ring transition state is disfavored when compared to a 6-centered ring transition state.^{188,179,189} Stable Ir(V) complexes that would be expected as intermediates in a OA/RE couple could not be located; such species rearranged to formally Ir(III) complexes upon geometry optimization. However, transition states corresponding to a CMD mechanism for both the *cis* and *trans* isomers of (^{dm}Phebox)Ir(OAc)₂(CH₄) were located. The free energy barrier to C—H bond activation of the methane in *cis*-(^{dm}Phebox)Ir(OAc)₂(CH₄) complex was calculated to be 30.9 kcal/mol relative to

(^{dm}Phebox)Ir(OAc)₂ plus methane while the free energy barrier of the *trans*-(^{dm}Phebox)Ir(OAc)₂(CH₄) complex was calculated to be 37.3 kcal/mol relative to ^{dm}PheboxIr(OAc)₂, thus $\Delta\Delta G^\ddagger = 6.4$ kcal/mol in favor of the *cis* complex (Figure 6.4a-d). Interestingly, although the *cis*-^{dm}PheboxIr(OAc)₂(CH₄) complex is less thermodynamically stable than the *trans*-^{dm}PheboxIr(OAc)₂(CH₄) complex, it is calculated to be the complex with the lower barrier to alkane activation.

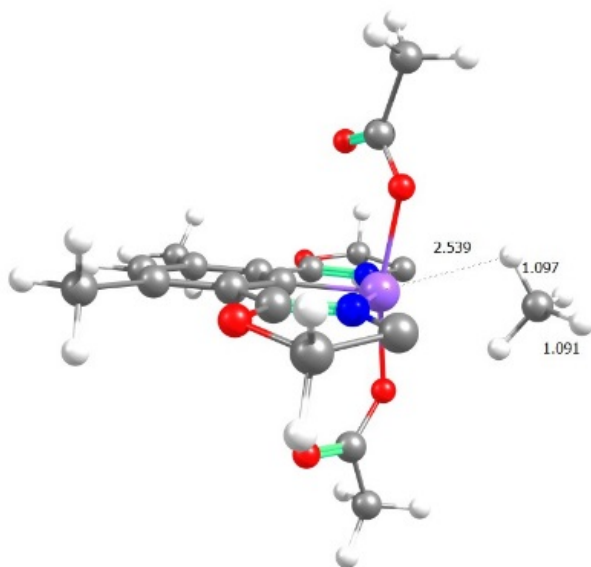
Another point of interest is the low calculated barrier to methane C—H bond activation from the *cis* σ -complex to the *cis*-CMD transition state (3.9 kcal/mol), Figure 6.3, whereas the barrier to activation from the *trans*-adduct complex to the *trans*-CMD transition state is much larger (21.1 kcal/mol). The reason for this is the preorganization inherent in the *cis*-CMD complex (Figure 6.4a) where one of the C—H bonds of methane is already lengthening in the methane adduct (computed bond length of 1.17 Å as compared to 1.09 Å in free methane). The calculated bond lengths in the *trans*- σ -methane complex do not show such a bond lengthening (values are all 1.09 - 1.10 Å). The lengthening of this C—H bond implies that there is some bond breaking already occurring in the σ -methane complex, which destabilizes the *cis*- σ -methane complex relative to the *trans*- σ -methane complex, but partially activates the C—H bond, resulting in a lower barrier to C—H bond activation. The lack of interaction in the *trans* complex can be seen as the two acetate groups rotate away from the methane ligand (Figure 6.4c).



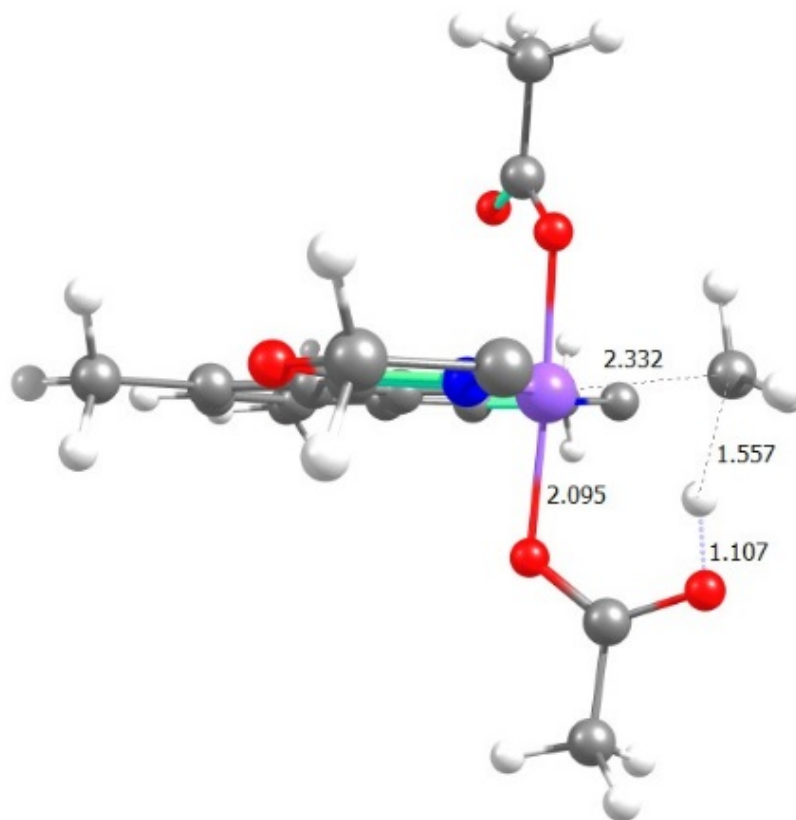
(a)



(b)



(c)



(d)

Figure 6.4 The structures of (a) *cis*-^{dm}PheboxIr(OAc)₂(σ-CH₄), (b) the CMD TS of *cis*-^{dm}Phebox(OAc)₂(σ-CH₄), (c) *trans*-^{dm}PheboxIr(OAc)₂(σ-CH₄), and (d) the CMD TS of *trans*-^{dm}PheboxIr(OAc)₂(σ-CH₄). The longest two methane C—H bond distances are shown (the remaining two are 1.085 Å). Methyl groups on the bisoxazoline rings of the ^{dm}Phebox ligand have been omitted for clarity. Iridium – purple, Oxygen - red, Nitrogen - blue, carbon - gray, hydrogen – white.

6.4 Impact of Ligand Modification

Having calculated that the ^{dm}PheboxIr complex more favorably reacts through a CMD mechanism than an oxidative addition/reductive elimination type mechanism, modifications to the supporting ligand that would facilitate C—H bond activation, particularly of methane, were investigated. It has been established through demonstration of an H/D exchange reaction that ^{dm}PheboxIr(OAc)₂(H₂O) reacts with octane at 160 °C without the need for external base.¹⁹⁴ However, if lower barriers could be achieved, milder conditions could be employed. Most

previous modeling studies of the CMD mechanism have focused on the effect of substrate^{195,196} so an investigation into the effect of catalyst modification would greatly increase our understanding and ability to develop more effective catalysts.

6.4.1 Effect of *para*-substitution on Aryl Linker

To determine the effect of varying the electronic properties of the phenyl spacer, Phebox ligands substituted with an electron donating dimethylamino group ($\sigma_p = -0.83$), an electron withdrawing nitro ($\sigma_p = 0.78$), or with the unsubstituted Phebox ligand were studied (Figure 6.5).⁶⁶ Similar free energy barriers, $\Delta G^\ddagger \sim 31$ kcal/mol were found for the C-H activation reactions for the complexes bearing ligands modified with these different substituents. The Hammett indifference implied by the results in Figure 6.5 is intriguing in light of the characterization of this mechanism as a deprotonation. One may posit that either the C-H activation event involves very little charge build up or there is only very weak electronic coupling between the orbitals of the arene backbone and the six-membered ring active site of the CMD transition state.

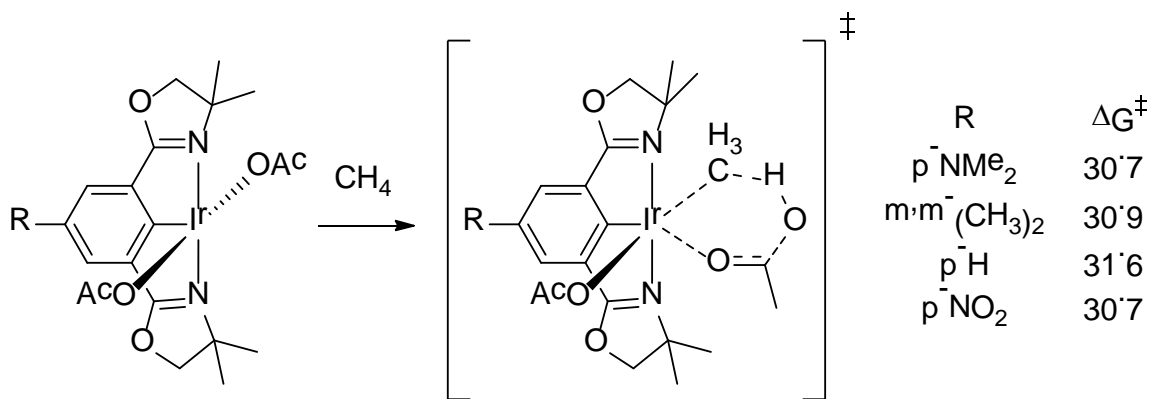


Figure 6.5 Free energy barriers (kcal/mol) for systems with *para*-substituents on the phenyl backbone.

6.4.2 Modifications of the Aryl Backbone

With the electronic modifications changing the barrier only slightly, the effect of exchange of the phenyl backbone with a heteroaryl backbone was investigated (Figure 6.6). Exchange of a pyridyl backbone for the phenyl backbone would result in an overall cationic complex. This change would be expected to increase the electrophilicity of the metal center. In the CMD mechanism for iridium the transition state is ambiphilic¹⁸⁸ and donation from the ligand to the metal is important for stabilization of the transition state. Increasing the electrophilicity of the metal may enhance that interaction and lower the barrier to C-H activation. Therefore, 2,6-pyrazine-bisoxazoline (Pyzbox), 2,6-pyridine-bisoxazoline (Pybox), and 3,5-pyridine-bisoxazoline (ParaNbox) ligands were modeled and the barriers for CMD were investigated (Figure 6.6) For this study the methyl groups on the phenyl backbone were not modeled for the different heteroaryl groups, so they are compared against the unsubstituted ^{dm}Phebox complex.

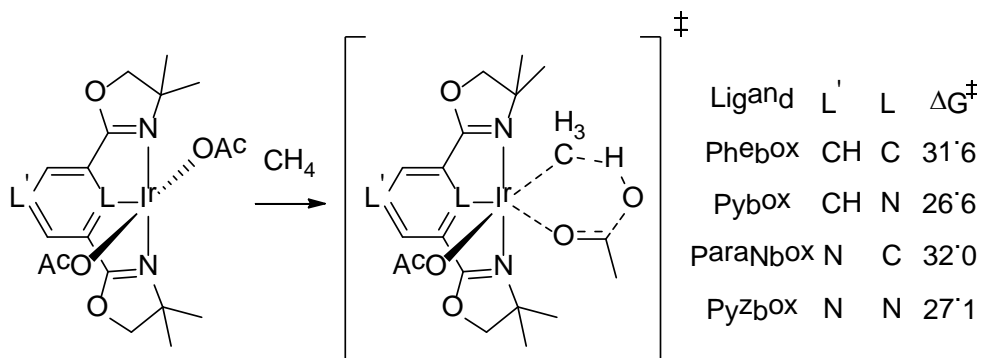


Figure 6.6 Free energy barriers (kcal/mol) for systems with nitrogen heterocycles as central ligand.

Changing the ligating atom from carbon (^{dm}Phebox) to nitrogen (Pybox) is calculated to lower the free energy barrier by 5.0 kcal/mol from 31.6 kcal/mol to 26.6 kcal/mol. This difference in free energy could be due to the exchange of the carbon ligating atom for a nitrogen atom, or

because the Pybox ligated complex is cationic and would therefore be expected to be more electrophilic. The ParaNbox ligated complex is calculated to have a 0.5 kcal/mol higher free energy barrier than Phebox for the activation of methane. Therefore, the simulations suggest that the decreased C—H activation barrier in the Pybox system relative to Phebox is not due to any change in the electronic properties of the aryl linker upon exchange of the phenyl backbone for a pyridyl backbone but is rather due to exchange of the anionic ligand for a neutral ligand. The barrier to methane activation for the Pyzbox ligated complex ($L = L' = N$) is 4.9 kcal/mol lower than the barrier for the ParaNbox ligated complex, similar to the difference between the Phebox and Pybox ligated complexes. It should be considered that in the gas phase charge effects may be exaggerated and the effects on the CMD barrier may be smaller in solution.

Periana *et al.* have shown that bipyrimidine ligands can facilitate electrophilic C-H bond activation in concentrated sulfuric acid solutions.¹³ Computational studies have suggested that the bipyrimidine stabilizes the complex against decomposition by retaining a bidentate binding mode while protonated.²⁷ Given that cationic systems promoted C-H cleavage, protonation or methylation of the ligand backbone could elicit the same effect for the Pyzbox and ParaNbox ligands. Thus, the barriers for the protonated, and methylated systems were investigated in the gas phase and compared to the parent complexes (Figure 6.7).

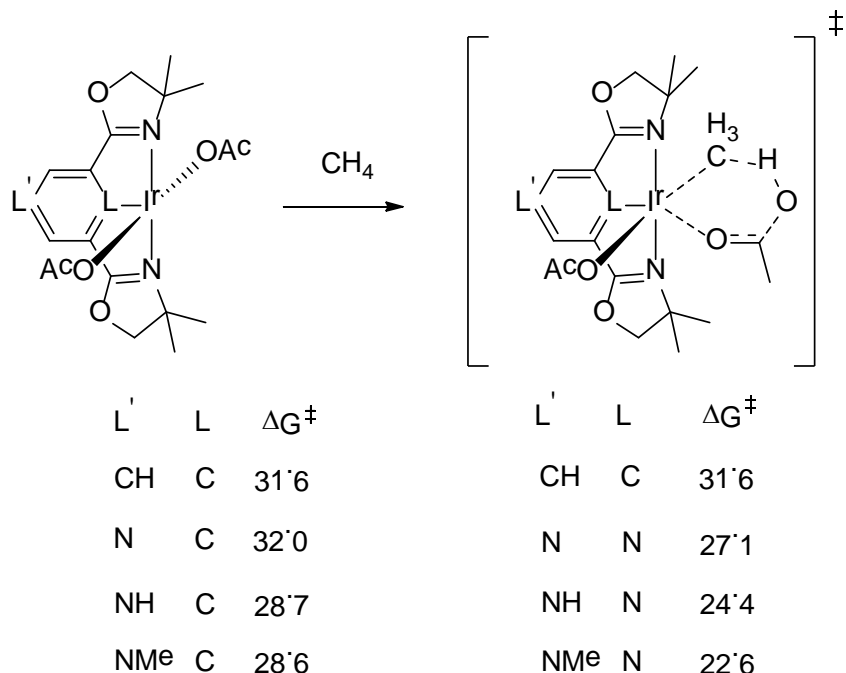


Figure 6.7 Free energy barriers (kcal/mol) for systems with protonated or methylated systems.

For the ParaNbox ligated system, both protonation and methylation lowered the free energy barrier by a similar amount (3.5 kcal/mol). For the Pyzbox ligand the free energy barriers show a distinction between methylation and protonation. The barrier for the methylated Pyzbox ligated system is calculated to be 1.8 kcal/mol lower than the protonated Pyzbox ligated complex. The large effect of protonation and methylation on the barrier to methane activation supports the proposal that a more electrophilic metal center facilitates C-H activation for this family of Ir-pincer complexes.

6.4.3 Effect of Pincer Arm Substitution

Complexes with alternate pincer arms were investigated to determine if oxazoline moieties were the optimal choice for pincer substituent. Carbenes, oxazolines with an additional methylene linker, and nitro groups were investigated as potential arms for the pincer ligand in this system (Figure 6.8). For these calculations, the methyl substituents on the center phenyl ring

were retained to better correspond to the experimental system. Exchange of the oxazoline ligands for unsaturated N-heterocyclic carbene ligands was calculated to have almost no effect on the free energy barrier. In light of the results for protonated and methylated pincer backbones, nitro groups were considered as a computational probe to model more electrophilic pincer arms. Even this very electron withdrawing group was not found to appreciably impact the barrier to methane activation. In summary, the CMD barriers seem fairly impervious to electronic modification of the pincer arms.

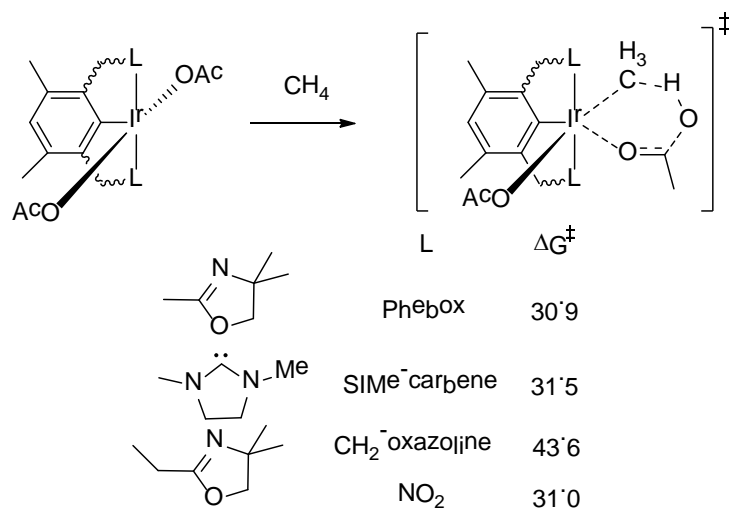


Figure 6.8 Free energy barriers (kcal/mol) for systems with modified side chains.

The impervious nature of the CMD mechanism to the ligand arms and electronic properties of the backbone may not be entirely unexpected. The CMD mechanism forms and breaks primarily σ -bonds. We hypothesize, therefore, that the σ -bonding orbitals, ($d_{x^2-y^2}$ and d_{z^2} in the typical coordinate system) would be expected to have the largest impact on reactivity. The d_{xy}^{dm} Phebox, and other modeled ligands, interact strongest with the $d_{x^2-y^2}$ orbital, while the forming Ir-Me interacts strongest with the d_{z^2} orbital. Since the ligand manipulations are in the plane perpendicular to the forming Ir-Me bond it is proposed that modification of the arms and

backbone does not substantially impact the energy of the d_{z^2} orbital and therefore would have a small impact on the barrier, as is observed computationally.

Homologation of the oxazoline moieties has a dramatic impact on the barrier raising it by 12.7 kcal/mol in free energy. These results imply that the steric impact of the pincer arms are more important than their electronic impact on Ir^{III} acetate CMD type C-H bond activation.

6.4.4 Effect of Modifying Acetate Base

Above it was proposed that the energy of the d_{z^2} orbital should have the largest effect on C-H activation barriers. Given that the spectator acetate ligand occupies the other lobe of the d_{z^2} (*i.e.*, is *trans* to the methyl group of the methane being activated in the TS, Figure 6.9), the effect of exchange of the acetate ligand for different carboxylate and acetamide ligands was deemed of interest (Figure 6.9). The more electron rich pivalate was calculated to lower the CMD barrier by 0.4 kcal/mol versus acetate. Bicarbonate, trifluoroacetate and acetamide activation (via the oxygen) were computed to have little effect on the free energy barrier, each raising it by less than 1 kcal/mol. Activation by benzoate raised the barrier by 1.8 kcal/mol. The calculated CMD barrier does not correlate with basicity as the barriers increase in the order R = Me₃C < CH₃ < CF₃ < HO < Ph, but pKa of the conjugate carboxylic acid increases in the order R = CF₃ < Ph < CH₃ < Me₃C < HO. Carbonate and acetamide activation (via the nitrogen) of methane were calculated to be much higher in energy (8 - 9 kcal/mol). Note that counterions were not modeled for carbonate so the overall complex is dianionic. The decreased electrophilicity in a dianionic system is expected to be the cause of the increased barrier in the carbonate system. The more favorable barrier ($\Delta\Delta G^\ddagger \sim 8$ kcal/mol) for the activation of methane by the oxygen rather than nitrogen atom of acetamide suggests that carboxylates are better bases than amides for this system.

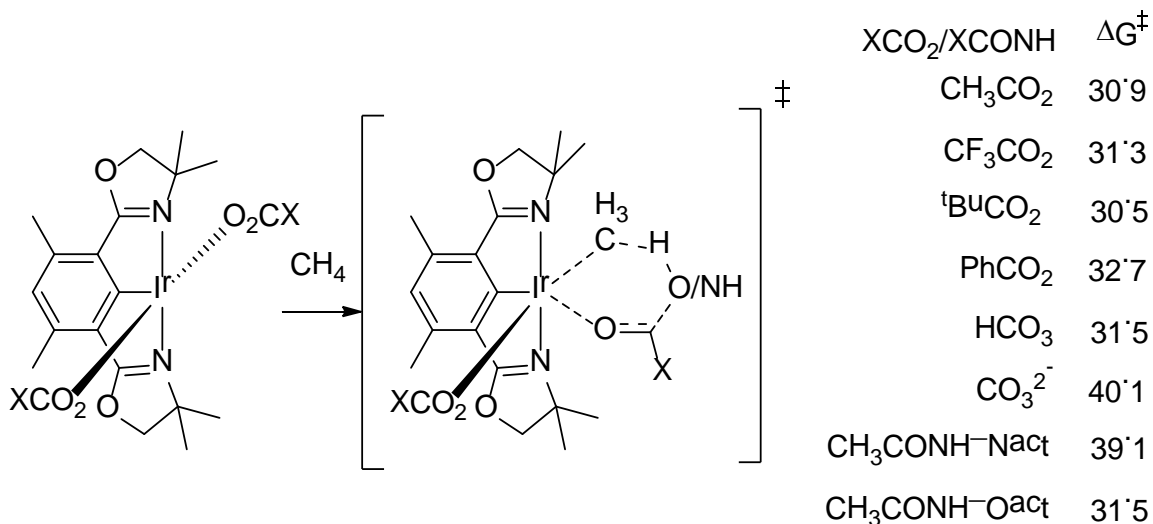


Figure 6.9 Free energy barriers (kcal/mol) for the activation of methane by various carboxylates and acetamide.

Given the observation that the CMD barrier does not correlate directly with basicity we considered that the spectator acetate might also modulate the activity of the complex. To test this hypothesis mixed acetate/trifluoroacetate systems were investigated. (Figure 6.10). When the acetate acting as the CMD base (R' in Figure 6.10) is exchanged for trifluoroacetate, the free energy barrier increases by 4.3 kcal/mol compared to the bis-acetate. However, if the spectator acetate is replaced by trifluoroacetate ($R = \text{CH}_3$, $R' = \text{CF}_3$, Figure 6.10), the barrier decreases by 0.9 kcal/mol. The first result is consistent with trends in basicity of RCO_2^- . The spectator carboxylate, being *trans* to the incoming methyl ligand, should allow more Ir-Me bond formation in the transition state and a lower barrier for the more weakly *trans* effecting trifluoroacetate spectator ligand. The magnitude of the ΔG^\ddagger in Figure 6.10 clearly indicates that the basicity of the carboxylate is of primary importance, while the *trans* influence/effect is secondary.

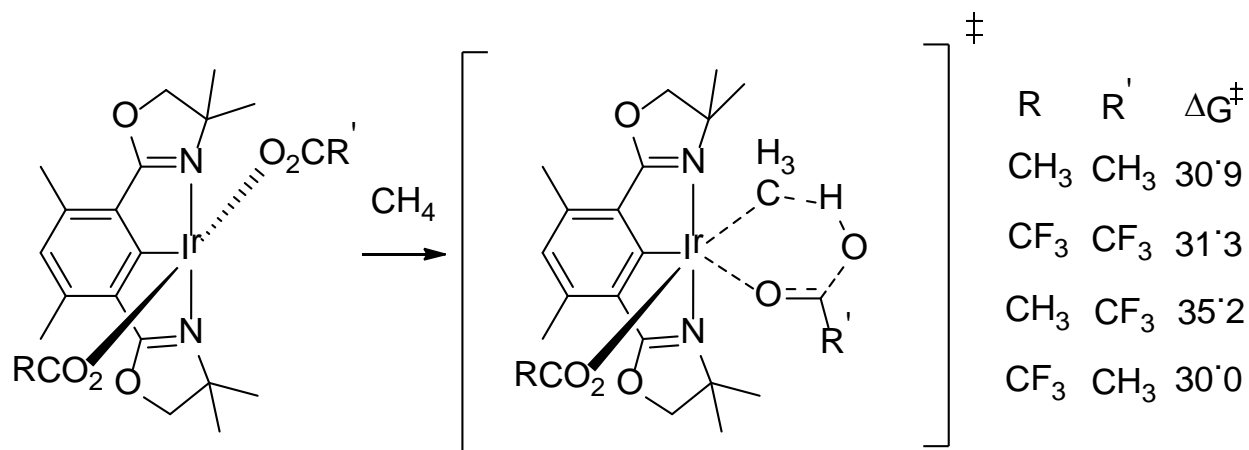


Figure 6.10 Free energy barriers for mixed acetate systems.

6.5 Summary and Conclusions

To best understand how to increase the activity of $(^{dm}\text{Phebox})\text{Ir}(\text{OAc})_2(\text{H}_2\text{O})$ toward cleavage of C—H bonds, the mechanistic details of the activation and the effect of ligand substitutions on the resulting barriers was studied using DFT. Several important conclusions in regards to the activation of alkane C—H bonds by Ir^{III} complexes via a concerted metalation deprotonation (CMD) mechanism have resulted. The most important of these are summarized here.

First, it was found that the *trans*- $(^{dm}\text{Phebox})\text{Ir}(\text{OAc})_2(\text{CH}_4)$ complex was more stable than the *cis*- $(^{dm}\text{Phebox})\text{Ir}(\text{OAc})_2(\text{CH}_4)$ complex. However, the preorganization inherent in the *cis*- $(^{dm}\text{Phebox})\text{Ir}(\text{OAc})_2(\text{CH}_4)$ lowers the barrier to the C—H activation transition state making the *cis* complex more active than the *trans* isomer. Presumably, the design of novel ligand sets that can ameliorate this preorganization penalty would be desirable, perhaps through the use of chelating bis-carboxylate ligands.

Second, the barrier to methane CMD by these Ir(III) pincer complexes was generally insensitive to modification of the pincer side arms, or changing the electronic properties of the

phenyl linker ligand through *para*-substitution. This insensitivity is proposed to be due to weak coupling between the orbitals that comprise the six-membered ring transition state of CMD with the π -orbitals of the arene backbone or the σ -orbitals of the arms, which lie orthogonal to the plane of the CMD reaction path. For the pincer arms, their steric impact was computed to be greater than their electronic impact.

Third, the carboxylate plays a dual role in the activation, as a base and as a spectator, and the two roles have opposite electronic demands. As a CMD base, more electron rich acetates are preferred as they should increase the basicity of the carboxylate thereby promoting the deprotonation. As the spectator, a more electron poor carboxylate facilitates reaction as it allows for greater Ir-Me bond character in the transition state due to a lower *trans* effect.

Fourth, exchange of a phenyl backbone for a heteroaryl backbone that ligates to iridium through a nitrogen leads to greatly lowered barriers. Similarly, protonation or methylation of the nitrogen in the *para*-position again leads to improved barriers. It is proposed that this is due to increased electrophilicity of these complexes. More electrophilic complexes should bind weak ligands, such as methane, stronger and binding of methane is energy intensive for this reaction. Also, the transition state is stabilized in part by electron donation from the substrate to the metal.¹⁸⁸ A more electrophilic metal should enhance this interaction as well. These results imply that cationic systems are likely to be the best options for further development of more active variants of these catalysts.

CHAPTER 7

CLOSING REMARKS AND CHAPTER SUMMARY

In Chapter 2 a computational study of the reductive functionalization of Rh^{III}-Me bonds in cationic bisbipyridine ligated Rh complexes of the form [(bpy)₂Rh(Me)X]⁺. The effect of modifying the bipyridine ligand, ancillary ligand, metal center, and nucleophile was studied to assist identification of reactive complexes for synthesis. Of the two isomers studied, the *cis* complex is more stable and more reactive than the *trans* isomer and these were the focus of further research. Singlet cobalt complexes have similar barriers to rhodium complexes, while triplet cobalt complexes are more reactive. Therefore, cobalt complexes would be promising candidates for further investigation. *Trans*-[(bpy)₂Rh(Me)X]⁺ complexes with various X groups (X = HO⁻, H⁻, H₃C⁻, Cl⁻, CO, and Py) were studied to determine the effect of the ligand trans to the Rh-Me bond upon barriers for reductive functionalization. Ligands that can accept electron density (Cl⁻, CO) lower the barrier significantly by facilitating reduction to Rh^I. Strong trans effect ligands (HO⁻, H⁻) also reduce the barrier by weakening the Rh-Me bond, but by a lesser extent than electron accepting trans ligands. The largest effect on the barrier came from manipulation of the bipyridine rings with electron donating substituents raising the barrier, but electron withdrawing ligands, specifically NO₂ substituents, lowering the barrier by 13.3 kcal/mol. These calculations highlighted the need for stabilization of the resulting Rh^I complex to promote reductive functionalization at Rh^{III}-Me bonds.

In Chapter 3 a complex was developed based on the properties suggested by our modeling efforts in the previous chapter. The 4,4',4''-trinitroterpyridine [(NO₂)₃terpy] ligand was selected as a scaffold that may promote reductive functionalization as it is electron poor and

could form a square planar Rh^I complex. Experimental collaborators showed that [(NO₂)₃terpy]Rh complexes undergo both oxidative addition of MeX at Rh^I and reductive functionalization of MeX at Rh^{III}. These reactions were studied computationally to better understand the mechanism and what factors controlled the reactivity of these complexes. To test the accuracy of the computational methods, it was calibrated by using bomb calorimetry to measure the enthalpy of addition of MeI to [(tBu)₃terpy]RhI and computations were found to be within 2 kcal/mol of the experimental value. Thus calibrated, the computations showed that the oxidative addition of MeX (X = Cl, I, O₂CCF₃) by 4,4',4''-tritylterpyridine [(tBu)₃terpy]RhCl was approximately 10 kcal/mol more favorable than the oxidative addition of the same MeX to [(NO₂)₃terpy]RhCl. The mechanism for the loss of MeCl from [(NO₂)₃terpy]Rh(Me)(Cl)₂ was also studied. The computed mechanism revealed an interesting facet, i.e., reductive functionalization is preceded by initial loss of halide to give the cationic [[(NO₂)₃terpy]Rh(Me)(Cl)]⁺. The release of the halide is facilitated by the high polarity of the nitromethane solvent. The increased electrophilicity of the cationic complex also explains the lowered barriers for the cationic complexes.

In Chapter 4 the same [(NO₂)₃terpy]Rh(Me)(Cl)(I) system was revisited, but this time in protic solvents. Acidic solvents have the added benefit of protecting the functionalized product, but Rh-Me bonds can undergo protonolysis under acidic conditions. Experimental collaborators studied the reductive functionalization of the [(NO₂)₃terpy]Rh(Me)(Cl)(I) system in acetic acid, trifluoroacetic acid, and water and observed only partial loss to protonolysis. The mechanism of this system was modeled in order to assess the relative barriers of the protonation and reductive functionalization pathways. The first difference was that solvents used, acetic and trifluoroacetic

acid, are both far less polar than the previous chapter. The lower polarity solvent increases the cost of dissociating the halide ligand and thus the barriers for the neutral six-membered and the cationic five-membered transition states are now approximately equal. The second effect of the new solvents was the potential for hydrogen bonding to the nucleophile and complex. Hydrogen bonding to the nucleophile raised the barrier for reductive functionalization, whereas hydrogen bonding to the complex lowered the barrier. Consideration of both effects raised the barrier by 4.4 kcal/mol. A final observation was that protonation of the Rh-Me bond was calculated to have a significantly higher barrier than reductive functionalization. However, the Rh-Me bond strength was calculated to be only 26.0 kcal/mol in $[(\text{NO}_2)_3\text{terpy}]\text{Rh}(\text{Me})(\text{Cl})_2$. The low bond dissociation free energy coupled with the higher reaction temperatures may allow for Rh-Me bond homolysis. Subsequent experiments with radical traps supported this prediction, but was not conclusive.

Hydrogenolysis of an iridium-methyl complex was the focus of Chapter 5. The mechanism of H-D exchange of the methyl and hydride ligands of $(\text{PONOP})\text{Ir}(\text{H})(\text{Me})^+$ (1) [PONOP = 2,6-bis(di-*tert*-butylphosphinito)pyridine] about exposure to molecular deuterium (D_2). Both oxidative and non-oxidative pathways were considered and oxidative hydrogen migration pathway was calculated to be the lowest energy pathway for hydrogen exchange. The calculated barriers for oxidative hydrogen migration and experimental barriers were in very close agreement providing further evidence for this pathway.

In chapter 6 the activation of alkanes by phebox iridium carboxylate complexes via the concerted metalation deprotonation (CMD) mechanism was studied to determine what ligands performed best. Most ligand modifications did not affect the CMD barrier significantly. Only aryl

backbones that would result in a cationic complex were calculated to decrease the barrier. Variation of the acetate ligand resulted in two disparate effects being elucidated. The carboxylate plays two roles, one is the base and the other is a spectator) within the reaction which have different electronic preferences. When the carboxylate that acts as a base is more electron rich, the barrier is reduced. More electron poor spectator carboxylate ligands are calculated to lower the barrier. The observed dichotomy led to the conclusion that only ligands that directly affect the d_{z^2} orbital are effective in lowering the CMD barrier.

In chapters 2 - 4 the focus is on the reductive functionalization of Rh-Me bonds. A complex was synthesized based on the computational predictions in chapter 2 and was shown to be active in both protic and aprotic media. This result may suggest that the same predictions could be useful to design new ligand sets to perform reductive functionalization. Assuming that other complexes that can accomplish reductive functionalization can be synthesized, the focus turns to the other step necessary to complete the proposed catalytic cycle, C-H activation. Of the three main suggestions towards synthesizing complexes active for reductive functionalization, at least one will disfavor oxidative addition as a route to C-H bond activation. Very electron poor ligands are necessary to help stabilize the Rh^I oxidation state, but by stabilizing the Rh^I center relative to the Rh^{III} oxidation state, naturally oxidative addition will be disfavored. Preliminary calculations on terpyRh^I systems suggested that oxidative addition of MeH is at least 35 kcal/mol uphill in free energy. With thermodynamics this unfavorable, the oxidation addition will be extremely slow and increasing the temperature may lead to homolytic processes of any resulting Rh-Me bond.

Two potential solutions would be to modify the ligand set to stabilize the Rh^{III} oxidation state. However, given the elevated temperatures necessary to perform the reductive functionalization, disfavoring the thermodynamics of reductive functionalization will only raise the barrier further. Another possibility is non-oxidative C-H activation as discussed in chapters 5 and 6, though, non-oxidative C-H activation would necessarily require an oxidant to complete the catalytic cycle. The C-H activation could occur either preceding the oxidation at a Rh^I center, or after the oxidation at a Rh^{III} center thereby adding potential flexibility in ligand selection. Concerted metallation-deprotonation seems a particularly promising mechanism as the carboxylate base can serve multiple roles in the catalytic cycle. First, it acts as the base during the CMD deprotonation. Second, depending on the carboxylate employed, it could serve as the nucleophile in the reductive functionalization. Third, as a bidentate ligand it could potentially dissociate an arm and act as a good leaving group/weak trans ligand for the reductive functionalization. Fourth, it may help stabilize cationic complexes by occupying a second coordination site, which has been calculated to favor both mechanisms. A potential drawback for non-oxidative methods is the need for an external oxidant. For fuel applications the oxidant would need to be inexpensive. Perhaps the best option would be molecular oxygen from air as it would essentially be free whether the dioxygen was used directly, or mediated by copper salts. However the Rh-Me bond homolysis in the terpy system could become further complicated with the use of dioxygen since it often promotes radical reactions.

An interesting further question for the non-oxidative C-H activation mediated by iridium complexes is how applicable are the conclusions of these particular systems to other iridium complexes? For example, the conclusion for the pheboxIr carboxylate system was that only those

ligands that specifically interacted with the orbitals participating in the CMD had a large effect on the barrier. For an octahedral complex with a meridional tridentate ligand the orbitals are distinct and this concept may be applied easily; however, in a complex with a facial ligand, especially the Cp* ligand that has been used previously for CMD, these orbitals are not as disparate. Research on a non C₃-symmetric tridentate facial ligand, such as a trispyrazoylborate where one pyrazoyl ligand has been replaced with an oxazolinylligand, could deduce whether this same orbital argument applies to facial ligands. A facial ligand has the added benefit of being able to use trans influence/effect properties to help modify the reactivity of more ligand binding sites to potentially reduce the CMD barrier further by easier binding of the alkane. For the hydrogenolysis of Ir-Me bonds by dihydrogen, perhaps the most interesting question is whether this reaction could be pushed in the opposite direction with an appropriate ligand scaffold. Metal hydrides can be formed by many processes such as C-H activation, protonation of metal centers, β-hydride elimination, and addition of hydrides to metal centers. If metal hydrides originating from any of these processes could selectively be converted into metal-methyl bonds by σ-bond metathesis, then not only could the metal-methyl bonds be formed but dihydrogen would be formed as a byproduct. Dihydrogen is a useful reagent for many reductions and in an industrial setting could be shuttled for use in other processes. This sequence would be unique in how alkane activation/functionalization is approached.

REFERENCES

- ¹ Olah, G. A. *Angew. Chem. Int. Ed.* **2005**, *44*, 2636.
- ² Speight, J. G. *Petroleum Refining: Technology and Economics*, **1999**,
- ³ Bruice, P. Y. *Organic Chemistry*; Prentice-Hall, Inc., **2001**, 3rd Ed.
- ⁴ C.D. Frohning, C.W. Kohlpaitner, in: B. Cornils, W.A. Herrmann (Eds.), *Applied Homogenous Catalysis with Organometallic Compounds: A Comprehensive Handbook in Two Volumes*, vol. 1, VCH Weinheim, **1996**
- ⁵ Schulz, H. *Appl. Cat. A* **1999**, *186*, 3-12.
- ⁶ Hansen J. B. in *Handbook of Heterogeneous Catalysis* (Eds.: G. Ertl, H. Knzinger, J. Weitkamp), VCH, Weinheim, **1997**, p. 1856
- ⁷ NIST database, <http://webbook.nist.gov/chemistry/> Accessed Feb. 10, 2015.
- ⁸ a) Sommer, J., Bukala, J. *Acc. Chem. Res.*, **1993**, *26*, 370-376 b) Davies, H. M. L.; Beckwith, R. E. *J. Chem. Rev.*, **2003**, *103*, 2861-2904. Arockiam, P. B.; Bruneau, C.; Dixneuf, P. H. *Chem. Rev.*, **2003**, *112*, 5879-5918. c) Arnold, P. L.; McMullon, M. W.; Rieb, J.; Kühn, R. E. *Angew. Chem. Int. Ed.* **2014**, *54*, 82-100.
- ⁹ a) Hashiguchi, B. G.; Bischof, S. M.; Konnick, M. M.; Periana, R. A. *Acc. Chem. Res.* **2012**, *45*, 885– 898. b) Jones, W. D., *Acc. Chem. Res.* **2003**, *36*, 140-146.
- ¹⁰ a) Pardue, D. B.; Mei, J. J.; Gunnoe, T. B.; Cundari, T. R.; *Inorg. Chem.*, **2014**, *53*, 2968-2975. b) Mei, J. J.; Carsch, K. M.; Freitag, C. R.; Gunnoe, T. B.; Cundari, T. R. *J. Am. Chem. Soc.*, **2013**, *135*, 1217-1220. c) McMullin, C. M.; Pierpont, A. W.; Cundari, T. R., *Polyhedron*, **2013**, *52*, 945-956. d) Figg, T. M.; Schoendorff, G.; Chiulukuri, B.; Cundari, T. R.; *Organometallics*, **2013**, *32*, 4993-4996.
- ¹¹ Shilov, A. E.; Shulpin, G. B. *Russ. Chem. Rev.* **1987**, *56*, 442–464.
- ¹² Periana, R. A.; Taube, D. J.; Evitt, E. R.; Loffler, D. G.; Wentrcek, P. R.; Voss, G.; Masuda, T. *Science* **1993**, *259*, 340–343.
- ¹³ Periana, R. A.; Taube, D. J.; Gamble, S.; Taube, H.; Satoh, T.; Fuji, H. *Science* **1998**, *280*, 560-564.
- ¹⁴ Goldberg, K. I.; Goldman, A. S. *Activation and Functionalization of C–H Bonds*; American Chemical Society: Washington, DC, **2004**; Vol. 885.
- ¹⁵ Stahl, S. S.; Labinger, J. A.; Bercaw, J. E. *Angew. Chem., Int. Ed.* **1998**, *37*, 2180–2192.

- ¹⁶ Jones, W. D. *Science* **2002**, *295*, 289–290.
- ¹⁷ Fulton, J. R.; Holland, A. W.; Fox, D. J.; Bergman, R. G. *Acc. Chem. Res.* **2002**, *35*, 44–56.
- ¹⁸ Olah, G. A.; Goepfert, A.; Prakash, G. K. S. *Beyond Oil and Gas: The Methanol Economy*, 2nd ed.; Wiley-VCH: Weinheim, Germany, **2009**.
- ¹⁹ Lau, W.; Kochi J. K. *J. Am. Chem. Soc.* **1986**, *108*, 6720-6732.
- ²⁰ Kao, L. C.; Hutson, A. C.; Sen, A. *J. Am. Chem. Soc.* **1991**, *113*, 700-701.
- ²¹ Nomura, S.; Uemura, S. *J. Chem. Soc. Chem. Commun.* **1994**, 129-130.
- ²² Hashiguchi, B. G.; Bischof, S. M.; Konnick, M. M.; Periana, R. A. *Acc. Chem. Res.* **2012**, *45*, 885–898.
- ²³ Jones, C.; Taube, D.; Ziatdinov, V. R.; Periana, R. A.; Nielsen, R. J.; Oxgaard, J.; Goddard, W. A. *Angew. Chem., Int. Ed.* **2004**, *43*, 4626–4629.
- ²⁴ Ahlquist, M.; Nielsen, R. J.; Periana, R. A.; Goddard, W. A. *J. Am. Chem. Soc.* **2009**, *131*, 17110-17115.
- ²⁵ Goldshleger, N. F.; Tyabin, M. B.; Shilov, A. E.; Shteinman, A. A. *Zh. Fiz. Khim. (Engl. Transl.)* **1969**, *43*, 1222-1223.
- ²⁶ Ahlquist, M.; Periana, R. A.; Goddard, W. A. *Chem. Commun.* **2009**, 2373–2375.
- ²⁷ Kua, J.; Xu, X.; Periana, R. A.; Goddard, W. A. *Organometallics* **2002**, *21*, 511-525.
- ²⁸ Stahl, S. S.; Labinger, J. A.; Bercaw, J. E. *J. Am. Chem. Soc.* **1996**, *118*, 5961-5976.
- ²⁹ Stahl, S. S.; Labinger, J. A.; Bercaw, J. E. *J. Am. Chem. Soc.* **1995**, *117*, 9371-9372.
- ³⁰ Jawad, J. K.; Puddephatt, R. J.; Stalteri, M. A. *Inorg. Chem.* **1982**, *21*, 332-337.
- ³¹ Jensen, M. P.; Wick, D. D.; Reinartz, S.; White, P. S.; Templeton, J. L.; Goldberg, K. I. *J. Am. Chem. Soc.* **2003**, *125*, 8614-8624.
- ³² Xu, X.; Fu, G.; Goddard, W. A.; Periana, R. A. *Stud. Surf. Sci. Catal.* **2004**, *147*, 499-504.
- ³³ Lin, M.; Sen, A. *Nature*, **1994**, *368*, 613-615.
- ³⁴ Xu, Z.; Oxgaard, J.; Goddard, W. *Organometallics*, **2008**, *27*, 3770-3773.
- ³⁵ Munz, D.; Meyer, D.; Strassner, T. *Organometallics*, **2013**, *32*, 3469-3480.
- ³⁶ Mylvaganam, K.; Bacskay, G. B.; Hush, N. S. *J. Am. Chem. Soc.* **1999**, *121*, 4633-4639.

- ³⁷ Xhu, H.; Ziegler, T. J. *Organomet. Chem.* **2006**, *21*, 4486-4497.
- ³⁸ Jones, W. D. *Inorg. Chem.* **2005**, *44*, 4475-4484.
- ³⁹ Evans, M. E.; Li, T.; Jones, W. D. *J. Am. Chem. Soc.* **2010**, *132*, 16278-16284.
- ⁴⁰ Vetter, A. J.; Rieth, R. D.; Brennessel, W. W.; Jones, W. D.; *J. Am. Chem. Soc.*, **2009**, *131*, 10742-10752.
- ⁴¹ Lewis, J. C.; Wu, J.; Bergman, R. G.; Ellman, J. A. *Organometallics* **2005**, *24*, 5737-5746.
- ⁴² Wang, C.; Ziller, J. W.; Flood, T. C. *J. Am. Chem. Soc.* **1995**, *117*, 1647-1648.
- ⁴³ Colby, D. A.; Tsai, A. S.; Bergman, R. G.; Ellman, J. A. *Accounts Chem. Res.* **2012**, *45*, 814-825.
- ⁴⁴ Gary, J. B.; Carter, T. J.; Sanford, M. S. *Top. Catal.* **2012**, *55*, 565-570.
- ⁴⁵ Rhinehart, J. L.; Manbeck, K. A.; Buzak, S. K.; Lippa, G. M.; Brennessel, W. W.; Goldberg, K. I.; Jones, W. D. *Organometallics*, **2012**, *31*, 1943-1952.
- ⁴⁶ Ueura, K.; Satoh, T.; Miura, M. *Org. Lett.* **2007**, *9*, 1407-1409.
- ⁴⁷ Li, X.; Yu, S.; Wang, F.; Wan, B.; Yu, X. *Angew. Chem. Int. Ed.* **2013**, *52*, 2577-2580.
- ⁴⁸ Wang, H.; Grohmann, C.; Nimphius, C.; Glorius, F. *J. Am. Chem. Soc.* **2012**, *134*, 19592-19595.
- ⁴⁹ Sherry, A. E.; Wayland, B. B. *J. Am. Chem. Soc.* **1990**, *112*, 1259-1261.
- ⁵⁰ Zhang, X.-X.; Wayland, B. B. *J. Am. Chem. Soc.* **1994**, *116*, 7897-7898.
- ⁵¹ Nelson, A. P.; DiMugno, S. G. *J. Am. Chem. Soc.* **2000**, *122*, 8569-8570.
- ⁵² Sanford, M. S.; Groves, J. T. *Angew. Chem.* **2004**, *116*, 598-600.
- ⁵³ Han, Y.-Z. Ph.D. Thesis, Princeton University, **1992**.
- ⁵⁴ Han, Y.-Z.; Sanford, M. S.; England, M. D.; Groves, J. T. *Chem. Commun.* **2006**, 549-551.
- ⁵⁵ Wu, B.; Zhang, J.; Yun, L.; Fu, X. *Dalton Trans.* **2011**, *40*, 2213-2217.
- ⁵⁶ Shestakova, E. P.; Varshavsky, Y. S.; Nikolskii, A. B. *J. Organomet. Chem.* **2005**, *690*, 3397-3404.
- ⁵⁷ Feller, M.; Diskin-Posner, Y.; Leitun, G.; Shimon, L. J. W.; Milstein, D. *J. Am. Chem. Soc.* **2013**, *135*, 11040-11047.
- ⁵⁸ a) Figg, T. M.; Cundari, T. R., *Organometallics* **2012**, *31*, 4998-5004. b) Conley, B. L.; Ganesh, S. K.; Gonzales, J. M.; Tenn, W. J.; Young, K. J. H.; Oxgaard, J.; Goddard, W. A.; Periana, R. A. *J. Am. Chem. Soc.* **2006**, *128*, 9018-9019. c) Brown, S. N.; Mayer, J. M. *J. Am. Chem. Soc.* **1996**, *118*,

12119–12133. d) Brown, S. N.; Mayer, J. M. *Organometallics* **1995**, *14*, 2951–2960. e) Figg, T. M.; Cundari, T. R.; Gunnoe, T. B. *Organometallics* **2011**, *30*, 3779–3785. f) Figg, T. M.; Webb, J. R.; Cundari, T. R.; Gunnoe, T. B. *J. Am. Chem. Soc.* **2012**, *134*, 2332–2339. g) Mei, J. J.; Carsch, K. M.; Freitag, C. R.; Gunnoe, C. R.; Cundari, T. R. *J. Am. Chem. Soc.* **2013**, *135*, 424–435.

⁵⁹Yoh, S-D.; Cheong, D-Y.; Lee, O-S. *J. Phys. Org. Chem.* **2003**, *16*, 63–68.

⁶⁰Renz, M.; Meunier, B. *Eur. J. Org. Chem.* **1999**, 737–750.

⁶¹Krüger, G.; Roodt, A.; Leipoldt, J.G.; van Eldik, R. *Inorg Chem.* **1989**, *28*, 3073–3076.

⁶²Lahuerta, P.; Latorre, J.; Martinez-Manez, R.; Garcia-Granda, S.; Gomez-Beltran, F. *Acta Crystallogr. C.* **1991**, *47*, 519–522.

⁶³Webb, J. R.; Figg, T. M.; Otten, B. M.; Cundari, T. R.; Gunnoe, T. B.; Sabat, M. *Eur. J. Inorg. Chem.* **2013**, *25*, 4515–4525.

⁶⁴Webb, J. R. Ph. D. Thesis, Univ. of Virginia, **2012**.

⁶⁵Kim, M. Y.; Seok, W. K.; Lee, H. N.; Han, S. H.; Dong, Y.; Yun, H. Z. *Naturforsch. B: Chem. Sci.* **2001**, *56*, 747–752.

⁶⁶Hansch, C.; Leo, A.; Taft, R. W. *Chem. Rev.* **1991**, *91*, 165–195.

⁶⁷Semproni, S. P.; Atienza, C. C. H.; Chirik, P. J. *Chem. Sci.* **2014**, *Advance Article*.

⁶⁸Obligacion, J. V.; Semproni, S. P.; Chirik, P. J. *J. Am. Chem. Soc.* **2014**, *136*, 4133–4136.

⁶⁹The σ^* orbitals were located as attack on the Rh-Me antibonding orbital would be expected, but the calculated energy values for the orbitals were positive and therefore deemed too circumspect for further analysis.

⁷⁰a) Penner, A.; Schröder, T.; Braun, T.; Ziemer, B. *Eur. J. Inorg. Chem.* **2009**, *29–30*, 4464–4470. b) Lo, L. T-L.; Ng, C-O.; Feng, H.; Ko, C-C. *Organometallics* **2009**, *28*, 3597–3600.

⁷¹a) Carrasco, A.C.; Pidko, E. A.; Masedeu-Bultò, A. M.; Lutz, M.; Spek, A. L.; Vogt, D.; Müller, C. *New J. Chem.* **2010**, *34*, 1547–1550. b) Robertson, J. J.; Kadziola, A.; Krause, R. A.; Larsen, S. *Inorg. Chem.* **1989**, *28*, 2097–2102.

⁷²Conifer, C. M.; Taylor, R. A.; Law, D. J.; Sunley, G. J.; White, A. J. P.; Britovsek, G. J. P. *Dalton Trans.* **2011**, *40*, 1031–1033.

⁷³Frisch, M. J. *et al. Gaussian 09*, Gaussian, Inc., Wallingford, CT, 2009.

⁷⁴Cossi, M.; Rega, N.; Scalmani, G.; Barone, V.J. *Comput. Chem.* **2003**, *24*, 669–681.

⁷⁵Cossi, M.; Barone, V.; Mennucci, B.; Tomasi, J. *Chem. Phys. Lett.* **1998**, *286*, 253–260.

- ⁷⁶Becke, A. D.; *J. Chem. Phys.* **1993**, *98*, 1372-1378.
- ⁷⁷Becke, A. D.; *J. Chem. Phys.* **1993**, *98*, 5648-5652.
- ⁷⁸Stevens, W. J.; Basch, H.; Krauss, M. *J. Chem. Phys.* **1984**, *81*, 6026-6033.
- ⁷⁹Cundari, T. R.; Stevens, W. J.; *J. Chem. Phys.* **1993**, *98*, 5555-5565.
- ⁸⁰Olah, G. A. and Molnár, Á.; *Hydrocarbon chemistry*, John Wiley, Hoboken, N.J., 2nd edn, 2003.
- ⁸¹Wittcoff, H.; Reuben, B. G.; Plotkin, J. S.; *Knovel Biochemistry Biology & Biotechnology Library – Academic Collection; Knovel Chemistry & Chemical Engineering Library – Academic Collection*, Wiley-Interscience, Hoboken, N.J., 2nd edn, 2004.
- ⁸²Tolman, W. B.; *Activation of small molecules: organometallic and bioinorganic perspectives*, Wiley-VCH, Weinheim, 2006.
- ⁸³Labinger, J. A.; *J. Mol. Catal. A: Chem.*, **2004**, *220*, 27.
- ⁸⁴Conley, B. L.; Tenn, W. J.; Young, K. J. H.; Ganesh, S. K.; Meier, S. K.; Ziatdinov, V. R.; Mironov, O.; Oxgaard, J.; Gonzales, J.; Goddard, W. A.; Periana, R. A., *J. Mol. Catal. A: Chem.*, **2006**, *251*, 8.
- ⁸⁵Crabtree, R. H., *J. Chem. Soc., Dalton Trans.*, **2001**, 2951.
- ⁸⁶Labinger; J. A., Bercaw, J. E. *Nature*, **2002**, *417*, 507.
- ⁸⁷Periana, R. A.; Bhalla, G.; Tenn, W. J.; Young, K. J. H.; Liu, X. Y.; Mironov, O.; Jones, C. J.; Ziatdinov, V. R. *J. Mol. Catal. A: Chem.*, **2004**, *220*, 7-25.
- ⁸⁸Webb, J. R.; Bolano, T.; Gunnoe, T. B. *ChemSusChem*, **2011**, *4*, 37.
- ⁸⁹Chepaikin, E. G. *Russ. Chem. Rev.*, **2011**, *80*, 363.
- ⁹⁰Goldshleger, N. F.; Shteinman, A. A.; Shilov, A. E.; Eskova, V. V. *Russ. J. Phys. Chem.*, **1972**, *46*, 785.
- ⁹¹ $\text{Rh}^+ \rightarrow \text{Rh}^{3+} + 2\text{e}^-$; $E^\circ = -0.158 \text{ V vs. PtCl}_4^{2-} + 2\text{Cl}^- \rightarrow \text{PtCl}_6^{2-} + 2\text{e}^-$; $E^\circ = -0.68 \text{ V}$.
- ⁹²Chemical Rubber Company, CRC Press, Cleveland, Ohio, 1978.
- ⁹³ $\text{Rh}^+ + \text{e}^- \rightarrow \text{Rh}$; $E^\circ = 0.6 \text{ V vs. Pt}^{2+} + 2\text{e}^- \rightarrow \text{Pt}$; $E^\circ = 1.18 \text{ V}$.
- ⁹⁴Manbeck, K. A.; Brennessel, W. W.; Jones, W. D. *Inorg. Chim. Acta*, **2013**, *397*, 140.
- ⁹⁵Kovach, J.; Brennessel, W. W.; Jones, W. D. *Inorg. Chim. Acta*, **2011**, *367*, 108.

- ⁹⁶ Luinstra, G. A.; Wang, L.; Stahl, S. S.; Labinger, J. A.; Bercaw, J. E. *J. Organomet. Chem.*, **1995**, *504*, 75.
- ⁹⁷ Luinstra, G. A.; Labinger, J. A.; Bercaw, J. E. *J. Am. Chem. Soc.*, **1993**, *115*, 3004.
- ⁹⁸ Atwood, J. D. *Inorganic and organometallic reaction mechanisms*, Wiley-VCH, New York, 2nd edn, 1997.
- ⁹⁹ Crabtree, R. H. *The organometallic chemistry of the transition metals*, Wiley-Interscience, Hoboken, N.J., 4th edn, 2005.
- ¹⁰⁰ Vigalok, A. *Chem. Eur. J.*, **2008**, *14*, 5102.
- ¹⁰¹ Vigalok A.; Kaspi, A. W. *Top. Organomet. Chem.*, **2010**, *31*, 19.
- ¹⁰² Ettore, R. *Inorg. Nucl. Chem. Lett.*, **1969**, *5*, 45.
- ¹⁰³ Goldberg, K. I.; Yan, J. Y.; Breitung, E. M. *J. Am. Chem. Soc.*, **1995**, *117*, 6889.
- ¹⁰⁴ Goldberg, K. I.; Yan, J. Y.; Winter, E. L. *J. Am. Chem. Soc.*, **1994**, *116*, 1573.
- ¹⁰⁵ Ruddick, J. D.; Shaw, B. L. *J. Chem. Soc. A*, **1969**, 2969.
- ¹⁰⁶ Yahav-Levi, A.; Goldberg, I.; Vigalok, A. *J. Am. Chem. Soc.*, **2006**, *128*, 8710.
- ¹⁰⁷ Yahav-Levi, A.; Goldberg, I.; Vigalok, A.; Vedernikov, A. N. *J. Am. Chem. Soc.*, **2008**, *130*, 724.
- ¹⁰⁸ Yahav-Levi, A.; Goldberg, I.; Vigalok, A.; Vedernikov, A. N. *Chem. Commun.*, **2010**, *46*, 3324.
- ¹⁰⁹ Arnold, P. L.; Sanford, M. S.; Pearson, S. M. *J. Am. Chem. Soc.*, **2009**, *131*, 13912.
- ¹¹⁰ Furuya, T.; Ritter, T. *J. Am. Chem. Soc.*, **2008**, *130*, 12834
- ¹¹¹ Kaspi, A. W.; Yahav-Levi, A.; Goldberg, I.; Vigalok, A. *Inorg. Chem.*, **2008**, *47*, 5.
- ¹¹² McMurtrey, K. B.; Racowski, J. M.; Sanford, M. S. *Org. Lett.*, **2012**, *14*, 4094
- ¹¹³ Racowski, J. M.; Gary, J. B.; Sanford, M. S. *Angew. Chem., Int. Ed.*, **2012**, *51*, 3414.
- ¹¹⁴ Whitfield, S. R.; Sanford, M. S. *J. Am. Chem. Soc.*, **2007**, *129*, 15142.
- ¹¹⁵ Powers, D. C.; Benitez, D.; Tkatchouk, E.; Goddard, W. A.; Ritter, T. *J. Am. Chem. Soc.*, **2010**, *132*, 14092.
- ¹¹⁶ Shen, X. Q.; Hyde, A. M.; Buchwald, S. L.; *J. Am. Chem. Soc.*, **2010**, *132*, 14076.
- ¹¹⁷ Mankad, N. P.; Toste, F. D. *Chem. Sci.*, **2012**, *3*, 72.

- ¹¹⁸ Scott, V. J.; Labinger, J. A.; Bercaw, J. E. *Organometallics*, **2010**, *29*, 4090.
- ¹¹⁹ Higgs, A. T.; Zinn, P. J.; Simmons, S. J.; Sanford, M. S. *Organometallics*, **2009**, *28*, 6142.
- ¹²⁰ Roy, A. H.; Hartwig, J. F.; *J. Am. Chem. Soc.*, **2001**, *123*, 1232.
- ¹²¹ Roy, A. H.; Hartwig, J. F.; *J. Am. Chem. Soc.*, **2003**, *125*, 13944.
- ¹²² Roy, A. H.; Hartwig, J. F.; *Organometallics*, **2004**, *23*, 1533
- ¹²³ Liu, H. ; Li, C. L.; Qiu, D. Tong, X. F.; *J. Am. Chem. Soc.*, **2011**, *133*, 6187.
- ¹²⁴ Pan, J.; Wang, X. Y.; Zhang, Y.; Buchwald, S. L.; *Org. Lett.*, **2011**, *13*, 4974.
- ¹²⁵ Petrone, D. A.; Malik, H. A.; Clemenceau, A.; Lautens, M.; *Org. Lett.*, **2012**, *14*, 4806.
- ¹²⁶ Maitlis, P. M.; Haynes, A. ; Sunley, G. J.; Howard, M. J.; *J. Chem. Soc., Dalton Trans.*, **1996**, 2187.
- ¹²⁷ Hartwig, J. F.; *Organotransition metal chemistry: from bonding to catalysis*, University Science Books, Sausalito, California, **2010**.
- ¹²⁸ Frech, C. M.; Milstein, D.; *J. Am. Chem. Soc.*, **2006**, *128*, 12434
- ¹²⁹ Lindner, E.; Wang, Q. Y.; Mayer, H. A.; Fawzi, R.; Steimann, M.; *Organometallics*, **1993**, *12*, 1865-1870.
- ¹³⁰ Pahls, D. R.; Groves, J. T.; Gunnoe, T. B.; Cundari, T. R.; *Organometallics*, **2014**, *33*, 1936-1944.
- ¹³¹ Haarman, H. F.; Ernsting, J. M.; Kranenburg, M.; Kooijman, H.; Veldman, N.; Spek, A. L.; van Leeuwen, P. W. N. M.; Vrieze, K.; *Organometallics*, **1997**, *16*, 887.
- ¹³² Behar, D.; Fessende, R. W.; *J. Phys. Chem.*, **1972**, *76*, 1710.
- ¹³³ Gilbert, B. C.; Larkin, J. P.; Norman, R. O. C.; *J. Chem. Soc., Perkin Trans.*, **1972**, *2*, 1272.
- ¹³⁴ Reszka, K. J.; Bilski, P.; Chignell, C. F.; Dillon, J.; *Free Radical Biol. Med.*, **1996**, *20*, 23.
- ¹³⁵ Feller, M.; Iron, M. A.; Shimon, L. J. W.; Diskin-Posner, Y.; Leitus, G.; Milstein, D.; *J. Am. Chem. Soc.*, **2008**, *130*, 14374.
- ¹³⁶ Gol'dshleger, N. F.; Es'kova, V. V.; Shteinman, A. A.; Shilov, A. E. *Russ. J. Phys. Chem.*, **1972**, *46*, 785-786.
- ¹³⁷ Lin, M. R.; Hogan, T. E.; Sen, A. *J. Am. Chem. Soc.* **1996**, *118*, 4574-4580.

- ¹³⁸ Muehlhofer, M.; Strassner, T.; Herrmann, W. A. *Angew. Chem., Int. Ed.*, **2002**, *41*, 1745–1747.
- ¹³⁹ Periana, R. A.; Mironov, O.; Taube, D.; Bhalla, G.; Jones, C. J., *Science*, **2003**, *301*, 814–818.
- ¹⁴⁰ Strassner, T.; Muehlhofer, M.; Zeller, A.; Herdtweck, E.; Herrmann, W. A. *J. Organomet. Chem.*, **2004**, *689*, 1418–1424.
- ¹⁴¹ Ahrens, S.; Zeller, A.; Taige, M.; Strassner, T., *Organometallics*, **2006**, *25*, 5409–5415.
- ¹⁴² Vargaftik, M. N.; Stolarov, I. P.; Moiseev, I. I. *J. Chem. Soc., Chem. Commun.* **1990**, 1049–1050.
- ¹⁴³ Strassner, T.; Ahrens, S.; Muehlhofer, M.; Munz, D.; Zeller, A. *Eur. J. Inorg. Chem.*, **2013**, 3659–3663.
- ¹⁴⁴ Kataja, K.; Song, X. M.; Huuska, M. *Catal. Today*, **1994**, *21*, 513–517.
- ¹⁴⁵ Gang, X.; Birch, H.; Zhu, Y. M.; Hjuler, H. A.; Bjerrum, N. J. *J. Catal.* **2000**, *196*, 287–292.
- ¹⁴⁶ Fortman, G. C.; Boaz, N. C.; Munz, D.; Konnick, M. M.; Periana, R. A.; Groves, J. T.; Gunnoe, T. *B. J. Am. Chem. Soc.*, **2014**, *136*, 8393–8401.
- ¹⁴⁷ Hashiguchi, B. G.; Konnick, M. M.; Bischof, S. M.; Gustafson, S. J.; Devarajan, D.; Gunsalus, N.; Ess, D. H.; Periana, R. A. *Science*, **2014**, *343*, 1232–1237.
- ¹⁴⁸ Hutson, A. C.; Lin, M. R.; Basickes, N.; Sen, A. *J. Organomet. Chem.*, **1995**, *504*, 69–74.
- ¹⁴⁹ Doi, K.; Togano, E.; Xantheas, S. S.; Nakanishi, R.; Nagata, T.; Ebata, T.; Inokuchi, Y. *Angew. Chem., Int. Ed.* **2013**, *52*, 4380–4383.
- ¹⁵⁰ Munz, D.; Strassner, T. *Angew. Chem., Int. Ed.*, **2014**, *53*, 2485–2488.
- ¹⁵¹ Liu, W. G.; Sberegaeva, A. V.; Nielsen, R. J.; Goddard, W. A.; Vedernikov, A. N. *J. Am. Chem. Soc.*, **2014**, *136*, 2335–2341.
- ¹⁵² Sberegaeva, A. V.; Liu, W. G.; Nielsen, R. J.; Goddard, W. A.; Vedernikov, A. N. *J. Am. Chem. Soc.*, **2014**, *136*, 4761–4768.
- ¹⁵³ Vedernikov, A. N., *Acc. Chem. Res.*, **2012**, *45*, 803–813.
- ¹⁵⁴ Boisvert, L.; Goldberg, K. I., *Acc. Chem. Res.*, **2012**, *45*, 899–910.
- ¹⁵⁵ Shilov, A. E.; Shul'pin, G. B., *Chem. Rev.*, **1997**, *97*, 2879–2932.
- ¹⁵⁶ Arndtsen, B. A.; Bergman, R. G.; Mobley, T. A.; Peterson, T. H. *Acc. Chem. Res.*, **1995**, *28*, 154–162.

- ¹⁵⁷ Jones, W. D.; Feher, F. J. *Acc. Chem. Res.*, **1989**, *22*, 91–100.
- ¹⁵⁸ Jones, W. D. *In Activation and Functionalization of Alkanes*; Wiley: New York, **1989**; pp 111–149.
- ¹⁵⁹ O'Reilly, M. E.; Pahls, D. R.; Webb, J. R.; Boaz, N. C.; Majumdar, S.; Hoff, C. D.; Groves, J. T.; Cundari, T. R.; Gunnoe, T. B. *Dalton Trans.*, **2014**, *43*, 8273–8281.
- ¹⁶⁰ Kushch, L. A.; Lavrushko, V. V.; Misharin, Y. S.; Moravsky, A. P.; Shilov, A. E. *Nouv. J. Chim.*, **1983**, *7*, 729–733.
- ¹⁶¹ Weinberg, D. R.; Labinger, J. A.; Bercaw, J. E., *Organometallics*, **2007**, *26*, 167–172.
- ¹⁶² Basickes, N.; Hogan, T. E.; Sen, A. J. *Am. Chem. Soc.* 1996, *118*, 13111–13112.
- ¹⁶³ (a) Thompson, M. E.; Baxter, S. M.; Bulls, A. R.; Burger, B. J.; Nolan, M. C.; Santarsiero, B. D.; Schaefer, W. P.; Bercaw, J. E. *J. Am. Chem. Soc.*, **1987**, *109*, 203. (b) Burger, P.; Bergman, R. G. *J. Am. Chem. Soc.*, **1993**, *115*, 10462. (c) Tilley, T. D. *Acc. Chem. Res.*, **1993**, *26*, 22. (d) Ziegler, T.; Folga, E.; Berces, A., *J. Am. Chem. Soc.*, **1993**, *115*, 636. (e) Niu, S.; Hall, M. B., *J. Am. Chem. Soc.*, **1998**, *120*, 6169. (f) Lin, Z. *Coord. Chem. Rev.*, **2007**, *251*, 2280. (g) Vastine, B. A.; Hall, M., *J. Am. Chem. Soc.*, **2007**, *129*, 12068.
- ¹⁶⁴ (a) Webb, J. R.; Munro-Leighton, C.; Pierpont, A. W.; Gurkin, J. T.; Gunnoe, T. B.; Cundari, T. R.; Sabat, M.; Petersen, J. L.; Boyle, P. D. *Inorg. Chem.*, **2011**, *50*, 4195. (b) Stern, D.; Sabat, M.; Marks, T. J. *J. Am. Chem. Soc.*, **1990**, *112*, 9558. (c) Osterloh, W. T.; Cornell, M. E.; Pettit, R., *J. Am. Chem. Soc.*, **1982**, *104*, 3759. (d) Khan, A. M.; McQuillin, F. J.; Jardine, I. *Tetrahedron Lett.*, **1966**, *7*, 2649.
- ¹⁶⁵ (a) Jordan, R. F.; Taylor, D. F. *J. Am. Chem. Soc.*, **1989**, *111*, 778. (b) Ramos, J.; Cruz, V.; Muñoz-Escalona, A.; Martínez-Salazar, J. *Polymer*, **2000**, *41*, 6161.
- ¹⁶⁶ Sadow, A. D.; Tilley, T. D. *J. Am. Chem. Soc.*, **2005**, *127*, 643.
- ¹⁶⁷ (a) Jones, W. D. *Acc. Chem. Res.*, **2003**, *36*, 140. (b) Lersch, M.; Tilset, M. *Chem. Rev.*, **2005**, *105*, 2471. (c) Hartwig, J. F.; Cook, K. S.; Hapke, M.; Incarvito, C. D.; Fan, Y.; Webster, C. E.; Hall, M. B. *J. Am. Chem. Soc.*, **2005**, *127*, 2538.
- ¹⁶⁸ Perutz, R. N.; Sabo-Etienne, S. *Angew. Chem., Int. Ed.* **2007**, *46*, 2578.
- ¹⁶⁹ Findlater, M.; Bernskoetter, W. H.; Brookhart, M. *J. Am. Chem. Soc.*, **2010**, *132*, 4534
- ¹⁷⁰ Complex 4 exhibits a 4H signal at –8.9 ppm. The structure is likely a highly fluxional η^2 -H₂ dihydride, as shown.
- ¹⁷¹ Perdew, J. P.; Burke, K.; Ernzerhof, M. *Phys. Rev. Lett.*, **1996**, *77*, 865.

- ¹⁷² (a) Martin, J. M. L.; Sundermann, A. *J. Chem. Phys.* **2001**, *114*, 3408. (b) McLean, A. D.; Chandler, G. S. *J. Chem. Phys.* **1980**, *72*, 5639. (c) Andrae, D.; Haußermann, U.; Dolg, M.; Stoll, H.; Preuß, H. *Theor. Chim. Acta*, **1990**, *77*, 123.
- ¹⁷³ Ghosh, R.; Emge, T. J.; Krogh-Jespersen, K.; Goldman, A. S. *J. Am. Chem. Soc.*, **2008**, *130*, 11317.
- ¹⁷⁴ Marenich, A. V.; Cramer, C. J.; Truhlar, D. G. *J. Phys. Chem. B*, **2009**, *113*, 6378.
- ¹⁷⁵ Maltby, P. A.; Schlaf, M.; Steinbeck, M.; Lough, A. J.; Morris, R. H.; Klooster, W. T.; Koetzle, T. F.; Srivastava, R. C. *J. Am. Chem. Soc.*, **1996**, *118*, 5396.
- ¹⁷⁶ Laponte, D.; Fagnou, K. *Chem. Lett.* **2010**, *39*, 111.8-1126.
- ¹⁷⁷ Ackermann, L. *Chem. Rev.* **2011**, *111*, 1315-1345.
- ¹⁷⁸ Biswas, B.; Sugimoto, M.; Sakaki, S.; *Organometallics* **2000**, *19*, 3895-3908.
- ¹⁷⁹ Davies, D. L.; Donald, S. M. A.; Macgregor, S. A. *J. Am. Chem. Soc.* **2005**, *127*, 13754-13755.
- ¹⁸⁰ Lu, P.; Boorman, T. C.; Slawin, A. M. Z.; Larrosa, I. *J. Am. Chem. Soc.* **2010**, *132*, 5580-5581.
- ¹⁸¹ Flegeau, E. F.; Bruneau, C.; Dixneuf, P. H.; Jutand, A. *J. Am. Chem. Soc.* **2011**, *133*, 10161-10170.
- ¹⁸² Davies, D. L.; Al-Duaij, O.; Fawcett, J.; Giardello, M.; Hilton, S. T.; Russel, D. R. *Dalton Trans.*, **2003**, 4132-4138.
- ¹⁸³ Feng, Y.; Lail, M.; Barakat, K. A.; Cundari, T. R.; Gunnoe, T. B.; Petersen, J. L. *J. Am. Chem. Soc.* **2005**, *127*, 14174-14175.
- ¹⁸⁴ Cannon, J. S.; Ou, L.; Liu, P.; Lan, Y.; O'Leary, D. J.; Houk, K. N.; Grubbs, R. H. *J. Am. Chem. Soc.*, **2014**, *136*, 6733-6743.
- ¹⁸⁵ Ikemoto, H.; Yoshino, T.; Sakata, K.; Matsunaga, S.; Kanai, M. *J. Am. Chem. Soc.* **2014**, *136*, 5424-5431.
- ¹⁸⁶ Li, L.; Brennessel, W. W.; Jones, W. D. *Organometallics* **2009**, *29*, 3492-3500.
- ¹⁸⁷ Zhang, Q.; Yu, H.-Z.; Li, Y.-T.; Liu, L.; Huang, Y.; Fu, Y. *Dalton Trans.* **2013**, *42*, 4175-4184.
- ¹⁸⁸ Ess, D. H.; Bischof, S. M.; Oxgaard, J.; Periana, R. A.; Goddard, W. A. *Organometallics* **2008**, *27*, 6440-6445.
- ¹⁸⁹ Davies, D. L.; Donald, S. M. A.; Al-Duaij, O.; Macgregor, S. A.; Pölleth, M. *J. Am. Chem. Soc.* **2006**, *126*, 4210-4211.

- ¹⁹⁰ Davies, D. L.; Donald, S. M. A.; Al-Duaij, O.; Fawcett, J.; Little, C.; Macgregor, S. A. *Organometallics* **2006**, *25*, 5976-5978.
- ¹⁹¹ Tenn, W. J.; Young, K. J. H.; Bhalla, G.; Oxgaard, J.; Goddard III, W. A.; Periana, R. A. *J. Am. Chem. Soc.* **2005**, *127*, 14172-14173.s
- ¹⁹² Boutadla, Y.; Davies, D. L.; Macgregor, S. A.; Poblador-Bahamonde, A. I. *Dalton Trans.*, **2009**, 5887-5893.
- ¹⁹³ Ito, J.; Kaneda, T.; Nishiyama, H. *Organometallics* **2012**, *31*, 4442-4449.
- ¹⁹⁴ Allen, K. E.; Heinekey, D. M.; Goldman, A. S.; Goldberg, K. I. *Organometallics* **2013**, *32*, 1579-1582.
- ¹⁹⁵ Gorelsky, S. I.; Lapointe, D.; Fagnou, K. *J. Am. Chem. Soc.* **2008**, *130*, 10849.
- ¹⁹⁶ Gorelsky, S. I.; Lapointe, D.; Fagnou, K. *J. Org. Chem.* **2012**, *77*, 658-668.
- ¹⁹⁷ Liu, F.; Pak, E. B.; Singh, B.; Jensen, C. M.; Goldman, A. S. *J. Am. Chem. Soc.* **1999**, *121*, 4086.
- ¹⁹⁸ Morales-Morales, D.; Lee, D. W.; Wang, Z.; Jensen, C. M. *Organometallics* **2006**, *20*, 1144.
- ¹⁹⁹ Renkema, K. B.; Kissin, Y. V.; Goldman, A. S. *J. Am. Chem. Soc.* **2003**, *125*, 7770-7771.
- ²⁰⁰ Krogh-Jespersen, K.; Czerw, M.; Summa, N.; Renkema, K. B.; Achord, P. D.; Goldman, A. S. *J. Am. Chem. Soc.* **2002**, *124*, 11404-11408.
- ²⁰¹ Cheng, C.; Kim, B. G.; Guironnet, D.; Brookhart, M.; Guan, C.; Wang, D. Y.; Krogh-Jespersen, K.; Goldman, A. S. *J. Am. Chem. Soc.* **2014**, *136*, 6672-6683.
- ²⁰² The four Ir-O bonds in Ir-O Bond lengths in PheboxIr(OAc)₂ for the two acetates are 2.04 Å, 2.07 Å, 2.41 Å, and 3.02 Å. This suggests there may be a second much weaker interaction between one acetate group and the open position of the iridium center.